Summer 5-3-2022

Non-destructive Evaluation of Concrete using Electrical Resistivity and Ultrasonic Wave Propagation

Justin Harris
University of Maine, justin.harris@maine.edu

NON-DESTRUCTIVE EVALUATION OF CONCRETE

USING ELECTRICAL RESISTIVITY AND

ULTRASONIC WAVE PROPAGATION

By

Justin Harris

B.S. University of Maine, 2020

A THESIS

Submitted in Partial Fulfillment of the

Requirements for the Degree of

Master of Science

(in Civil Engineering)

The Graduate School

The University of Maine

August 2022

Advisory Committee:

Dr. Eric N. Landis, Professor of Civil and Environmental Engineering, Advisor

Dr. Keith A. Berube, Associate Professor of Mechanical Engineering Technology

Dr. Stephanie Wood, Research Civil Engineer, U.S. Army Engineer Research and Development Center

NON-DESTRUCTIVE EVALUATION OF CONCRETE

USING ELECTRICAL RESISTIVITY AND

ULTRASONIC WAVE PROPAGATION

By Justin Harris

Thesis Advisor: Dr. Eric N. Landis

An Abstract of the Thesis Presented
in Partial Fulfillment of the Requirements for the
Degree of Master of Science
(in Civil Engineering)
August 2022

With the intent to investigate the relationship between concrete physical properties and non-destructive evaluation techniques (NDE), several experiments were performed. Specimens were made at varying geometries using a range of different concrete mixes under several different curing conditions. These specimens were subjected to a combination of electrical resistivity and ultrasonic wave propagation measurements. One part of this study investigated determining the orientation of steel fibers using electrical resistivity. This resulted in the fabrication of a four-probe square device with the potential capabilities of determining fiber orientation. The other part of this research applied ultrasonic wave propagation via through-transmission along with electrical resistivity via the uniaxial method. The results from this uncovered an exponential relationship between the pulse wave velocity and formation factor for saturated specimens. With the formation factor's relationship to strength and microstructural properties, this relationship may lead to predicting strength and pore structure using relationships to a simple ultrasonic property.

DEDICATION

I dedicate this work to my brother, Trace.

ACKNOWLEDGEMENTS

I would like to begin by thanking my advisor, Dr. Eric Landis, for his invaluable guidance over these past few years. My graduate studies here at the University of Maine will be an experience I will never forget.

Next, I would like express my gratitude for the other members of my thesis committee, Dr. Keith Berube from the University of Maine and Dr. Stephanie Wood from the U.S. Army Engineering Research and Development Center, who took the time to review my thesis and act on my examination committee.

I'd like to acknowledge the assistance I received from the other graduate students throughout this project, including Aidan Carlson, Parinaz Belalpour Dastjerdi, JJ Holstein, Alyssa Libby, Amir Haddad Kolour, and Mairead Thistle. From small advice to assistance with specimens themselves, your contributions are greatly appreciated. I'd also like to thank all of the professors I had throughout my undergrad and graduate studies courses.

I would also like to thank all the people whose friendship made my duration here at the University of Maine all the more enjoyable: Stephanie Carito, Trevor Chaput, Lauren Cusson, Sean Decker, Jilleon Farrell, Jens Hansen, Benjamin Homes, Sarah Labbe, Llewellyn Searing, Timothy Simien, and Elliot Stinchfield.

Finally, I'd like to thank my family for their undying and unconditional love, support and encouragement over my time at the University of Maine. My appreciation has no bounds.

TABLE OF CONTENTS

LIST OF FIGURES

CHAPTER 1
INTRODUCTION

Throughout the past two decades, there has been increasingly more interest and resources designated to the non-destructive evaluation of concrete and other cementitious materials. Non-destructive evaluation refers to the assessment of chemical and physical properties of a material that is non-intrusive, that is, it does not affect the state of the material. The ability to analyze materials is vital to the monitoring of existing structures, and holds value in determining where funds should be allocated. While removing pieces of existing structures and performing tests to determine the status of the material is effective, this practice would also cause further deterioration of the structure. Consequently, the problem has been posed: How can concrete be effectively and efficiently monitored and evaluated through non-destructive means? In attempts to create a solution to this question, several non-destructive evaluation techniques have been employed with the intent to estimate the characteristics of concrete. These methods include: ground penetrating radar (GPR), x-ray, infrared tomography, and acoustic emissions amongst others. GPR measures reflected electromagnetic waves, x-ray methods take advantage of the energy absorption of radiation waves, infrared tomography uses heat maps of specimens for evaluation, and acoustic emissions focuses on the emitted waves of a material undergoing stress. Often, the pitfalls of these techniques are the inapplicability in the field, cost effectiveness, or inability to gather the necessary information through a single technique. As a result, this thesis attempts to combine the abilities of two different forms of non-destructive evaluation in order to gather more information on cementitious materials. The first technique, electrical resistivity, has become a popular technique due to the simplicity, relatively low cost, rapid testing, and little to no necessary specimen preparation. The second technique, ultrasonic wave propagation, requires a bit more setup, but can be evaluated at different levels of complexity in order to gather all of the possible information.

The electrical resistivity of concrete describes concrete's capability to withstand the flow of ions when subjected to an electrical field. Resistivity is the inverse of conductivity, both conceptually and analytically, which is concrete's ability to catalyze the flow of ions through its pores (Layssi 2015). Alternatively, electrical resistivity can be depicted as two components: the ionic conductivity of free evaporable water, and conduction through unreacted cement particles and gel-water (Tang, 2016). In recent years, standards have been introduced for resistivity of concrete in the forms of ASTM C1760-12 (withdrawn) and ASTM C1876-19 along with AASHTO TP 95-11 (ASTM 2012, Tang 2016, ASTM 2019). Despite the introduction of standards from ASTM and AASHTO, there is still a gap between knowledge in the field and industry practice. For this thesis, electrical resistivity has been selected as a tool to evaluate concrete due to its nature of application through concrete, having the potential to provide information on transport properties and permeability (Layssi 2015, Tang 2016).

Ultrasonic wave propagation involves recording information on mechanical waves sent through a specimen of interest. The term ultrasonic refers to sending these waves at a frequency higher than the audible limit of humans, which is approximately 20 kHz (Hassefras 2019). For materials that are relatively homogeneous and isotropic, ultrasonic wave propagation can be simple and straightforward, but for materials that are heterogeneous and anisotropic such as concrete, things can become more complicated by the introduction of the various forms of attenuation. Attenuation refers to the loss of energy that occurs in various forms as an acoustic wave is propagated through a material. The interest in ultrasonic wave propagation stems from the interpretation of this energy loss and the information it can theoretically provide on materials and their current state, including damage, flaws, etc. Ultrasonic wave propagation has been chosen as a tool for this thesis due to the potential information it can provide on the microstructural properties of concrete.

The purpose of this thesis is to further answer the question of, can concrete be more effectively assessed in a non-destructive manner by combining the results from multiple non-destructive evaluation techniques? In order to do so, this thesis proposes combining the two aforementioned non-destructive evaluation techniques. This thesis is structured by beginning with a literature review and background on the two non-destructive evaluation techniques. This is followed by a chronological presentation of the four experiments performed in pursuit of an answer to the previously stated hypothesis. After this, a summary and conclusion will be given attesting to the implications of the findings from this thesis.

CHAPTER 2
LITERATURE REVIEW

This chapter will cover the two non-destructive methods utilized during the experiments to be discussed in chapter 3. The background, methodology, and previous research are what gave the inspiration and rationale for these experiments to be conducted.

2.1 Electrical Resistivity

Electrical resistivity of concrete is tool that can be used in various scenarios, including rapid chloride intrusion, setting time, early age characteristics, fiber orientation and compressive strength amongst others (Farooq 2009, Sanish 2013, Azarsa 2017). As previously mentioned, electrical resistivity is a product of the pore solution within concrete. Initially, the pore solution in concrete begins as the water within the mix, but as the water and cement react, ions are released into the solution. Primarily, these ions will consist of calcium (Ca^{2+}), hydroxide (OH^-), potassium (K^+), sodium (Na^+), and sulfate (SO_4^{2-}) (Spragg 2013, Sharisha 2017). The proportion of these ions present in the pore solution is contingent on the cement mix used, the amount of water in the mix, and the extent to which curing has occurred. In general, the hydration of cement in concrete can be broken down into five periods: initial hydrolysis, induction, acceleration, deceleration, and diffusion (Farooq 2009, Landis 2017). Initial hydrolysis (also known as pre-induction) occurs first when calcium (Ca^{2+}) and hydroxide (OH^-) ions from the surface of the cement are introduced into the solution. This period typically lasts tens of minutes and does not form any hydration products, but does setup the solution for reaction products. Following this period is induction, which is characterized by a buildup of calcium and hydroxide ions along with the slow precipitation of semi-crystalline calcium-silicate-hydrate (C-S-H) and low heat release. The heat release during hydration is depicted in Figure 2.1. The third period is acceleration, which is marked by the formation of solid C-S-H and calcium hydroxide (CH). The acceleration period also includes a decrease in porosity and availability of water. Additionally, there is an increase in heat which peaks at the beginning

of the fourth phase, deceleration. Deceleration is defined by a decreased rate of hydration product formation, due to the reduced porosity and availability of water due to the CH and C-S-H formed. Finally, is diffusion, which is a continuation of deceleration, in which there is a slow growth of CH and C-S-H as long as there is existing unreacted concrete and water. Throughout the hydration of concrete, the concentration of calcium and sulfate ions decrease in the solution while the concentration of sodium, potassium, and hydroxide ions increase, which is important pertaining to the electrical conductivity of a concrete solution (Farooq 2009, Landis 2017). As previously mentioned, the difference in these proportions are a result of cement composition, water availability, and level of curing that has occurred. Along with the ion composition in the solution of the concrete, another important factor in the electrical resistivity of concrete is permeability. Permeability is a parameter that encompasses the complex pore structure in cementitious materials. As pores in concrete vary in shape and size, they can be categorized into several different groups: pores located in the hydrated cement paste (capillary pores, gel pores, air voids), pores in aggregates, pores between the interfacial transition zone of the aggregates and cement binder, and internal discontinuous pores cause by temperature and humidity changes. (Tang 2016).

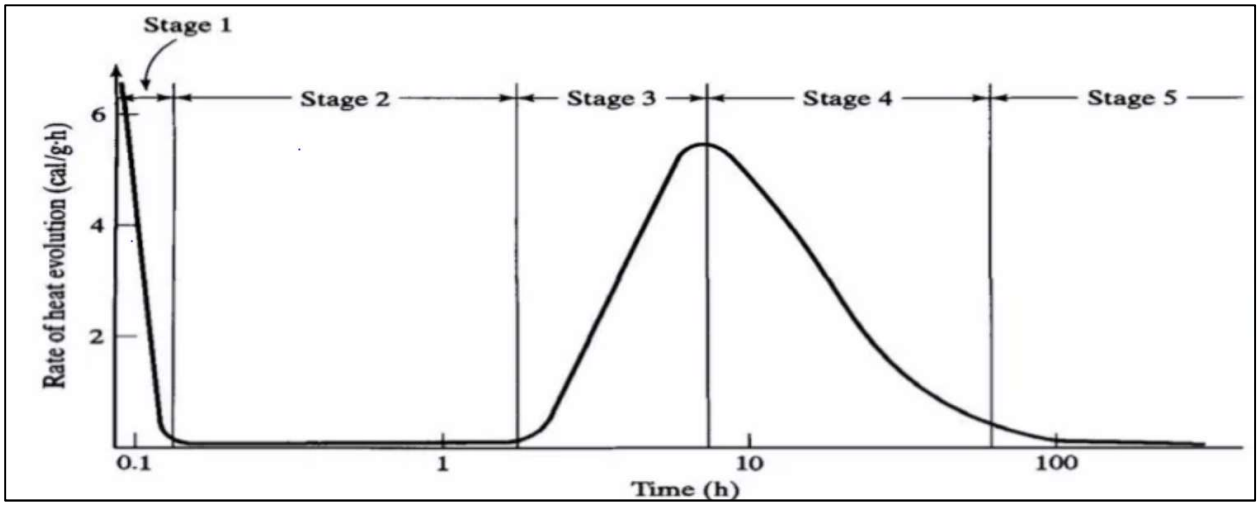

Figure 2.1: Rate of heat evolution during hydration of tricalcium silicate (Landis 2017)

2.1.2 Direct Current vs Alternating Current

Now that electrical resistivity of cementitious materials has been introduced, some background will be presented on electrical resistivity. First, direct current (DC) vs alternating current (AC). Direct current methods are the simpler of the two methods, but have several drawbacks that can make DC methods unsuitable for concrete measurements. In general, direct current methods emit an electrical current from an artificial source in order to create an electrical potential field through the specimen of interest (Seidel 2007). This is often done using electrodes on both sides of the specimen along with another pair of electrodes that measure the electrical potential difference across the specimen. In short, a known voltage is applied and the measured current can be used to determine the resistance using Ohm's Law (Rajabipour 2006).

$$Z = \frac{V}{I}$$

Where Z is the impedance in Ohms, V is voltage in volts, and I is the current in amperes.

The drawbacks of DC methods are the likely culprit for the lack of literature for these methods on concrete. The greatest disadvantage of DC methods is the issue of polarization that is caused by constant DC excitation in concrete specimens. Concrete is a porous material, and depending on the saturation of specimen, may exhibit capacitance properties, that is, it can hold an electric charge. Due to the nature of DC methods, substantial polarization effects can occur on the boundaries between the electrodes and concrete surfaces along with the interface between the pore solution and the solids surrounding the pores (Rajabipour 2005, Layssi 2015, Tang 2016). In total, there are five types of polarization that can occur with DC methods, including: dipole polarization or alignment of electrical dipoles along the direction of the electrical field, atomic polarization or altering the distance between opposite charged atoms, electronic polarization or movement between the electron cloud and nucleus, interfacial polarization or buildup of electrical charge at interfaces, and double layer polarization at an

interface. These forms of polarization are best visualized in Figure 2.2. The other major drawback to direct current methods, is that high voltages (around 60 volts) are often necessary in order to negate noise on readings, which can emit heat generation which could potentially alter the microstructure of the specimen (Rajabipour 2005, ASTM 2019).

Due to the limitations of direct current methods, alternating current methods are recommended for determining properties of concrete. Alternating currents can be applied at lower voltages (in the tens to hundreds of millivolts compared to tens of volts) which minimizes the concern of microstructure alteration due to heat transfer (Rajabipour 2006). Additionally, alternating currents avoid the issue of polarization since the polarization of the electrodes is shifted with the direction of the current, and the electrical properties of the concrete matrix are not influenced (Woo 2004, Solgaard 2012, Layssi 2015, Tang 2016).

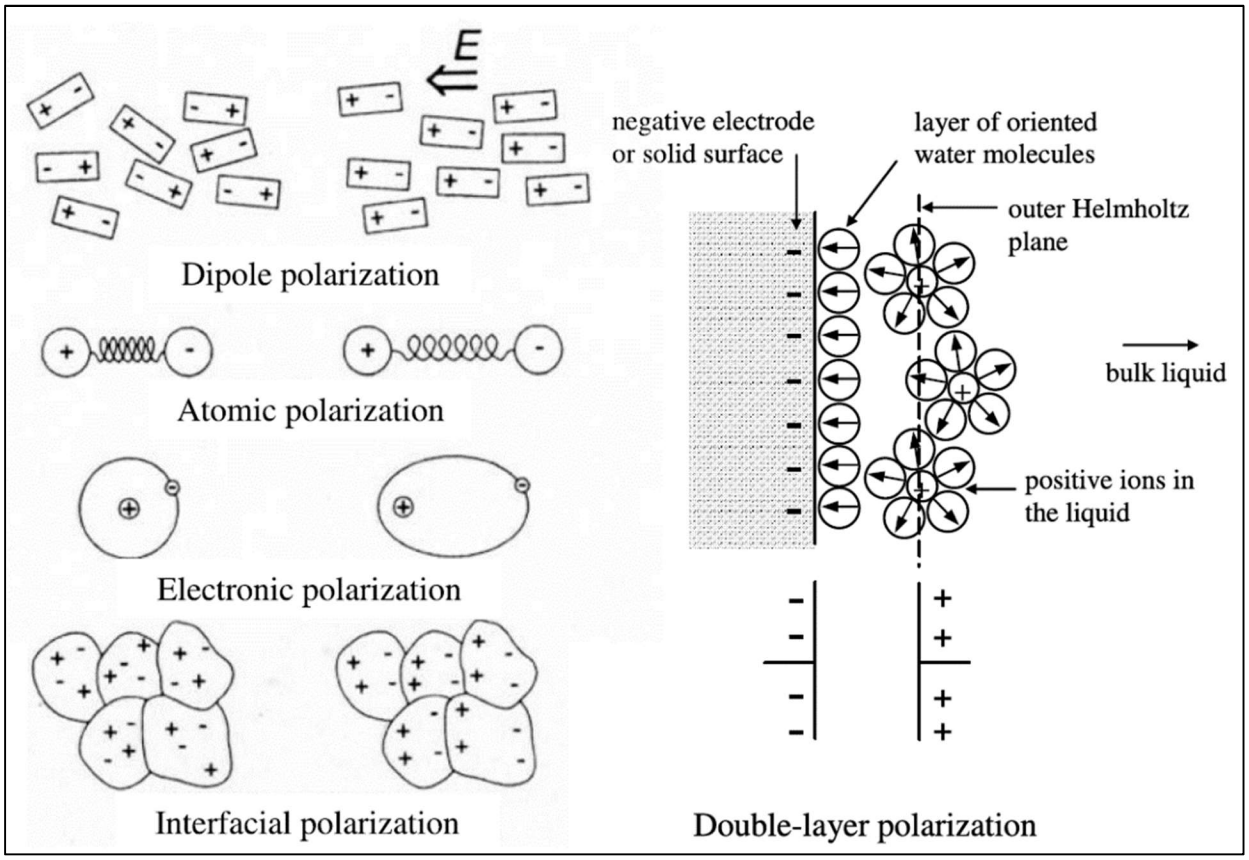

Figure 2.2: Types of polarization that occur due to direct current excitation (Rajabipour 2005)

2.1.3 Electrical Impedance Spectroscopy

For a multi-phase material such as concrete, the electrical properties are an accumulation of the different materials, the volume ratio between the materials, and the formation of the microstructure (Macdonald 1987, Rajabipour 2006). At a single frequency of alternating current, different phases of a material vary in relaxation time, that is, time to equilibrium for each phase is different. Due to this nature of electrical response, a single phase of a material may find resonance and dominate the response at a given frequency (Rajabipour 2006). This knowledge can be utilized by taking measurements across a spectrum of frequencies to gather more information about the microstructure. This method, electrical impedance spectroscopy (EIS), also referred to as alternating current impedance spectroscopy (ACIS), is an alternating current method which works with both the real and imaginary impedances (Rajabipour 2004, Rajabipour 2006, Tang 2016, Hu 2019). This is typically expressed in the form of a Nyquist plot, which has the two impedances on the horizontal and vertical axes, and typically includes two arcs, one corresponding to low frequency (in the mHz-kHz range), and one for high frequency (in the kHz-MHz range) (Rajabipour 2004, Rajabipour 2006). The low frequency arc displays information about the bulk-electrode interface properties, and the high frequency arc displays information regarding the bulk properties of the concrete. Typically, plots will look similar to that depicted in Figure 2.3, and can provide information on properties such as chloride ion permeability, freeze-thaw, creep, fiber dispersion and steel corrosion resistance (Woo 2004, Ravikumar 2013, Zhu 2017, Hu 2019). In terms of equipment, a typical setup for electrical impedance spectroscopy may look similar to those depicted in Figure 2.4.

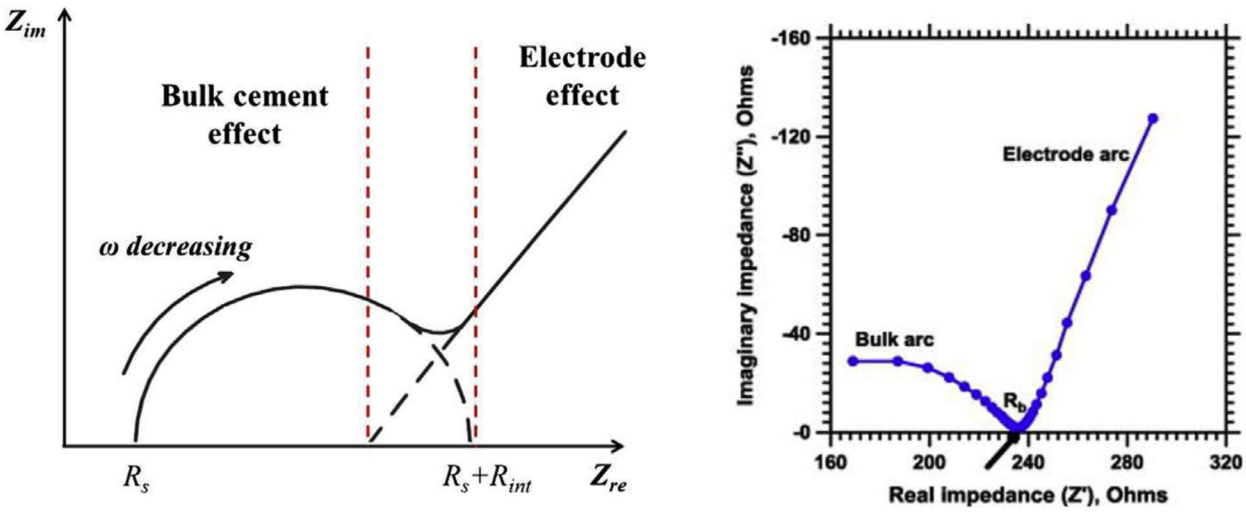

Figure 2.3: The theoretical (left) and measured (right) Nyquist plot from AC impedance spectroscopy (Ravikumar 2013, Zhu 2017).

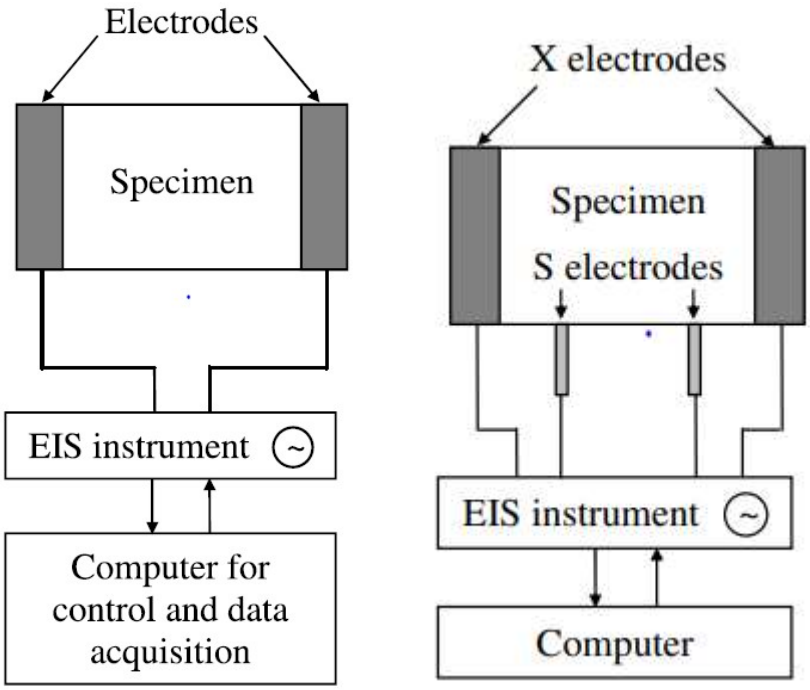

Figure 2.4: Typical EIS equipment setup for two-point (left) and four-point (right) measurements. (Rajabipour 2006)

2.1.4 Further Background on Alternating Current Methods

There are several forms of application for alternating current methods used to determine physical properties of concrete (Layssi 2015, Azarsa 2017). As previously mentioned, the concept of impedance is used for electrical resistivity methods. This property, impedance, is denoted by the term Z, and can represented as a complex number.

$$Z = Z' + jZ''$$

This complex number is split into two properties, the real portion, the resistance Z' or R, and the imaginary portion, the reactance Z'' or X (Layssi 2015). Alternatively, the impedance is often denoted as the absolute value of the impedance, |Z| and a phase angle, ø. By plotting these two terms, the resistance will be on the x-axis and the reactance will be on the y-axis as depicted in Figure 2.5 (Layssi 2015, Shirisha 2019). The resistance is the property of interest here, and can be found through the relation below.

$$R = |Z| \cdot \cos(\emptyset)$$

Often, the phase angle is small, thus when this is true,

$$\cos(\emptyset) \approx 1, \qquad Z \approx R$$

And Ohm's law can be transformed into, (Rajabipour 2006, Layssi 2015, Shirisha 2019)

$$R = \frac{V}{I}$$

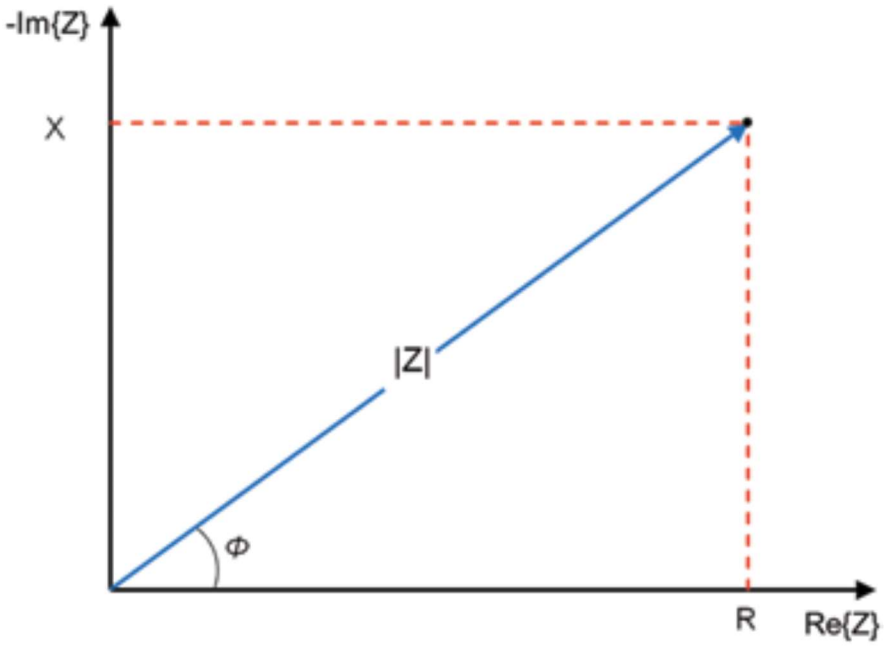

Figure 2.5: Graphical representation of the relationship between Impedance, Resistance, and Reactance (Layssi 2015)

The resistance is a property that is dependent on the geometry of the specimen, thus the term resistivity ρ, is introduced to generalize the electrical properties of a specimen by the following relation:

$$\rho = k \cdot R$$

where k is a geometric constant that is dependent on the geometry of the specimen or the method being used (Rajabipour 2006, Spragg 2013, Layssi 2015, Shirisha 2019). The geometric constant k will be discussed more when introducing applications for alternating current methods in section 2.1.5. The importance of the resistivity term will be revealed shortly; first some microstructural properties must be introduced.

The resistivity, amongst other physical properties, is strongly influenced by two microstructural parameters, the connectivity and porosity. Connectivity is a value that portrays the interconnectedness of the pores within a pore system, while the porosity represents the ratio of pore volume to the volume

of the entire specimen (Spragg 2013, Shirisha 2019). Both parameters are independent of the specimen geometry, but due to the confusion caused by the similarities between the two, they are also combined by taking the multiplicative inverse of their product, which is denoted as the formation factor (Weiss 2013, Layssi 2015, Shirisha 2019). This relation is shown in the equation below.

$$F = \frac{1}{\beta \Phi}$$

Where *F* is the formation factor, ϕ is the porosity, and β is the connectivity.

The formation factor is included in the Nernst-Einstein relationship, which relates diffusion constants and the resistivity values of the specimen and the pore solution of the specimen. This relationship goes as follows:

$$\frac{D_o}{D} = F = \frac{\rho}{\rho_o}$$

Where ρ is the effective or total electrical resistivity, ρ_o is the resistivity of the pore solution, D_o is the self-diffusion coefficient which describes how different ions make their way through dilute solutions, and *D* is the bulk diffusion coefficient (Weiss 2013, Layssi 2015, Shirisha 2018). Several studies have been performed showing that the formation factor is strongly correlated with microstructural properties, hence the interest in this value (Spragg 2013, Sallehi 2018, Weiss 2018). Figure 2.6 gives a visual depiction of the pore resistivity, porosity, and connectivity.

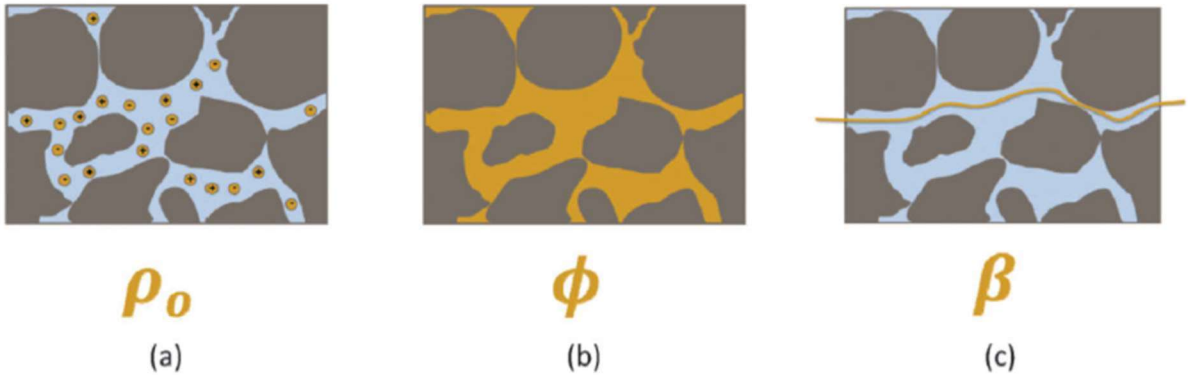

Figure 2.6: Microstructure parameters (a) pore solution resistivity (b) porosity and (c) connectivity (Spragg 2013)

Another potential value of interest for resistivity measurements, is the determination of the tortuosity. The tortuosity term refers to the ratio of the length between the two probes being used, or length of the specimen, and the distance traveled through the specimen to get from one end to the other. This ratio can be represented by the equation below and this term is depicted in figure 2.7 (Shirisha 2019).

$$\Lambda = \frac{L}{L_e}$$

Where Λ is the tortuosity, L is the length of the specimen, and L_e is the effective length, or length of the path traveled from one end of the specimen to the other.

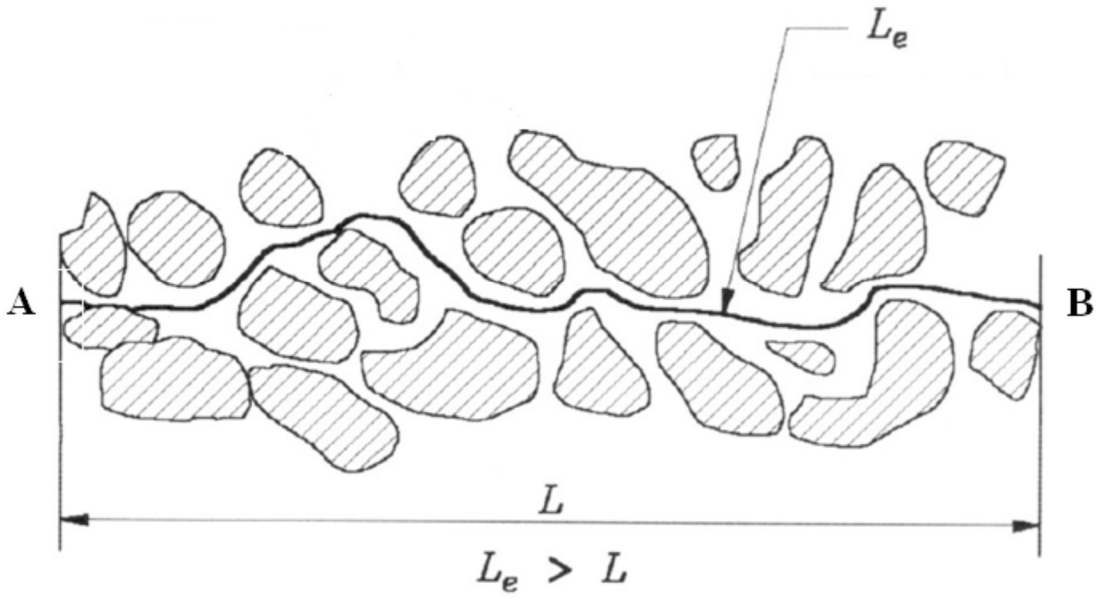

Figure 2.7: Depiction of effective length L_e, vs the length of the specimen L (Sharisha 2019)

Often, in order to relate the tortuosity to the formation factor, another term, the tortuosity factor, is introduced, which can be determined by the equation below (Sharisha 2019).

$$T_m = (\frac{L_e}{L})^2$$

Where T_m is the tortuosity factor. The tortuosity factor can then be related to formation factor as follows:

$$T_m = \emptyset \cdot F$$

To this point in time, there is no known technique or measurement method that can estimate this factor, hence the introduction of this relation. Another form of tortuosity is the geometric tortuosity factor, which is simply the square of tortuosity,

$$\tau_m = \Lambda^2$$

This value is used in relation to the formation factor as follows:

$$F = \frac{\tau_m}{\Phi_p \delta}$$

and

$$\Phi_p = \Phi_{cap} + \Phi_{gel}$$

where Φ_p is the total porosity, Φ_{cap} is the capillary porosity, Φ_{gel} is the porosity of the C-S-H gel pores, and δ is constrictivity (Sharisha 2019). The constrictivity is a parameter that characterizes the bottlenecking of the continuous pore system within a material, which is visually depicted in Figure 2.8. This parameter can be calculated by solving the below for constrictivity.

$$\delta = \frac{\tau_m}{\Phi_p \cdot F}$$

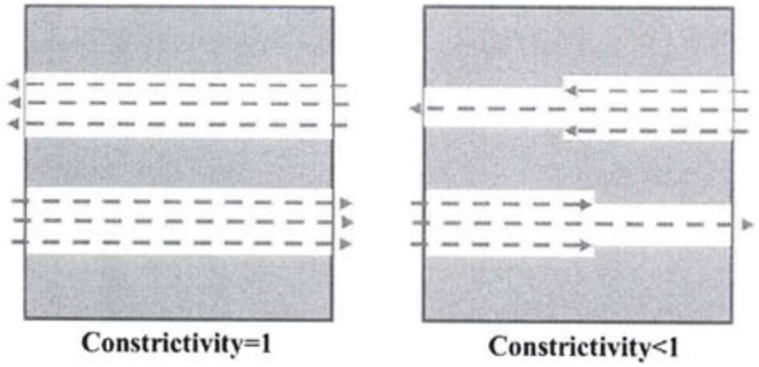

Figure 2.8: Visual representation of constrictivity (Sharisha 2019)

2.1.5 Alternating Current Methods

There are two primary AC methods used to determine physical properties of concrete, both depicted in Figure 2.9. The first of which is the uniaxial method. The uniaxial method, or bulk electric resistivity test, is the simplest of the options. This method is performed by placing two parallel metal plates with sponges on opposite sides of a concrete specimen. The sponges are used to create a proper electrical connection. An alternating current is then run through the concrete specimen and the change in potential is taken. The frequency range for this method is 0.1 kHz to 10 kHz. For this method, the geometric factor k is determined as

$$k = \frac{A}{L}$$

where *A* is the cross-sectional area of the specimen, and *L* is the length of the specimen. This method is often used for measuring chloride intrusion in concrete. The benefits of this method are that the method is very fast and simple. The downfalls of this method are that information can only be gathered on an existing structure if there are specimens poured from the same mix, or a chunk of the structure is taken out to make measurements on, which would make the test no longer a non-destructive evaluation. If specimens are poured from the same mix as the existing structure, they likely will not have endured the same environmental effects, which may alter the response (Rajabipour 2006, Spragg 2013, Layssi 2015, Azarsa 2017, Sharisha 2019).

The second method is the four-point method. In the four-point method, or Wenner probe method, the apparatus aligns four equally spaced probes in an array. An alternating current is applied by the two outside probes while the two inside probes measure the potential, with acceptable frequencies ranging from 0.01 to 10 kHz. The geometric factor k is determined as

$$k = \gamma a$$

Where γ is 2π for most geometries and a is the spacing between probes (Rajabipour 2006, Spragg 2013, Layssi 2015, Azarsa 2017, Sharisha 2019).

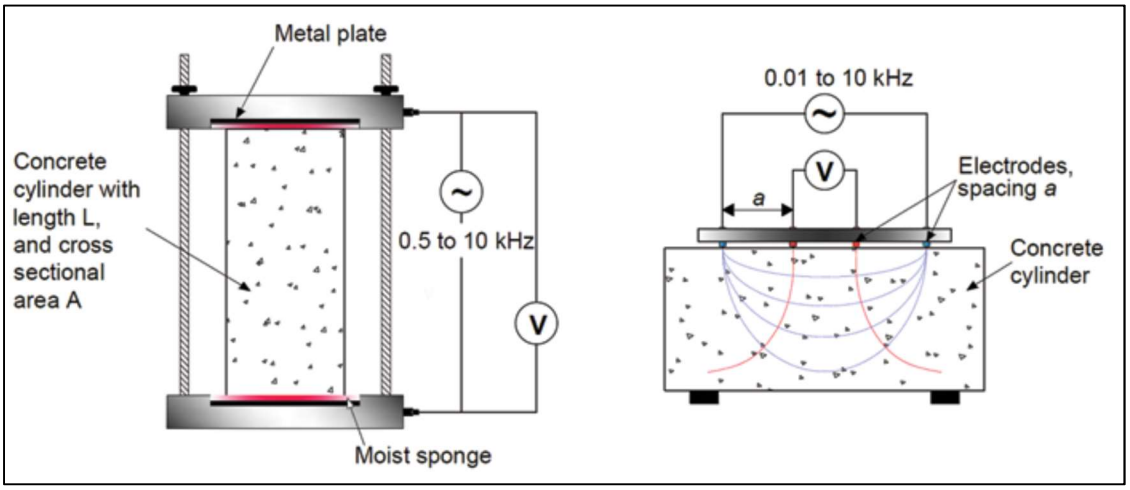

Figure 2.9: Electrical resistivity techniques: (a) uniaxial method; and (b) four-point (Wenner probe) method (Layssi 2015)

It should be noted that the depth of penetration for this is typically considered to be about half of the distance between the probes. The benefit of this method includes the ability to take measurements on any specimen given the specimen dimensions exceed that of the distance between the outside probes. The potential downside to this method is that several readings may be needed to get an accurate estimate of the total resistivity of a specimen since this method takes measurements within a local area (Rajabipour 2006, Lataste 2008, Spragg 2013, Layssi 2015, Azarsa 2017, Sharisha 2019).

An emerging technique is one that is used in determining the orientation of steel fibers within concrete. The interest in determining fiber orientation in concrete is that the distribution and orientation of these fibers are known to have considerable impact on the mechanical properties of the material as a whole (Lataste 2008, Barnett 2009, Solgaard 2013, Martinie 2013). Lataste et al. propose determining a high or low resistivity axis (Lataste 2008). Since the conductivity of steel is several magnitudes higher than that of concrete, this axis represents the line of lowest or highest orientation of fibers, as the presence of fibers along an axis will significantly reduce the measured resistivity (Lataste 2008, Barnett 2009). It should be noted that the low resistivity axis represents the axis with a high alignment of fibers, and the high resistivity axis represents the axis with a low alignment of fibers, since metals are very conductive relative to concrete, and resistivity is the inverse of conductivity. This axis is determined by using a modified four-point method, with the probes oriented in a square formation, and rotating the center of the probe at angle increments, as depicted in Figure 2.10. In doing so, the resistivity can be determined at each point, and the magnitude of the measurement at each angle will represent how much fibers are aligned along the axis that is being measured (Lataste 2003, Lataste 2008, Barnett 2009, Martinie 2013). Using the following relationship, the anisotropy can be found for a given area on a specimen:

$$\log(A_n) = \log({}^{\rho_i}/_{\rho_j})$$

where ρ_i and ρ_j are the resistivity in perpendicular directions. The value of A_n expresses the anisotropy of the fibers, with a value of 0 representing complete isotropy

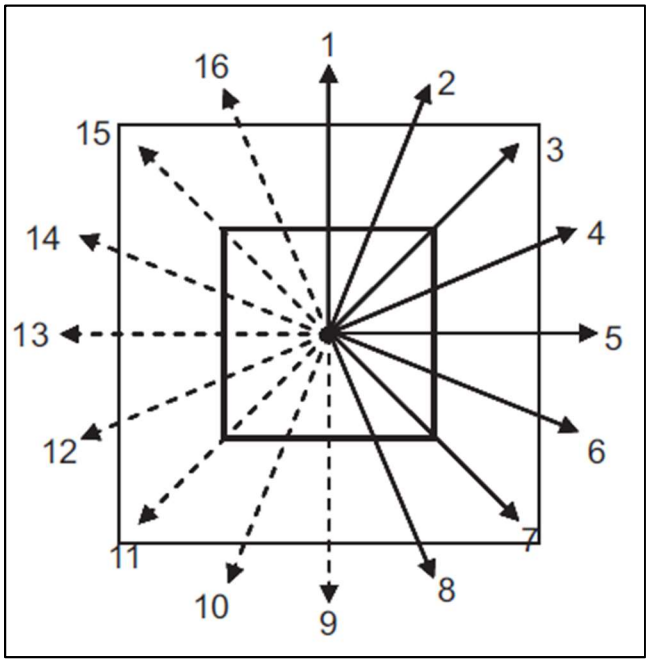

Figure 2.10: Rotation method for fiber orientation determination (Lataste 2008)

2.1.6 Factors Affecting Measurements

There are several variables that are important to consider and control when taking electrical resistivity measurements. The first variable to consider is temperature. Changes in temperature can alter the ion mobility within a specimen, and as the temperature increases, the measured resistivity will decrease (Polder 2001, Rajabipour 2006, Spragg 2013, Solgaard 2013, Azarsa 2017). As previously mentioned, resistivity is a measurement of the ability of a material to withstand the flow of ions, so temperature's ability to alter ion mobility will have a great effect on resistivity measurements. In general, a change in a single degree Celsius, will alter the measured resistance by 3% in wet specimens and 5% in dry specimens (Polder 2001, Layssi 2015, Azarsa 2017). A visual representation of the effect of temperature on measurements can be seen in Figure 2.11. This figure shows that about a 30°C change in testing temperature can double the electrical resistivity.

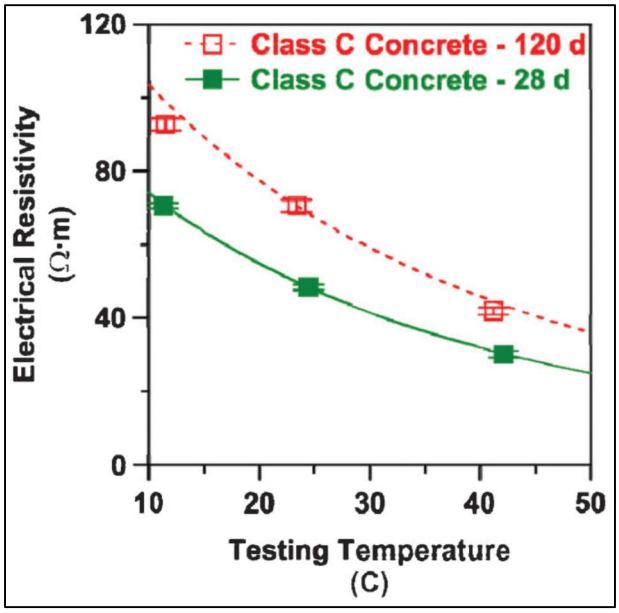

Figure 2.11: Influence of specimen temperature on measured resistivity (Spragg 2013)

Another important variable to consider is moisture content of the degree of saturation. The amount of moisture within concrete will determine the availability of fluid within the pore network of a specimen. This allows for increased ion mobility, and thus an increase in the degree of saturation will result in a decrease in resistivity. Based on a study by Larsen et al, a change in moisture content by 11% can triple the measured resistivity, and a 22% change can increase the measured resistivity six fold (Larsen 2006, Azarsa 2017). Due to the sensitivity of this variable, Weiss has introduced the concept of including a saturation factor defined by Archie's law. This relationship is typically expressed by the following:

$$f(S) = S^m$$

where S is the saturation and m is archie's constant, which typically ranges between 3 and 5 for concrete, and is determined experimentally (Weiss 2013). This saturation factor ranges from 0 to 1, with 1 being at full saturation. This relationship is then used to normalize measured values of resistivity for moisture by the relationship:

$$F = \frac{\rho}{\rho_o} f(S)$$

Another variable that affects resistivity measurements is one that has been briefly discussed, specimen geometry. As shown in section 2.1.5, the geometric constant k is dependent on the testing method and also dependent on the geometry of the specimen. For the four probe method, the geometric constant was given as 2π multiplied by the spacing of the probes. This is not entirely accurate for all geometries. A study by Morris et. Al. (1996) introduced a cell constant that should be introduced for uncommon cylinder dimensions, slightly altering the geometric coefficient. This cell constant is incorporated as follows:

$$\rho_{adj} = \frac{\rho_{disp}}{K}$$

Where ρ_{adj} is the resistivity adjusted for the specimen dimensions, ρ_{disp} is the calculated resistivity, or resistivity displayed by industrial equipment, and K is the cell constant that adjusts display resistivity. The values of K can be seen in the plots of figure 2.12.

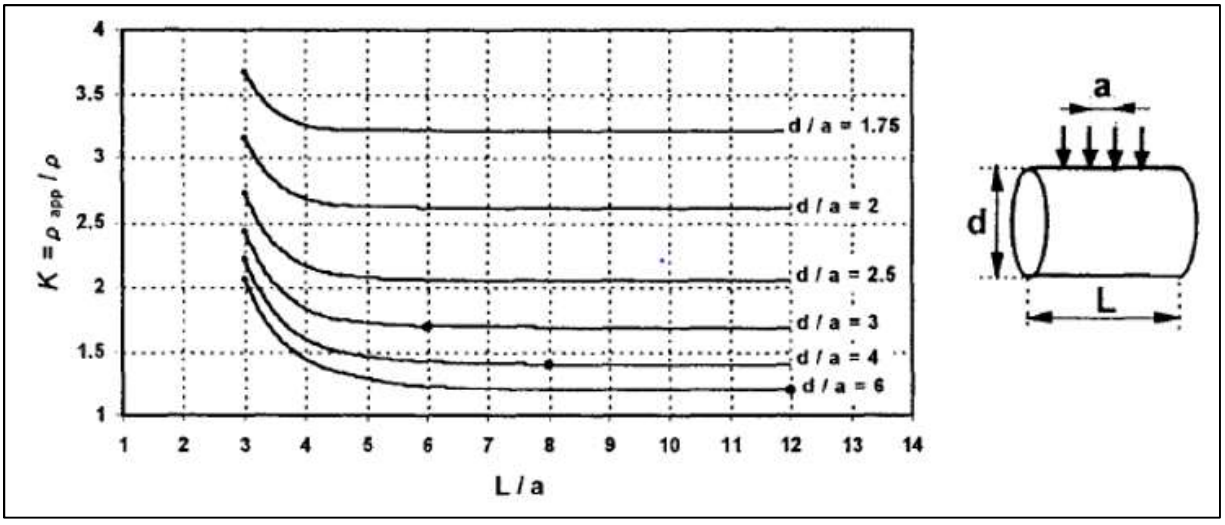

Figure 2.12: Values of cell constant *K* for adjusted resistivity (Morris 1996)

2.1.7 Past Attempts to Isolate Variables

In this study, the use of a multi method system will be implemented with the intent to gather more information by correlating the two methods applied to the same sets of specimens. Studies in the past have attempted to isolate variables in order to make predictions on the characteristics of concrete, dating back to the 1920s when electrical resistivity was used to estimate the setting time of cement paste (Shimizu 1928). These studies have had varying levels of success, which is what gives credence to the attempt to do so here, but with the application of the multi-method system concept, which may open the door to gathering more information on concrete while exhausting less resources than what would otherwise be required.

There are already existing standards for using electrical resistivity to estimate rapid chloride intrusion in concrete using the bulk resistivity method (ASTM 2019). Weiss investigated the relationship between the formation factor and the rapid chloride penetration test, proposing that formation factor replace the test due to mathematical equivalence (Weiss 2016, Weiss 2018). Weiss also estimated the time before repairs due to corrosion to concrete based on the formation factor of the concrete (Weiss 2017, Weiss 2018).

Many studies have investigated the development of electrical resistivity and conductivity as concrete and cementitious materials age (Hansson 1983, Li 2007, Sant 2010, Weiss 2013, Sanish 2013, Sharisha 2017). These studies found a steep increase in resistivity initially, which then plateaus similar to the compressive strength of concrete as age of concrete increases.

Other studies investigated the relationship between resistivity and porosity. Sanish et al. estimated the early age porosity of cement-based materials using electrical conductivity via Archie's Law, Generalized Effective Media and the Bruggeman-Hanay Model (Sanish 2013). Zaccardi et al. and

Sant el al. investigated the relationship between porosity and resistivity values (Sant 2010, Zaccardi 2014).

Sallehi et al. summarized the past attempts to predict the formation factor using porosity, Maxwell proposed a relationship between these two values in 1904 as:

$$F = \frac{3 - \phi}{2\phi}$$

Slawinski proposed a relationship for solid soil particles in 1926 as:

$$F = \frac{(1.3219 - 0.3219\phi)^2}{\phi}$$

Archie's law was applied for this relationship in 1942 as:

$$F = \phi^{-m}$$

Where m is Archie's constant and typically ranges between 3 and 5 for cementitious materials. This equation was then modified by Atkins and Smith to include a coefficient representing the geometric tortuosity of porous materials as

$$F = A\phi^{-m}$$

where A is the geometric tortuosity coefficient (Maxwell 1904, Slawinski 1926, Archie 1942, Atkins 1961, Sallehi 2018).

Another variable that has been investigated in regards to resistivity is moisture. Weiss et. al. (2013) introduced the saturation function as previously mentioned. Henkenseifken et. al. (2009) compared the electrical resistivity of cement mortar to water-cement ratio, which found that the

greatest change in resistivity occurred at the lowest water-cement ratio and the change is resistivity is relatively small at greater water-cement ratios (Spragg 2013).

Overall, all these studies are what garner the confidence to isolate variables in this thesis.

2.2 Ultrasonic Wave Propagation

Ultrasonic wave propagation is a non-intrusive, non-destructive evaluation technique that has been applied to a variety of materials since the 1900's. Early on, some of the greatest successes of ultrasonic wave propagation resided in metals. Studies such as Bratina et al. (1962) and Joshi et al. (1972) assessed the damage to metal that had undergone fatigue damage by measuring the attenuation of longitudinal waves. Attenuation is a characteristic of a material that refers to the energy loss by an ultrasonic wave when the wave is sent through it. This will be discussed more in depth later in this chapter. In such studies, the most abundant mechanisms of degradation were in the form of micro cracks and non-linear deformation, which concrete structures experience as well. Additionally, more success using attenuation was found, in the manner of determining the pore size distribution of polycrystalline materials in some metals (Papadakis 1968). Theoretical background on determining flaws in metals through the use of ultrasonic wave propagation can be found through many studies such as the one performed by Roney (1950). For general background on ultrasonic wave propagation in solids, the reader is referred to the reading by Kolsky (1963). Further studies of ultrasonic wave propagation have been performed to the likes of measuring the multiple scattering of linear waves in composite materials which allowed for the determination of fiber interaction and average strain (Yang 1994).

2.2.1 Ultrasonic Wave Propagation in Concrete

In comparison to the early success of ultrasonics in metals, advances in the evaluation of concrete through ultrasonics methods have been much fewer. This lack of success stems from the challenge of defining microstructural properties for a material with its components randomly scattered throughout. On a large scale, in the range of meters, concrete can be considered homogeneous, but on the microscopic scale, the range of air voids, aggregates, and reaction products within the cement matrix can make characterization a troubling task. The length scale of different materials within cementitious mixtures are depicted in figure 2.13.

Many studies have attempted to define physical and microstructural properties of concrete through the means of ultrasonic measurements. To begin, an understanding of the effect of each of the particles within concrete, in addition to the cracks of varying sizes and abnormalities, along with their interactions, are vital to the utilization of these techniques. Some older studies have attempted to analyze concrete using ultrasonic attenuation and dispersion. Suaris et al. (1985) performed compression tests on concrete specimens with a ring attached to hold a transducer around the circumference of a concrete cylinder. The results of this study found a significant change in the amplitude of waveforms and a miniscule change in ultrasonic wave velocity. This demonstrated the potential for using ultrasonic attenuation to measure damage in concrete specimens that are undergoing cyclic loading cycles. Landis et al. studied the effect of aggregates on the scattering of longitudinal waves.

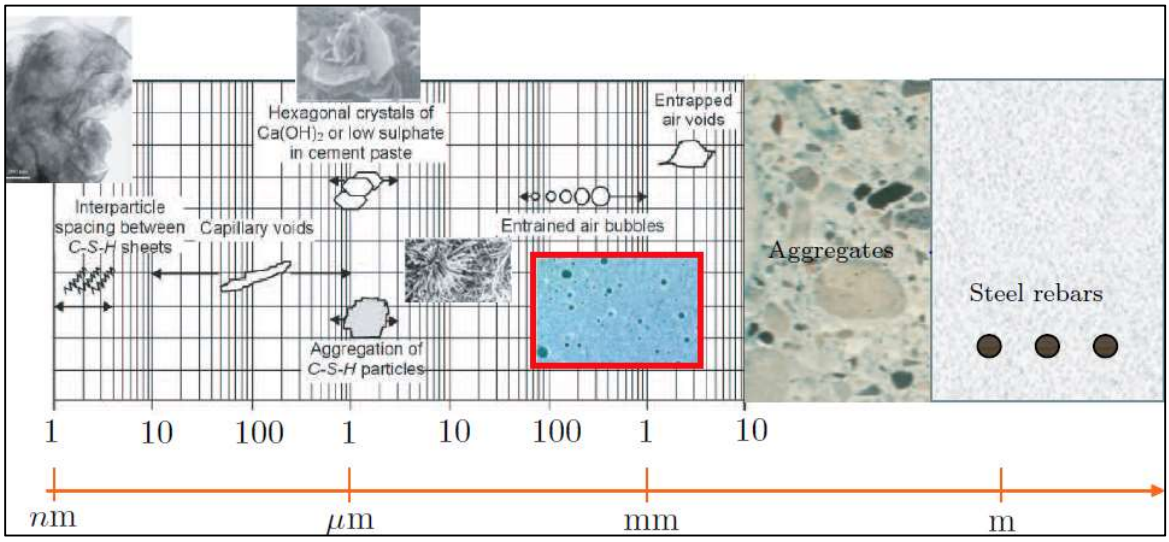

Figure 2.13: Length Scale of Substances within Cementitious Materials (Punarai 2006)

This research found a link between the characteristics of attenuation and the inhomogeneity of the concrete (Landis 1995). More recent studies have continued the trend of attempting to determine the relationship between characteristics of attenuation, and microstructural properties of materials, such as strength and porosity. Abdullah and Sichani performed a study on the relationship of attenuation

coefficients and different properties of cement and plaster. The results of this study found that varying types of cement and water cement ratios affected the values of attenuation (Abdullah 2009).

Popovics et al. performed a test using one sided measurements to measure the velocity of longitudinal waves and Raleigh waves, which found that one sided methods could find comparable results to that of through transmission methods (Popovics 1998). Yamen et al. compared the differences between the direct and indirect methods in finding ultrasonic pulse velocity. In doing so, this study found that the error between the two methods for determining the ultrasonic pulse velocity was about 2% (Yaman 2001). The conclusion from this is that the two methods can be interchangeable for such purposes, and the decision regarding which method to use should be based on other factors. Kewalramani et al. introduced artificial neural networks for analysis of ultrasonic data in concrete. This study investigated the relationship between the compressive strength of concrete and ultrasonic pulse velocity. This study found that the ultrasonic pulse velocity could predict the strength of concrete with an error of less than 25% for most values (Kewalramani 2006). Aggelis et al. combined ultrasonic pulse velocity with acoustic emissions. The acoustic emissions method is one that utilizes sound waves to determine cracks and other flaws. This study found that the combination of the two worked very well in conjunction. The ultrasonic pulse velocity was effective in finding existing cracks within specimens, while acoustic emissions was useful for finding the smaller, more active cracks during loading (Aggelis 2009). Laskar et al. performed a study on the effect of flaws on ultrasonic pulse velocity. This study found that ultrasonic pulse velocity was significantly affected by flaws. This being said, the effect of flaws a depth of 300 mm from the surface had negligible effects (Laskar 2020). Gebretsadik et al. (2021) studied the effect of steel fibers on ultrasonic pulse velocity. This study found that the ultrasonic pulse velocity increased up to a fiber content of 2%, and then would decrease thereafter. All of these studies are relevant to this thesis as this thesis will also focus on the ultrasonic pulse velocity as one of the characteristic values from ultrasonic measurements.

Shah et al. (2000) studied the effect of strength on ultrasonic measurements. In this study, it was found that signal transmission is much more sensitive to changes in strength, while pulse velocity was changed much less. The study finds that a 25% reduction in the Young's modulus results in only a 3% change in ultrasonic pulse velocity, while the signal transmission was affected by 31%, and as this reduction continues, so does the disparity. This study also assessed the effects of microcracks on these values. Isleyici (2005) studied the effect of surface roughness on ultrasonic measurements. This study found that as the surface roughness increased, the transmitted sound pressure decreased. This was an expected outcome due to the energy loss of scattering. This study also found that lower frequency transducers were less affected by the surface roughness compared to higher frequency transducer. Along with this, the conclusions of this research suggest utilizing at least two different measurement frequencies in order to correct for the error caused by surface roughness. Aggelis et al. (2007) performed a study with the intent of evaluating the effectiveness of large crack maintenance on bridges. This was done by evaluating the transit time of Raleigh wave and longitudinal waves before and after the crack was filled with epoxy or any other fill. This study found a significant reduction in transit time for the two waves after the fill was placed, indicating that the entire void was filled and effective. Zamen (2000) analyzed crack growth using fractal analysis of ultrasonic waves as a means of damage assessment. This study analyzed data in phase-space rather than the frequency domain, which prevented the loss of data by working in the frequency domain. Lootens et al. (2020) utilized the reflection method for measuring the strength of concrete over time during quasi static compression tests. This study took advantage of the ultrasonic equipment's ability to constantly measure with proper setup. The conclusion of this study was that the reflection method is viable for normal concrete, but further study would have to be done to determine the efficacy of this method for high performance concrete. Alnuaimi et al. (2021) also monitored concrete, but monitored the curing of concrete, using linear and nonlinear methods. This study found that both linear and nonlinear methods are viable

methods for monitoring the curing of concrete. All of these studies are important to this thesis, from considering the effect of strength on ultrasonic measurements, to effects of surface roughness, and monitoring of concrete using ultrasonic measurements.

Many studies have investigated the ultrasonic spectral energy density and the ability to fit this curve to coefficients of attenuation. Weaver (1998) studied the spectral energy density in aluminum foam. This study concluded that values were reasonable given the limited knowledge of the theoretical background at the time. Since then, Anugonda (2001) studied scattering in concrete, Becker et al. (2003) introduced glass bead aggregates to further influence scattering, Punurai et al. (2007) studied the diffuse ultrasound, and Deroo et al. (2009) studied diffuse ultrasound for damage assessment. All the aforementioned research serve as the basis for the two studies that this thesis mimics most for the ultrasonic testing. These studies, Hassefras, (2019) and Landis et al, (2020) compare diffuse ultrasound and X-ray CT. The principles of ultrasound used in these studies are laid out in the next section.

2.2.2 Principles of Ultrasonic Testing

Ultrasonic testing using mechanical waves, juxtapose to the electromagnetic waves that X-ray techniques utilize (Krautkramer 1968). These waves consist of oscillations of discrete particles that propagate along a direction. These waves are governed by three equations of motions in isotropic elastic solids, one for each of the three principle axes. These three equations can be manipulated to produce the wave equation, which is the equation shown below (Kolsky 1963).

$$\rho \frac{\partial^2 \Delta}{\partial t^2} = (\lambda + 2\mu)\nabla^2 \Delta$$

Where ρ is the material density, Δ is the dilatation, or sum of the strains along each axis, λ is Lame's constant, μ is the rigidity modulus, and ∇^2 is the Laplacian operation. Through this equation, it is found

for extended elastic mediums that for waves with no rotation, the waves will travel with velocity c_1, and waves with no dilatation travel at velocity c_2 as defined by the equations below (Kolsky 1963).

$$c_1 = [\frac{\lambda + 2\mu}{\rho}]^{\frac{1}{2}}$$

$$c_2 = (\mu/\rho)^{\frac{1}{2}}$$

The first type of wave is known as a irrotational wave, more commonly known as a dilatation wave, or a P-wave. The second type of wave is known as a equivoluminal wave, more commonly known as a distortion or S-wave. These two types of waves are the only two types of wave to exist for isotropic solids that are unbounded. For the case of mediums bounded on a surface, Raleigh waves may propagate. Raleigh wave effects decrease significantly with depth, and have the characteristics of propagating at a notably lower velocity (Kolsky 1963). There are two primary forms of propagation in waves. The first is longitudinal waves, which oscillate the same direction as the direction of propagation. The second type of propagation include transverse waves or shear waves, which oscillate perpendicular to the direction of propagation, as depicted in figure 2.14.

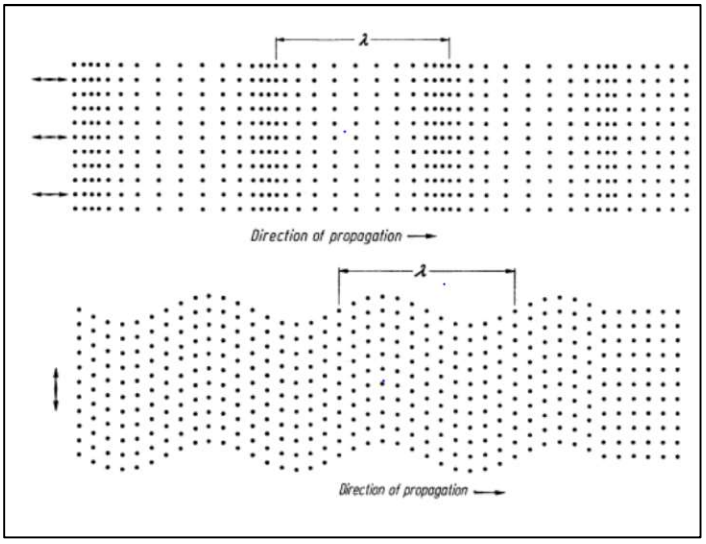

Figure 2.14: Depiction of longitudinal wave (top) and shear wave (bottom) (Krautkramer 1968)

Knowledge of the different types of waves are important to understanding the causes of energy loss in mediums such as concrete. The law of refraction is an important concept to understand for scattering within heterogeneous materials. When a wave meets an interface, it meets at an angle of incidence, often transcribed as α_e. This event results in a reflected wave and a refracted or transmitted wave. The angle at which these waves travel relative to the boundary are governed by the general law of refraction as shown below. Further explanation of this concept is depicted in Figure 2.15.

$$\frac{\sin \alpha_I}{\sin \alpha_{II}} = \frac{c_I}{c_{II}}$$

Where I and II denote the two waves involved in either a reflection or refraction scenario, α correspond to the angle of incidence, reflection, or refraction, and *c* is the acoustic velocity (Kolsky 1962, Krautkramer 1968). Often, both reflection and refraction will occur in these situations, with the exception of these circumstances occurring at critical angles, although critical angles are not germane to this thesis as they are a special case of the law of refraction.

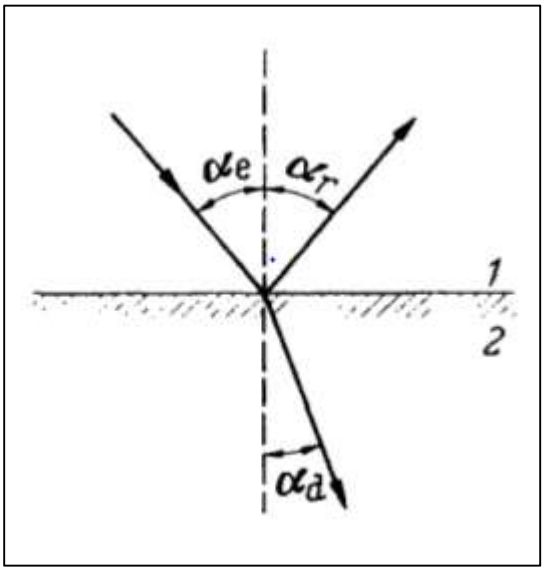

Figure 2.15: Depiction of the law of refraction (Krautkramer 1968)

2.2.3 Attenuation

As previously mentioned, attenuation is a measurement of energy loss for mechanical waves, or the decay rate of the total energy as a wave propagates through a material. Attenuation is often caused by inhomogeneity within a medium, thus for a material such as concrete, attenuation can be important to a higher level of understanding of concrete microstructure using ultrasonic measurements. Thus, research such as this study attempt to further understand the relationship between these characteristics of attenuation and microstructural properties of concrete. In general, attenuation can be categorized into two separate classes, intrinsic attenuation, and extrinsic attenuation.

The most prominent form of extrinsic attenuation is beamspreading. Beamspreading refers to phenomenon that occurs in transducers of finite size. Transducers emit a wave field when activated, and depending on the ratio of the diameter of the transducer to the wavelength of the mechanical waves being propagated, a radiation pattern may cause a strongly divergent wave field. The approximate pressure wave in a wave field at point x is defined by the relation below.

$$p(x) = p_o \cdot \frac{\pi d^2}{4 \cdot x \cdot \lambda}$$

Where p_o is the initial pressure produced by the transducer. This equation shows that increasing the diameter to wavelength ratio results in a higher pressure. The equation below represents the pressure wave reduction due to beamspreading (Punurai 2006):

$$p(x) = 2p_o \cdot \sin(\pi \frac{d}{\lambda} \sqrt{0.25 + \left(\frac{x}{d}\right)^2} - \frac{x}{d})$$

where d is the diameter. As shown in this equation, the diameter to wavelength ratio greatly affects the pressure reduction due to beamspreading (Punurai 2006). This equation can be better understood using Figure 2.16 which depicts how the divergence of the wave field are dependent on the relationship

between the diameter and wavelength. As shown in this figure, there is a significant reduction in the divergence of the beam by tripling the diameter to wavelength ratio (Punurai 2006). This all being said, the extrinsic attenuation is independent of the material and its properties, making it of less significance for this study.

For intrinsic attenuation, there are two primary mechanisms in play, absorption and scattering. Absorption characterizes dissipation of energy in mechanical waves. For linear elastic materials, the energy that would be dissipated can be stored without loss, as the material is elastic. This being said, concrete is often categorized as a viscoelastic material due to its varying phases.

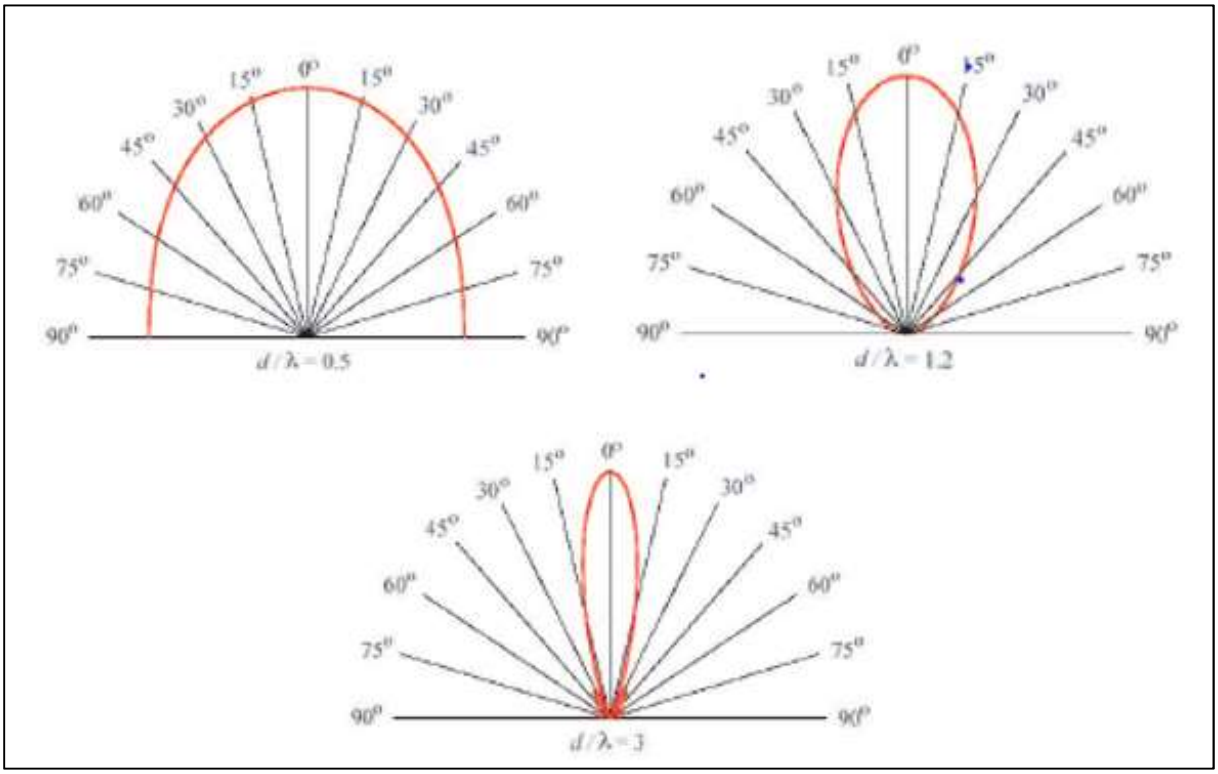

Figure 2.16: Effect of beamspreading based on diameter to wavelength ratio

As a result, the relationship between stress and strain become dependent on time, causing the hysteresis effect (Punurai 2006). In short, the strain is not able to keep up with the alteration in stress throughout the specimen, which causes friction between the strain regions. This friction creates temperature gradients, and such energy attributing to temperature gradients results in permanent energy loss.

Scattering is an effect that occurs at boundaries between materials of differing elastic properties, and refers to the dispersion of ultrasonic waves within a medium. This form of attenuation is important in concrete, due to the distributed phases throughout the material (aggregates, cement, water, voids, etc.). Scattering can present itself at any inhomogeneity within a medium, and for low spatial densities, the loss due to a single scatter event is independent of that of others. The loss due to a single scatter event can be quantified by what is known as the single scattering theory (Roth 1993, Punurai 2006). Thus, the effect produced from single scattering events is the summation of the individual single scattering events. Although, waves may experience multiple scattering events, especially in a medium such as concrete, which introduces the multiple scattering effect, making the evaluation of scattering significantly more complicated (Punurai 2006, Hassefras 2019). For these theories, scattering is assumed to be isotropic, meaning the waves scatter equally in every direction, rather than anisotropic. The difference between these two are depicted in Figure 2.17.

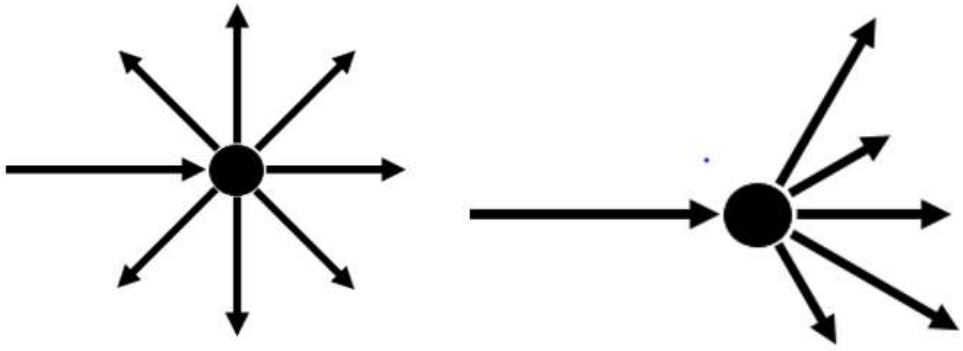

Figure 2.17: Isotropic scattering (left) and anisotropic scattering (right)

2.2.4 Ultrasonic Testing Methods

There are three primary testing methods for ultrasonic wave propagation. While there are other less common test methods such as noncontact methods (Ongpeng 2018) and wave reflection method (Lootens 2020), this section will go over the more prominent testing methods: direct transmission, indirect transmission, and semi-direct transmission method (Laskar 2020). All three methods utilize two transducers in a pitch-catch arrangement as shown in Figure 2.18.

The direct transmission method aligns the ends of the two transducers on parallel sides of the specimen. This method sends the ultrasonic waves directly from the transmitting transducer to the receiving transducer. The indirect transmission method applies the transmitting and receiving transducers to the same side of the specimen, which is useful in the field when only one side of the specimen is available. The indirect method can also be applied by angling the transmitting transducer. The semi-direct transmission method involves setting up the two transducers on adjacent sides of the specimen. For all three methods, the length defined as L for the ultrasonic pulse velocity is simply the distance between the heads of the transducers, as defined in Figure 2.18.

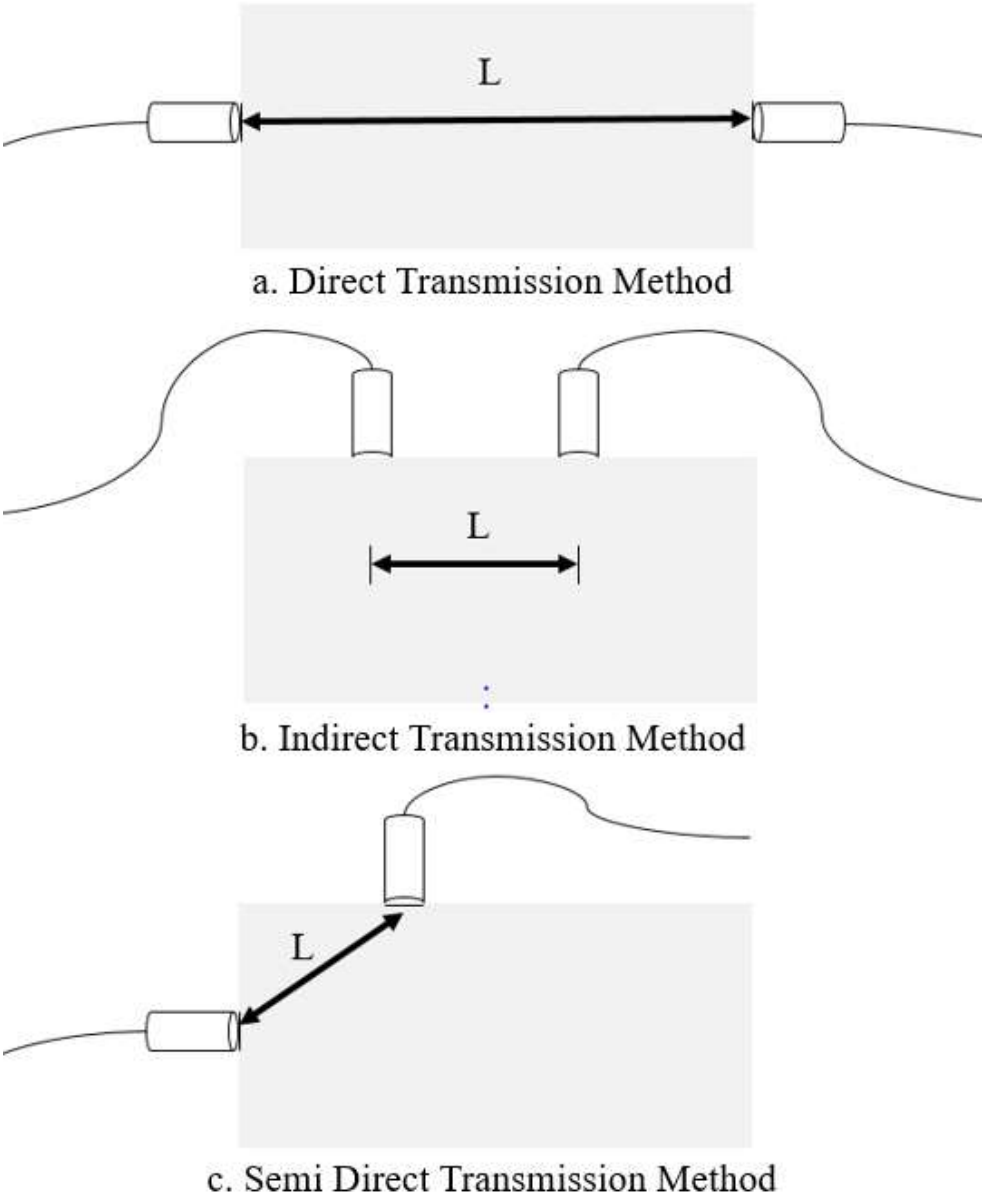

Figure 2.18: Schematic of Common Ultrasonic Testing Techniques

CHAPTER 3
METHODS, DATA ANALYSIS, AND RESULTS BY EXPERIMENT

This chapter will go through each separate experiment in this thesis, starting with the methodology and background that gives credence to performing the experiment, followed by the specimen preparation, equipment used, results, discussion, and a reflection on the problems that occurred with some insight as to how to improve on the experiments for future research.

3.1 Experiment 1: Fiber Orientation

3.1.1 Methodology

The first experiment began in February 2021. The methodology of this test was similar to that described in section 2.1.5, but due to the available equipment at the time, a Wenner probe was used oppose to the four-probe square array which is the recommended configuration. This methodology follows that of Lataste et al. and Barnett et al. and will be further described below (Lataste 2008, Barnett 2010). The hypothesis for this test was that for specimens without steel fibers, there would be no apparent resistivity axis, as there was not steel fibers to greatly influence the resistivity along an axis, so there would only be minor differences due to the anisotropic and heterogeneous nature of concrete. For specimens with fibers, there would be local resistivity axis along the flow of the concrete when the concrete was poured.

The methodology for using electrical resistivity to determine fiber orientation in concrete involves taking several measurements at individual points on the specimen, but at varying orientations. As proposed by the aforementioned studies, one means of doing so is to take several points on the surface of the specimen, then rotate the measurement device about this point, taking measurements at 22.5^{o} increments until a complete rotation about the center point is complete. After doing so, plotting the value of the resistivity in polar coordinates, with the angle corresponding to which it was taken at,

can allow for the visualization of a resistivity axis. Such a resistivity circle may look similar to that seen in Figure 3.1.

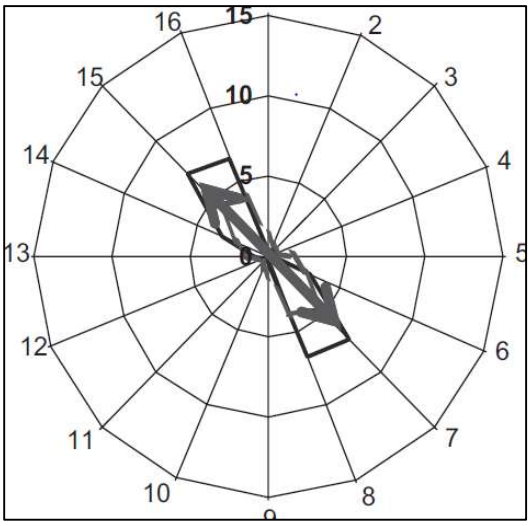

Figure 3.1: Visual Representation of a Resistivity Axis (Lataste 2010)

The importance of the resistivity axis, is that this axis represents the direction for which there is the smallest density of fibers oriented parallel to that direction. This is known due to the difference in resistivity between concrete and steel fibers (Barnett 2008, Lataste 2010, Martinie 2013). Intuitively, metals are typically quite conductive materials, while concrete is not a conductive material. Alternatively, concrete is a material that records high values of resistivity, while steel records low values of resistivity. Knowing this, the presence of steel fibers within concrete will affect the measured values of resistivity (Martinie 2013). If the steel fibers within a concrete specimen are oriented along the axis for which measurements are being taken, then the effects of the steel fibers will be great. In such a case, the apparent resistivity will be much less than that of concrete without steel fibers embedded. Alternatively, if the orientation of the steel fibers is perpendicular to the axis that the current is being injected into, then the measured resistivity will be similar to that of concrete without fibers. Thus, plotting this will reveal the axis for which the resistivity is highest and lowest, or where the fiber orientation density is lowest and highest. By doing this at multiple spots on the surface of a concrete

specimen, the local orientation of fibers at each point can be made, and a general idea of global fiber orientation can be obtained. A visual representation of this can be seen in Figure 3.2.

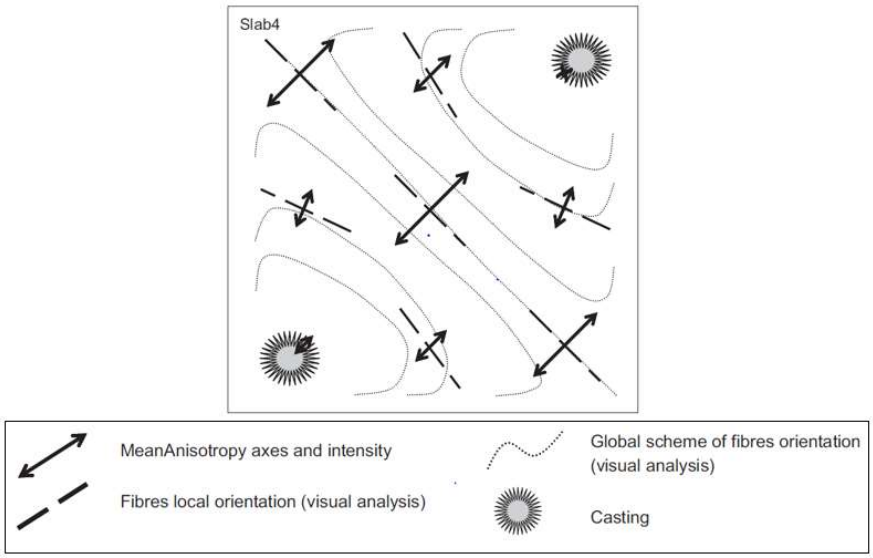

Figure 3.2: Global fiber orientation on a concrete plate (Lataste 2010)

This method of measuring at incremental orientations allows for the calculation of anisotropy. Anisotropy is a measurement of how equally dispersed the fibers are within a concrete specimen. Isotropy would be achieved if all fibers and physical properties of the concrete were dispersed equally in all directions, which would equate to a value around 0.5 for anisotropy based on different models (Martinie 2011, Martinie 2013). For a heterogeneous material such as concrete, along with fibers embedded within the concrete, this is an extremely unlikely event. Thus anisotropy is measured in order to get an idea of the fiber dispersion locally, and then globally by means of a collective set of local anisotropies. Martinie proposed that anisotropy is measured as the ratio of conductivities along perpendicular axes, as shown in the equation below:

$$\log_{10} An_i = \log_{10} \frac{\sigma_{ai}}{\sigma_{aj}}$$

Where An_i is the anisotropy at the ith point, σ_{ai} and σ_{aj} are perpendicular conductivities of the ith axis (Martinie 2013).

3.1.2 Specimen Manufacturing and Curing

For the choice of mix, ultra-high performance concrete (UHPC) was used. The exact mix proportion used is tabled in Figure 3.3. The procedure for creating the specimens started by equipping the proper safety equipment, which included closed end shoes, long sleeve clothes, and an N95 mask to filtrate the silica particles. Additionally, the dusk collector was turned on to further decrease the likelihood of inhaling silica particles. Then, one of the homemade wooden molds was placed inside a large trash bag. The dimensions of the molds and the use of the large trash bag will be discussed later in this chapter. Next, the components of the mix were weighed on an electrical balance. To do so, buckets were placed on the electrical scale and tared, then the component would be added until reaching the desired mass. The bucket would then be placed under a dusk collector. The water and ADVA 198 were weighed last to avoid the effect of evaporation which could have caused there to be a loss of mass for the water component of the mix.

Mix Component	Mix Proportion	Mass (lb)	Mass (g)
Portland Lime Cement	1	7.240	3284.1
Silica Fume	0.176	1.274	578.0
Silica Sand	1.234	8.935	4052.6
ADVA 198	0.032	0.232	105.1
Water	0.234	1.694	768.5
Steel Fibers	0.007	0.051	23.0
Total	2.683	19.426	8811.3

Figure 3.3: Mix proportions for high performance concrete

For mixing, a large BakeMax BMPM012 12-quart planetary mixer device was used. First, the dry ingredients of the mix were poured into the mixing bowl in the order of silica fume, Portland lime cement, then silica sand. After the components were added, the mixing bowl was then attached firmly to the mixer, and the flat beater was attached. The mixing bowl was then elevated using the crank such that the flat beater almost touched the bottom of the mixing bowl. For heavier loads, wooden boards were placed under the mixing bowl in order to support the mixer apparatus in holding the mixing bowl

up while mixing. This setup can be seen in Figure 3.4. Then, the planetary mixer was turned on low until the dry components were sufficiently blended. The mixer should be put on low for mixing the dry components as the increased kinetic energy at higher mixing settings can cause the dry components to spill out of the mixing bowl. Next, the water and ADVA 198 were mixed together in a separate container. Then, approximately half of this mix was added to the dry components and mixed in the large mixing bowl. At this time, the mixing setting was increase to give the mixer more power for blending the mix components. Following this, the water and ADVA 198 mixture was slowly added to the mixing bowl while mixing, until the mix began to "kick over." The term 'kick over" describes the moment when the UHPC mix begins to flow into a liquid-like material. This typically requires approximately 80-85% of the water and ADVA 198 mixture based on the proportions in Figure 3.3. At this time, if fibers were included in the mix design, they were added to the mixer. For this experiment, one specimen was made with fibers and one was made without fibers due to the availability of the mix components. Shortly after this, the mixer was turned off and the mixing bowl was removed from the mixer apparatus. The mixing bowl was then poured into the wooden mold, and the location(s) from which the mix was poured was marked on the plastic bag on the wooden mold. Then, the mold was placed into the wet room. The following day, the mold was removed from the wet room and hit on the bottom side with a hammer until the concrete specimen fell out of the mold. The specimen was then marked where the concrete had been poured from. The specimen was then placed in the wet room until measurements were taken.

Figure 3.4: The BakeMax planetary mixer setup for mixing HPC

The inner dimensions of the mold were selected to be 12”x12”x1.5” for the concrete panels. The thickness of 1.5” was chosen to allow for adequate depth of penetration for electric currents. For the Resipod surface resistivity device that was already in stock, the distance between probes was about 1.5” inches, and the depth of penetration for surface resistivity probes is generally considered to be half to the entire distance between probes (Lataste 2008). Since the forms were made from wood, using form oil would likely require the disassembly of the entire mold for each use to get the specimen out of the mold. Alternatively, by placing the mold inside a large plastic trash bag, the concrete does not form a strong connection to the plastic bag and can be removed from the mold without disassembly.

3.1.3 Procedure

As described in section 3.1.1, for each specimen, measurements were taken at several locations at degree increments. An example of what this looks like is displayed in Figure 3.5. The measurements from this experiment were performed the day after the specimens were cast. To begin this procedure, the locations to take measurements at were marked on each specimen. This was first done by making a circle around the measurement point using a compass and pencil. Then, using a protractor, the angle increments were marked on the circle using a marker. Following this, a container was filled with water to a few inches in depth. Due to availability, a Proceq Resipod wenner probe device was used. The probes of this device were submerged into the container of water in order to fill the reserves before use. Filling the reserves with water allow for a more sufficient electrical connection (Proceq 2017). Following this, measurements were taken along the four circles shown in Figure 3.5 at each angle increment using the Resipod device. Measurements were recorded in a lab notebook for each angle.

Figure 3.5: A wooden mold (left) and a sample specimen with circle markings (right)

3.1.4 Data Analysis and Results

The data analysis was performed on the experimental data following the procedure from section 3.1.3. This analysis was done using Microsoft Excel. First, this data was converted from polar to Cartesian coordinates, and plotted for each circle. This is done simply using the following relations:

$$x = r \cdot cos\emptyset$$

And…

$$y = r \cdot sin\emptyset$$

An example of what one of these plots would look like can be seen in Figure 3.6. The plot on the left is from a specimen without fibers, and the plot on the right is from a specimen with steel fibers. Theoretically, the plot without fibers makes sense, due to the lack of steel fibers, there should be no apparent resistivity axis and the resistivity should be similar along every orientation. For the specimen with steel fibers, since the concrete was poured into a single corner of the mold, it would be anticipated that there would be a resistivity emanating from that corner from which the concrete was poured. Based on Figure 3.1 from section 3.1.1, there would appear to be no dominating or clear resistivity axis yet again. To add more context, the four resistivity circles for the specimen with steel fibers are overlaid onto the specimen in Figure 3.7. This figure indicates that there is no apparent global resistivity axis that can be determined based on the data from this procedure. In the figure, the red star designates the corner from which the UHPC mix was poured from, and one would anticipate that the fibers would align along the direction of the flow until the edges where the wall effect may take place (Lataste 2008, Bennet 2010). The wall effect is a boundary condition that will cause fibers to align parallel to a surface of the mold as the mix approaches the boundaries of the mold itself. This effect was avoided by taking measurements closer to the center of the specimen, as this effect typically only occurs on the edges of

the specimen where the walls of the mold existed during pouring. Regardless, it is evident that the results for this experiment are inconclusive.

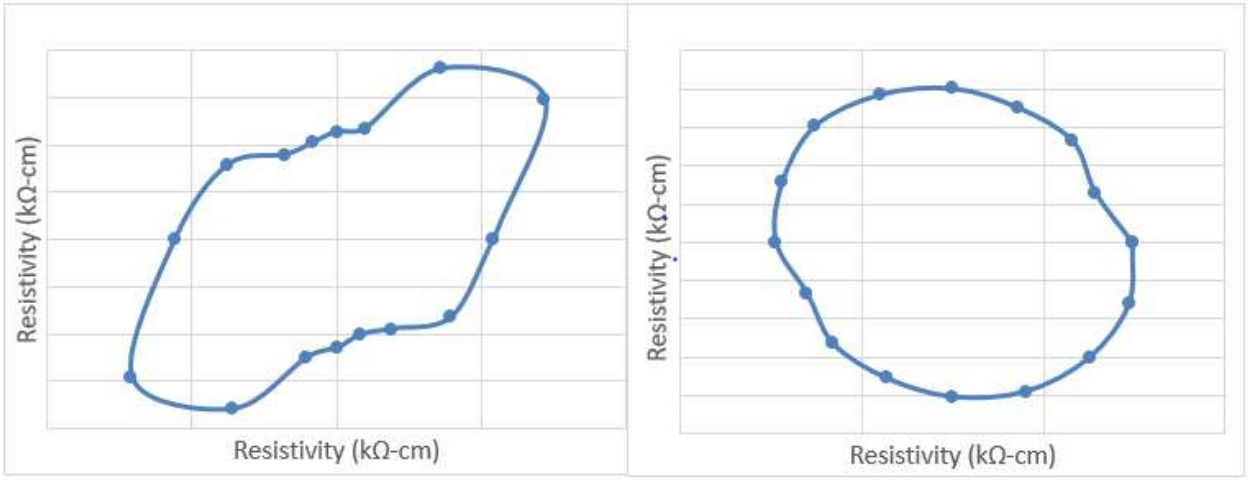

Figure 3.6: Resistivity vs orientation plots for specimens without fibers (left) and with steel fibers (right)

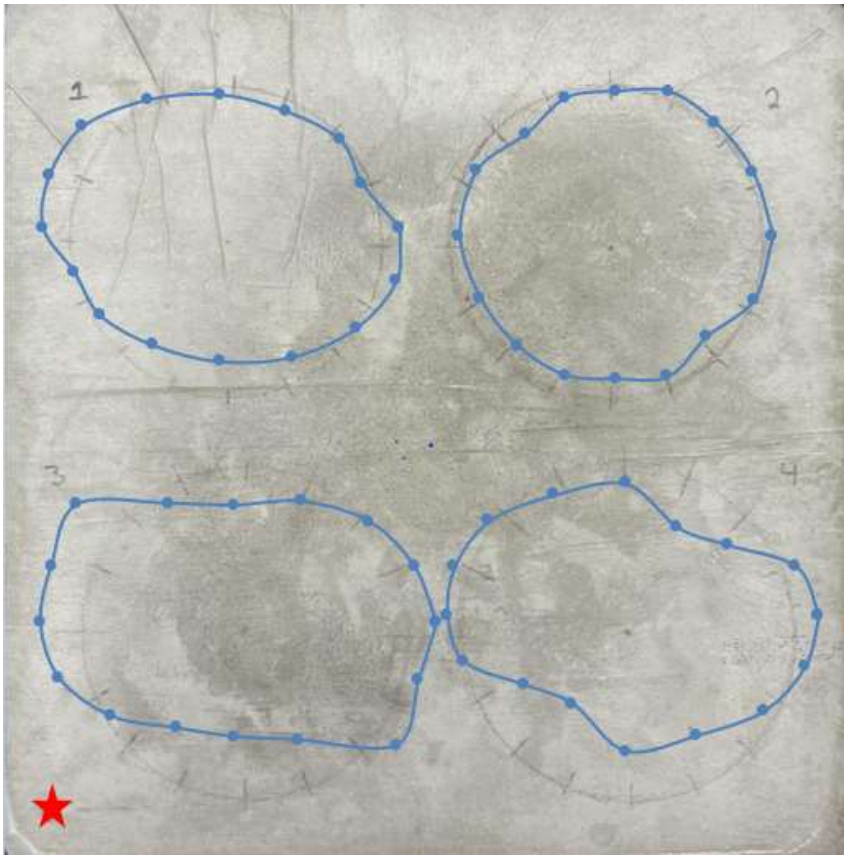

Figure 3.7: Resistivity vs orientation plots overlaid onto plate specimen

3.1.5 Conclusions

The hypothesis for this experiment was that there would be resistivity axes for specimens with fibers, and there wouldn't be any for specimens without fibers. Based on figures presented, the hypothesis for the specimens without fibers was reinforced, but the hypothesis for specimens with steel fibers was not. There are several possible reasons for why the results from this test were found to be inconclusive, one of which could be that the fibers were dispersed in a fairly isotropic manner. This would be unlikely, especially due to the fact that the fibers were all poured from the same location in the mold. Alternatively, as suggested by Lataste et al. (2008), the Wenner probe may have too much interference and polarization for these measurements due to the linear array of probes. Thus, the implementation of a square formation of the probes may be more suitable for such experiments.

3.1.6 Plans for improvement

As discussed in section 3.1.5., the most logical plan for improvement upon this experiment would be to choose a new apparatus to take measurements with. Due to the success of Lataste et al. (2003, 2008), it would seem that the four-probe square device would be the most logical means of determining the fiber orientation within the plate specimens. The device used in these studies appears to be a Megger DET5/4D earth tester, as shown in Figure 3.8. At the time of this study, this model was discontinued and considered obsolete, so the plan for improvement was to obtain a newer model of this device and manufacture a four-probe square device.

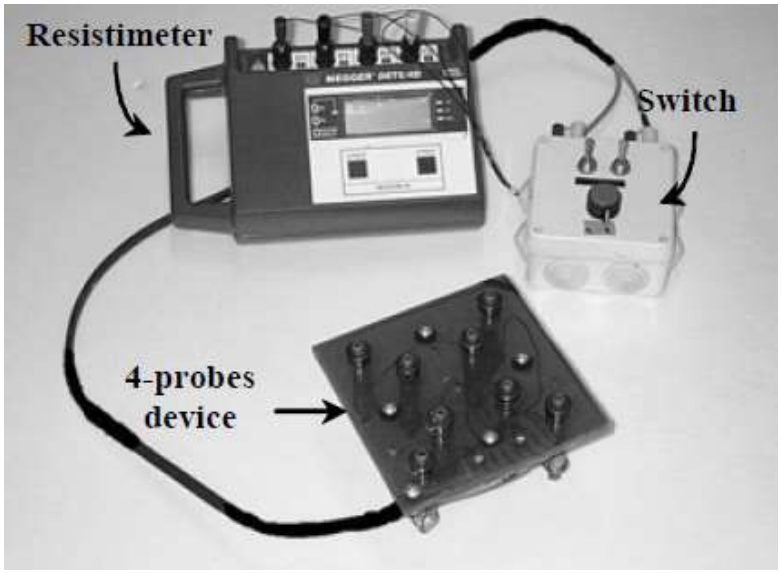

Figure 3.8: Image of the four-probe square device (Lataste 2003)

3.2 Experiment 2: Multi Method Setup

3.2.1 Methodology

The second experiment of this thesis took place in September 2021. The methodology of this section combines the non-destructive evaluation techniques of electrical resistivity and ultrasonic wave propagation. The purpose of doing this is based in the belief that a single non-destructive evaluation technique is not sufficient enough to extract all of the desired information out of a specimen. The concept of using a multi method system is not a novel concept in the evaluation of concrete, as several studies have investigate concrete in this manner with varying success. (Zhang 2007, Rivard 2009, Vesely 2014, Vesely 2015, Mazloom 2017).

For electrical resistivity, the uniaxial method was used. As discussed in section 2.1.5, the uniaxial method involves placing specimens between two metal electrode plates, and measuring the resistance through the specimen. This method was selected due to its easy application for the specimen dimensions chosen, along with the availability of existing equipment. The primary property of interest for these measurements was the formation factor of the concrete. As previously discussed, the formation factor is a property combining microstructural properties of concrete, and is representative of the state of the pore system within a specimen. The means by which the formation factor was determined will be thoroughly explained in section 3.2.3.

For ultrasonic wave propagation, the direct transmission method was used. As discussed in section 2.2.4, this method involves setting up transducers on parallel sides of the specimen, with one transducer outputting ultrasonic waves (the transmitting transducer), and the other transducer receiving the ultrasonic waves after they have passed through the specimen (the receiving transducer). The properties of interest for this method were ultrasonic pulse velocity, attenuation coefficient, the

diffusivity coefficient, and the disspation coefficient. The means by which these properties were determined will be explained in section 3.2.3.

The hypothesis of this experiment, was that by combining these two non-destructive evaluation techniques on specimens of varying curing age and water content, that a relationship between the two methods could be found that would allow for the determination of more information on the properties of the material being tested.

3.2.2 Specimen Manufacturing and Curing

In order to achieve the proposed hypothesis, concrete mixes of varying water-to-cement ratios were used. To cover the wide range of water-to-cement ratios used for common concrete mixes, water-to-cement ratios of 40%, 50%, and 60% were used for these specimens. The proportions of each component for the different concrete mixes were determined using the procedure outline by Landis (Landis 2017). These proportions can be found in the table below.

Mix Component	Proportion: 40% W/C	Proportion: 50% W/C	Proportion: 60% W/C
Water	0.082	0.083	0.083
Cement	0.206	0.165	0.138
Course Aggregate	0.444	0.447	0.449
Fine Aggregate	0.269	0.305	0.330

Figure 3.9: Concrete mix proportions by mass, with 3% air entrainment.

For the mixing procedure, the specifications laid out in ASTM C192 were followed. First, form oil was applied to the inside of the molds, and the hole on the bottom of the molds was taped over. For this experiment, 4”x 8” cylinder molds were selected. Next, the mix components were weighed out individually using empty buckets and a scale. Mix components were weighed out in grams. For mixing, a large concrete mixer from Multiquip was used, as shown in Figure 3.10. First, the course aggregate was

added to the mixer. Following this, approximately 30% of the water component was added and the mixer was turned on. After the mixer was turned on, the rest of the mix components were added to the mixer in the order of fine aggregate, cement, and the remaining water component. The mixer was left on for the next three minutes, then turned off for three minutes. During the rest period, concrete was scraped off the inside of the mixer using a large aluminum utility scoop to free up some of the mix that was stuck to the mixer, and maintain the proper mix proportions. Following the rest period, the mixer was turned on for another two minutes, and then the mix was poured into a large plastic bin. The bin was then moved next the vibration table. The mix was then poured into the cylinder molds in three lifts. After each lift, the cylinders were placed on the vibration table and the table was turned on briefly. Following the third lift, the molds were moved into the wet room. In total, there were five specimens for each mix.

Figure 3.10: Mixer used for creating concrete specimens

The next day, the molds were removed from the wet room and the tape was removed from the bottom of the molds. Then, pressurized air was used on the hole in the bottom of the molds to facilitate pushing the concrete specimen out of the mold. The specimens were then marked based on their mix and curing conditions. The naming for the concrete cylinders were determined based on the following pattern, first the water-to-cement ratio as a percent (40, 50, 60), followed by the curing condition (A for air dried, B for lime bath, and S for sealed), and finished with the specimen number for this group (01 or 02).

As previously stated, the curing conditions for the specimens fell into three groups, air dried, lime bath, and sealed. The air dried specimens were stored in Boardman hall room 120, the sealed specimens were wrapped with plastic wrap, and the lime bath specimens were placed in an enclosed lime bath located in the concrete lab in the basement of Boardman hall. The purpose of using these different curing conditions was to take measurements on specimens under a variety of water contents. The specimens kept in the lime bath would be the specimens with the highest degree of saturation, as they were constantly submerged in water, the sealed specimens maintain approximately the same water content that they had when they were first set, and the air dried specimens would lose water content over time.

3.2.3 Procedure

For the procedure, resistivity and ultrasonic measurements were taken on each specimen daily for 28 days, with the exception of a few days due to unexpected circumstances. Mass was also recorded for each specimen daily. For this process, the specimens would be tested by curing condition to reduce the time outside of their curing. For the sealed specimens, the plastic wrap had to be removed and new plastic wrap had to be applied. Each group of specimen would be placed in a cart to move from the curing location, to the resistivity setup, and the ultrasonic wave propagation setup. It is recommended that a paper towel is placed under the concrete specimens to prevent dusk, pebbles, etc. from sticking to the bottom of wet specimen, as to prevent interference in measurements.

For resistivity, the RCON2 Concrete Bulk Resistivity Device was used. To use this device, a contact sponge was placed on top of the bottom metal electrode plate. For each measurement, the specimen was placed on top of the contact sponge, then another contact sponge was placed on top of the specimen, followed by the top electrode plate. Then, the four threaded rods attached to the bottom plate were slotted into the top plate, and the knobs for each rod were twisted until the connection was firm. The connection cables were then connected to the electrode plates, and the measurement device. The measurement device was then plugged into an outlet and turned on. This setup is shown in Figure 3.11. Following this, measurements were recorded in a lab notebook. It should be noted, this measurement device produces readings in impedance and a corresponding phase angle, and so long as the phase angle was low (less than 5^{o}), the impedance was considered to be the resistance based on the small angle approximation. As explained in section 2.1.4, the resistance is equal to impedance multiplied by the cosine of the phase angle. Finally, after measurements were taken on each specimen, the apparatus was disassembled and the contact sponges were submerged in water.

Figure 3.11: Setup for RCON2 bulk resistivity meter

For ultrasonic wave propagation, several parts were used for the measurement system. This system is depicted in Figure 3.12. For this setup, a high voltage pulser, two transducers, a data acquisition device (DAQ), and a laptop were used. The high voltage pulser used was a Panametrics Model 5058PR, the two transducers were 150 kHz transducers made by Proceq, and the data acquisition device was a National Instruments USB-6361. In this system, the high voltage pulser was set to maximum voltage, and a frequency of 20 kHz. From the pulser, two cables were run, one to the transmitting transducer from the transmitting output, and the other was run directly to the data acquisition device from the sync-out output on the pulser. When pulses are sent, the output is sent at a high voltage through the transmitting transducer, and sent at a much lower voltage to the data acquisition device, the importance of this will be explained shortly. Ultrasonic transducers are piezoelectric, meaning that they contain a crystal such that, when a strain is applied, a charge is emitted.

The reverse is also true, when the voltage is applied to the transducer, a strain is produced. The crystal within the transducers converts the electrical charge into a wave at 150 kHz. Thus, when charge is run to the transducer from the pulser, the ultrasonic wave is emitted. This wave travels through the specimen being measured, and the receiving transducer gathers the information from the wave after it has traveled through the specimen. The receiving transducer relays this charge to the data acquisition device, which sends the information to the laptop. The laptop records the data using a program called NI DAQExpress, a software included with the data acquisition device. Within this software, is a limited version of LabVIEW called LabVIEW VI. The specifics of this code work due to running two cables from the pulser. The code used for data acquisition via LabVIEW needs to know when to begin recording. If the code begins running when the input is non-zero, then it would begin running as soon as the receiving transducer sent signal to the data acquisition device (disregarding the miniscule amount of time required for the signal to pass through the cables to the data acquisition device). If this occurs, then there would be no way to determine the transit time through the specimen, as the first point in the data would be the signal arrived through the receiving transducer.

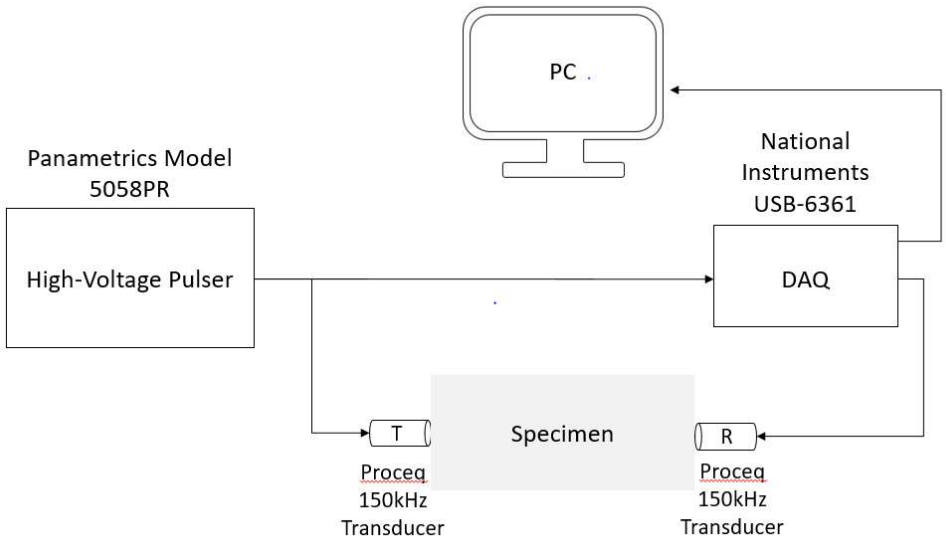

Figure 3.12: Drawing of ultrasonic wave propagation setup

In the case of this experiment, by running a cable from the sync-out output on the pulser to a digital input on the data acquisition device, the input from the sync out can be used as a programmable function input, or PFI. The sync-out also sends this signal at a low voltage, such not to overload the data acquisition device. This digital signal then determines when the software begins recording data, and thus the transit time can be determined based off of this. It should be noted that the difference between the time for the signal to run through the two cables is considered negligible. When this code is used, the software records and saves the information for each event, for a given number of points before and after the event begins. In this case, for each ultrasonic measurement, fifty events would be recorded each time, so that signal averaging could be utilized, reducing noise. Each event contains 8000 data points, 1000 before, 7000 after the event occurs. Considering the data is recorded at 2 MHz, these events are lasting a very short amount of time, which allows the ability to record 50 events per specimen per day to be feasible in regards to time. It should also be noted that vacuum grease was used a couplant for the contact between the transducers and the specimens. A thin layer of vacuum grease was applied and wiped off for each measurement to prevent particles interfering from specimens already tested, and to maintain consistency between specimens. Couplants are used to increase the repeatability of data (Dugmore 2002, Netshidavhini 2012) and create a better ultrasonic contact, similar to water used as a couplant for electrical resistivity measurements.

At the end of 28 days, the concrete specimens were tested for compressive strength following ASTM C39. This was done in hopes of drawing a correlation between the compressive strength and the properties found from the ultrasonic and electrical resistivity measurements.

3.2.4 Data Analysis

For the electrical resistivity measurements, Microsoft Excel was used for data analysis. The property of interest for these measurements was the formation factor. The formation factor was determined through the relationship below.

$$F = \frac{\rho}{\rho_o}$$

Using the recorded values of resistance, the bulk resistivity could be found through the relationship

$\rho = k \cdot R$

where

$$k = \frac{A}{L}$$

And *k* is the cell constant, *A* is the area of the cross section, and *L* is the length of the specimen. The dimensions of the cylinders were all the same, so a constant value for the cell constant could be used. The other value that needed to be determined in order to find the formation factor was the pore resistivity. Considering that measurements were taken daily, and considering the different curing conditions, it would be unfeasible to extract the pore solution from each specimen daily in order to determine values for this property to correspond with each bulk resistivity value. As a result, the Virtual Cement and Concrete Testing Laboratory (VCCTL) was used for estimating this quantity. The VCCTL is software that allows for the creation of unique concrete mixes, and simulates values such as porosity, pore resistivity, etc. as shown in figure 3.13. It should be noted that the pore resistivity in the VCCTL is output in Siemens per meter. Siemens are the multiplicative inverse of ohms, thus a conversion must be made so that the units of the bulk resistivity and pore resistivity are the same when determining the formation factor.

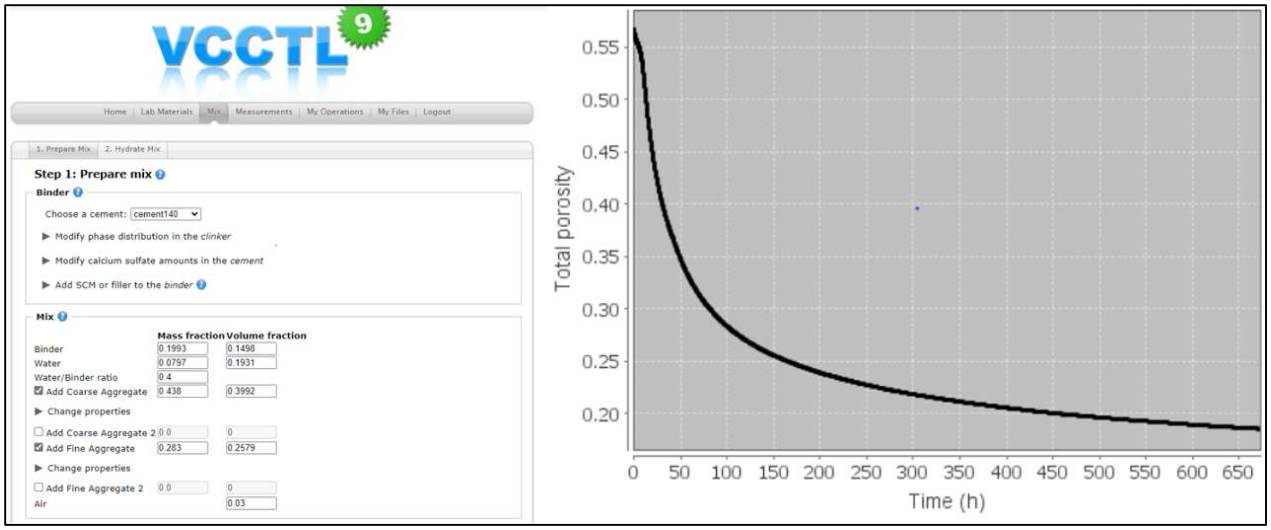

Figure 3.13: Mix input and output for VCCTL

For the ultrasonic data, more sophisticated data analysis had to be employed, so Matlab was used for the data analysis. The data output from the NI DAQExpress software is formatted into a Microsoft Excel file, so the first steps were to transfer these files over to Matlab and perform data averaging for each measurement. An example of what one of these plots looks like after data analysis can be seen in Figure 3.14.

The ultrasonic pulse velocity was one property of interest. This value is determined by the relationship below.

$$v = \frac{L}{t}$$

Where *v* is the ultrasonic pulse velocity, *L* is the distance between the transducers, and *t* is the transit time. The transit time was determined by finding the first break in the curve, or onset of the curve, and subtracting that time from when the wave was sent.

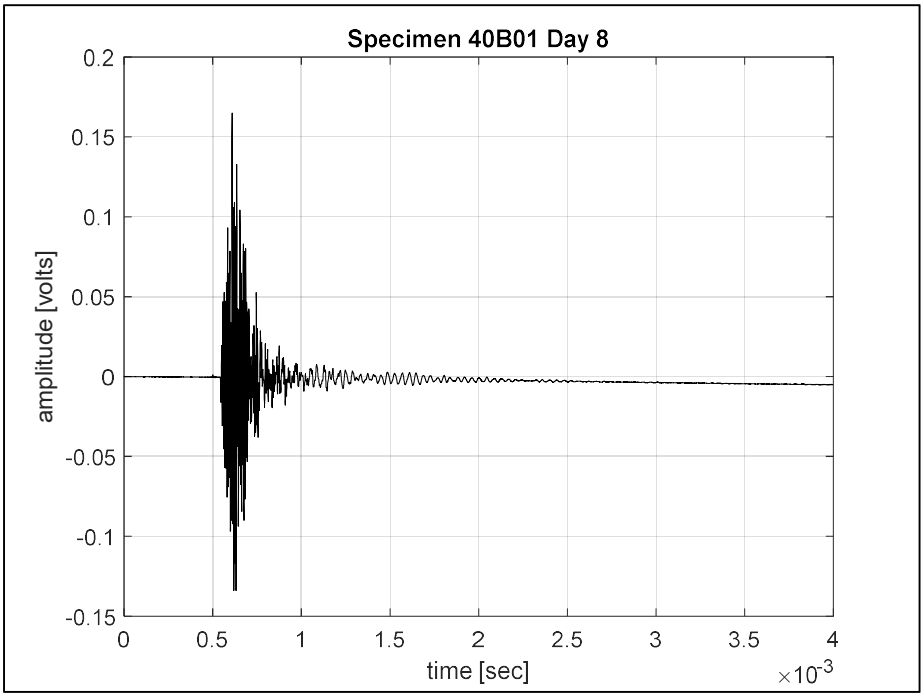

Figure 3.14: Sample ultrasonic wave plot after signal averaging

The next property of interest is the total attenuation. The total attenuation was calculated following the procedure prescribed by Philippidis (2004), which was later used by both Ju et al (2017) and Hassefras (2019). For this procedure, a reading was taken with the two transducers face to face, with no specimen in between. This reading would act as the data for determining the initial amplitude. This would then be compared to the data for measurements taken through the specimens. For each data set, a fast fourier transform was performed. The maximum value for the initial amplitude data set in the frequency domain would be denoted as A_o, and the maximum value in the frequency domain for other data sets would be denoted as A_x. The total attenuation of the specimen for the data can be found using the relationship below (Philippidis 2004).

$$\alpha = -\frac{20}{L}\log(\frac{A_x}{A_o})$$

Where L is the distance traveled between the two transducers. The advantage of this method is that the effects of the coupling is negated, as both readings include the same coupling conditions, which negates the factor of extrinsic attenuation. The resulting value signifies the intrinsic attenuation, which is the portion of the attenuation that characterizes the material, as discussed in section 2.2.3 (Philippidis 2004).

Next, there are the values of the diffusivity and dissipation. These two values are representative of the two major components of intrinsic attenuation, absorption and scattering, respectively. These two values are determined by means of the diffusion approximation. Outlined by Becker et al. (2003), the diffusion approximation determines a value for the spectral energy density for a given ultrasonic signal in the time-domain. This is done by dividing this time-signal into overlapping time windows, in this case 90% was used. A Hamming window is then applied to the individual time windows in order to remove artificial lobes and smooth the edges. Next, the fast fourier transform is taken of each time window, and the output of this transform is squared. The outcome of this is called the power spectrum. The power spectrum is then integrated over a certain frequency bandwidth centered around the measuring frequency, which would be 150 kHz for this experiment, producing an approximation of the spectral energy density. This is considered an approximation of the spectral energy density, as it differs from the true spectral energy density based on a factor emanating from the coupling conditions and transducer efficacy (Becker 2003). The diffusivity and dissipation coefficients are then determined by a fitting of the diffusion equation, shown below.

$$E(r,t,f) = \frac{P_o}{2\sqrt{D\pi t}} e^{-r^2/(4Dt)} e^{-\sigma t}$$

Where E(r,t,f) is the spectral energy density, *r* is the length of the specimen, *t* is the time, *f* is the frequency, P_o is the power spectrum, *D* is the diffusivity coefficient, and σ is the dissipation coefficient.

This equation was fitted using a non-linear least squares regression. An example of one of these curve fits can be seen in figure 3.15, which is similar to that found in literature (Hassefras 2019).

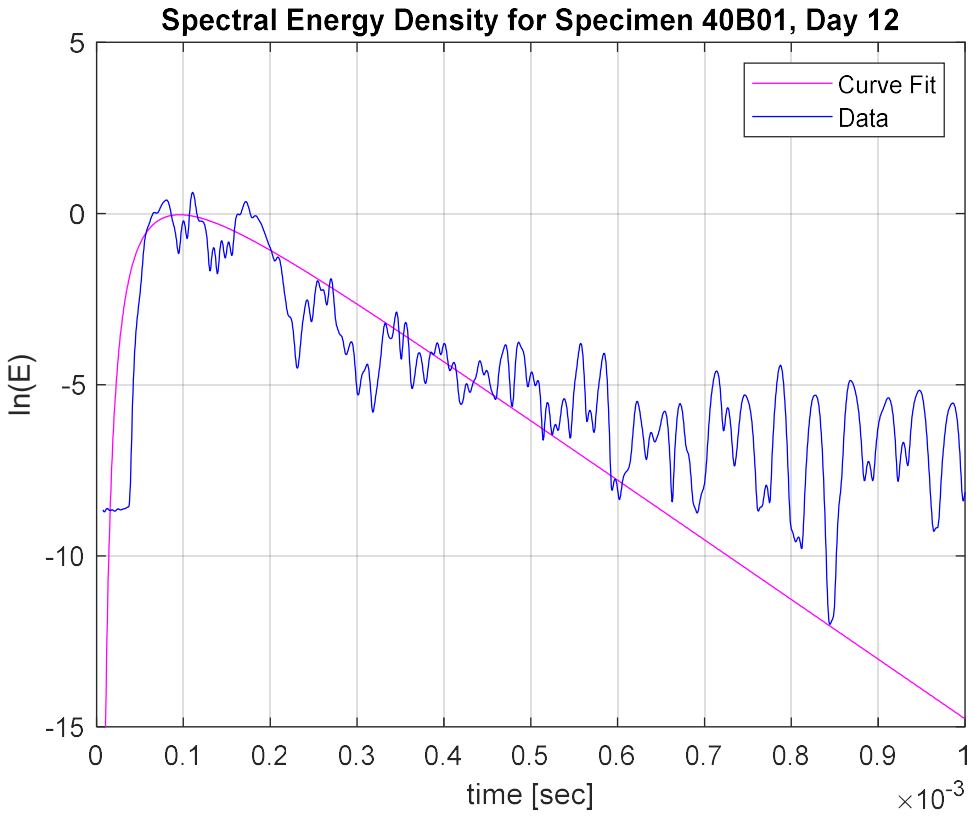

Figure 3.15: Example for diffusion equation curve fit

3.2.5 Results

For this experiment, there were many variables to evaluate across, including curing age, water-to-cement ratio, along with properties compared amongst each other including formation factor, ultrasonic pulse velocity, attenuation, diffusivity, and dissipation. This section will summarize the findings across these axes. Throughout this section, there will be several plots including multiple data sets. To differentiate between the data, cylinders with 40% water content had blue markers, cylinders with 50% water content had red markers, and cylinders with 60% water content had black markers. Cylinders that were air dried had a plus sign as a marker, cylinders that were saturated in lime water had

a circular marker, and sealed specimens had an x as a marker. This is more clearly defined in the table below.

	40% W/C Ratio	50% W/C Ratio	60% W/C ratio
Air Dried	+	+	+
Lime Bath	○	○	○
Sealed	×	×	×

Figure 3.16: Plot markers for experiment two

First, the values of formation factor were compared with curing age, shown in Figure 3.17. To begin with, since the specimens that were sealed and air dried were not fully saturated, they would need a saturation function to adjust for the fact that they are not fully saturated for the determination of formation factor, as discussed in chapter 2.1.6. The inability to determine a saturation function stems from not knowing the mass of the specimens at the oven dry state. That all being said, the important thing to take away from this plot is that the formation factor has a tendency to increase as the curing age increases, and is relatively similar for each water-to-cement ratio.

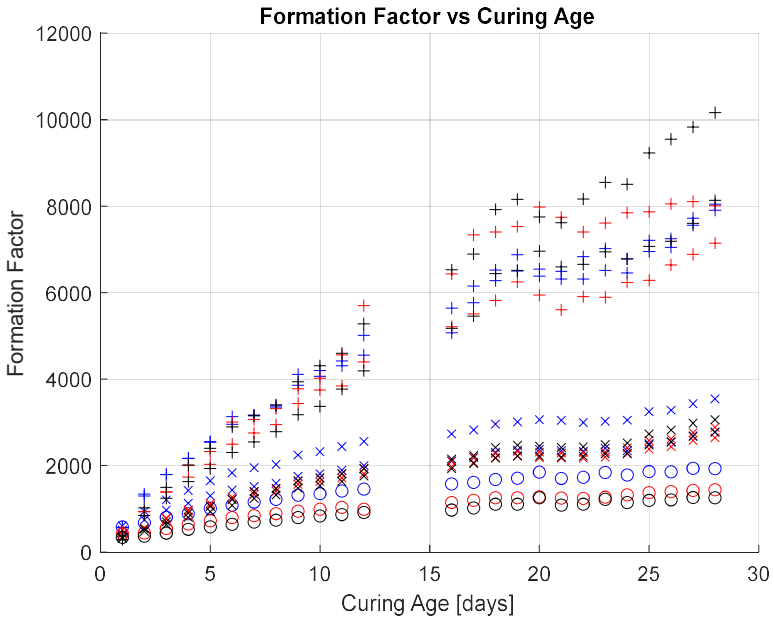

Figure 3.17: Formation factor vs curing age

The formation factor on the 28th day was then compared to the compressive strength determined on the 28th day. Since compressive strength tests are destructive, these tests were only performed once, and the formation factor on this day would be the most applicable comparison between the peak load and the formation factor. The plot of this relationship is shown in Figure 3.18. As shown in this figure, the cylinders made from mixes with lower water-to-cement ratios have higher compressive strength, as anticipated. For their respective curing conditions, these specimens also tend to have higher formation factors, although this relationship is not perfect, which may be due to the lack of a saturation function.

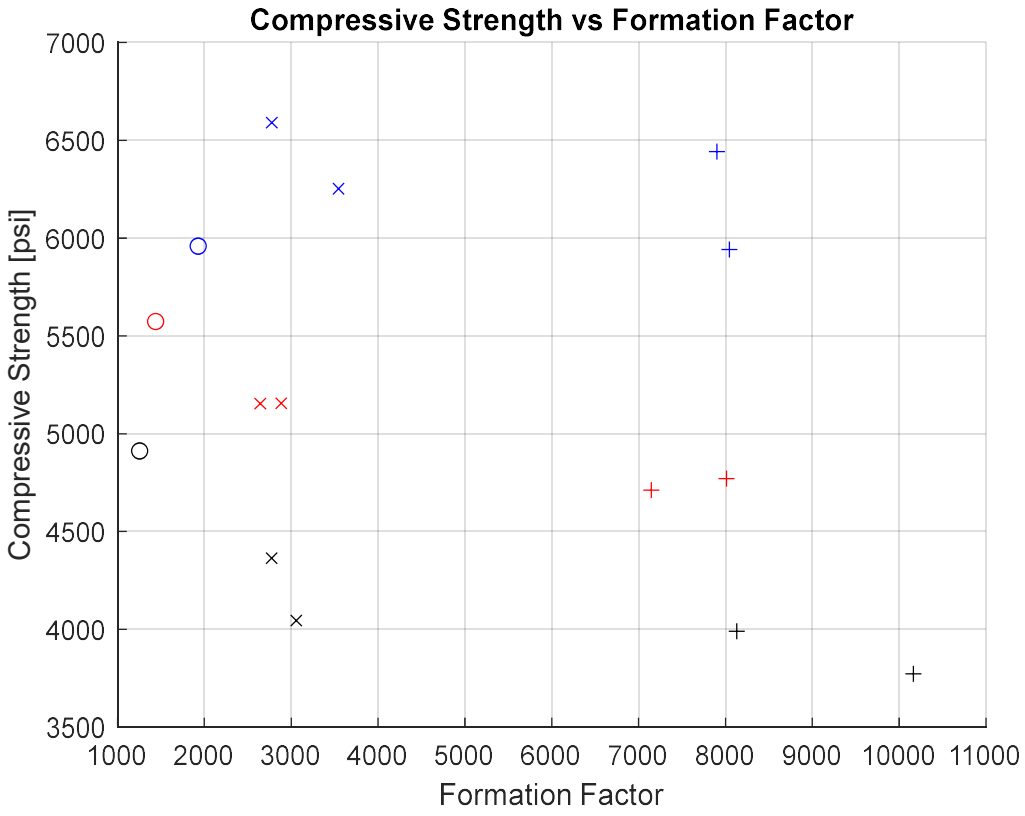

Figure 3.18: Compressive strength vs formation factor

Next, the ultrasonic pulse velocity was compared with curing age, shown in figure 3.19. This relationship is clear, at the early concrete age, the increase in ultrasonic pulse velocity is high, but quickly plateaus after about 10 days. The results show that the ultrasonic pulse velocity is higher for specimens that have higher degrees of saturation, and mixes with lower water-to-cement ratios. The significance of this plot is the relationship between the ultrasonic pulse velocity based on the mix proportions, as it appears the mixes that performed with higher compressive strength display higher ultrasonic pulse velocities, with variances due to the curing conditions. The curing conditions that result in a higher degree of saturation appear to produce a slightly greater ultrasonic pulse velocity based on the other specimens of the same mix.

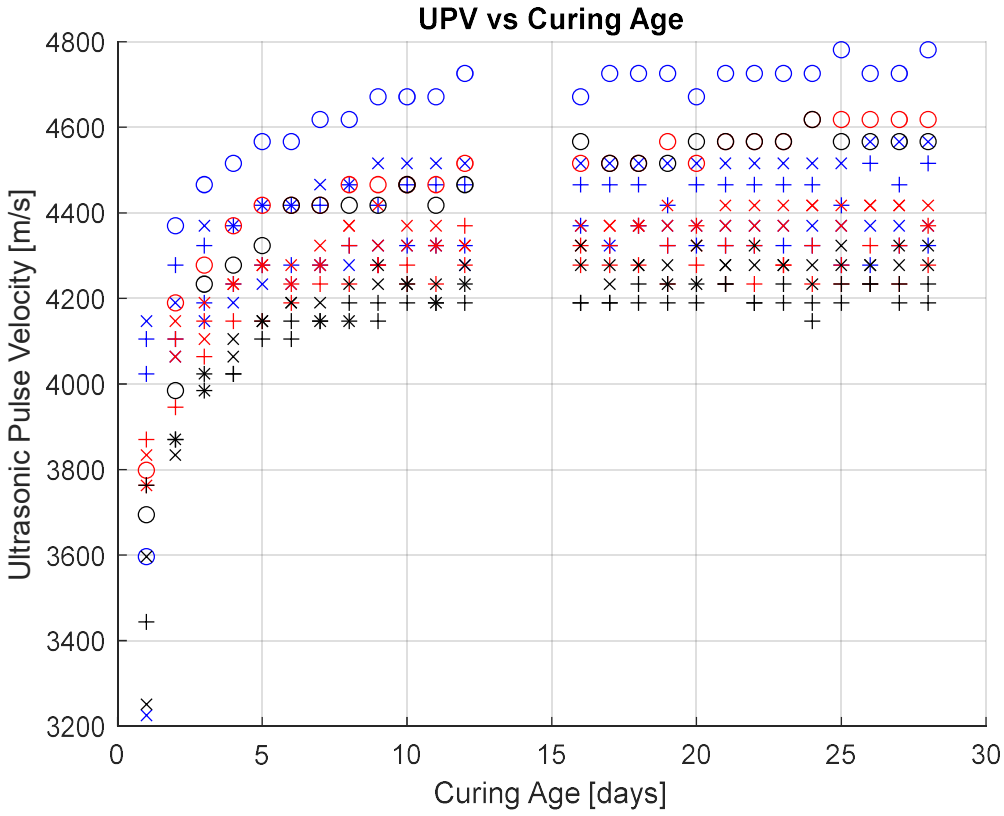

Figure 3.19: Ultrasonic pulse velocity vs curing age

Based on the relationship previously discussed, the next course of action was to investigate the relationship between the ultrasonic pulse velocity and the compressive strength more directly. Thus, similar to the formation factor, the ultrasonic pulse velocity recorded on the 28th day was compared with the compressive strength determined on the 28th day. This relationship is shown in Figure 3.20. This figure shows a positive correlation between the ultrasonic pulse velocity and compressive strength, and this correlation seems to be even stronger when focused on the data for the individual curing conditions.

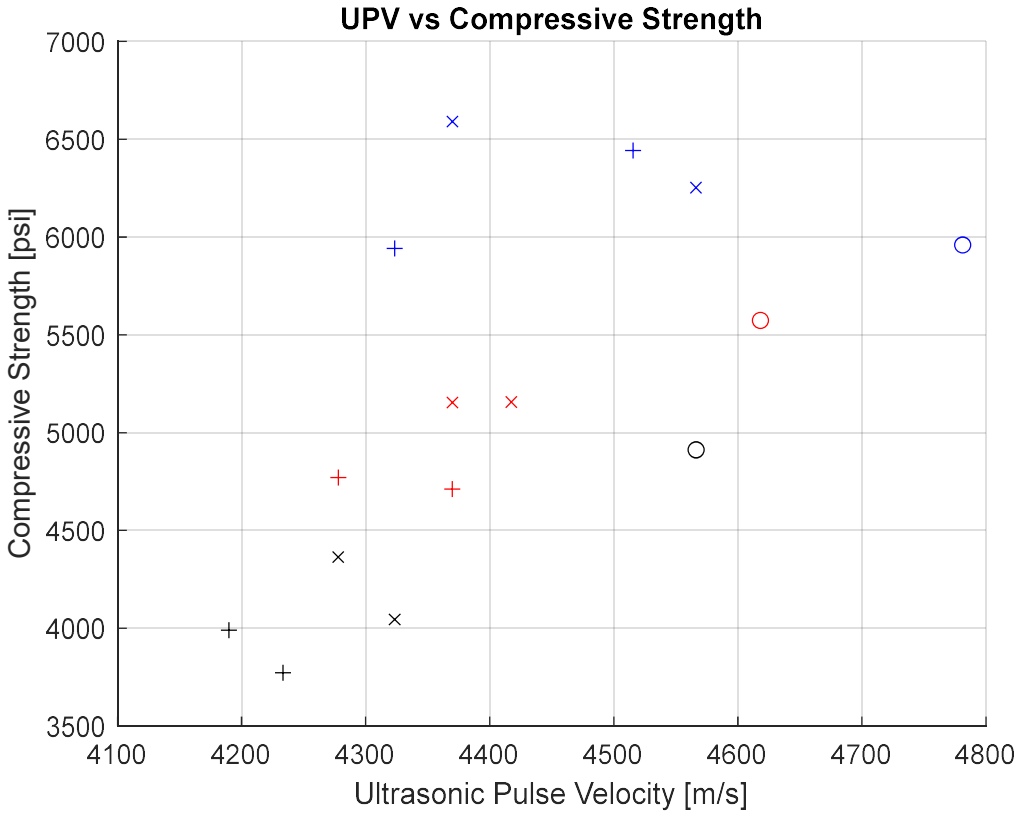

Figure 3.20: Ultrasonic pulse velocity vs compressive strength

Next, the total intrinsic attenuation coefficient was compared with curing age and compressive strength, as shown in Figure 3.21. Looking at the curing age comparison plot, for some specimens the attenuation peaks at the beginning, dips in the middle, then increases afterwards, such as the saturated specimens, while other specimens are scattered across the plot with no apparent trend. Overall, there appears to be a slight decrease in total attenuation as the curing age increases, although the data is fairly scattered and has a wide margin. For the comparison with compressive strength, the measurements from the 28th day were used again. For this comparison, there appears to be a negative correlation between the two variables. There appears to be a correlation between the attenuation coefficient and the compressive strength than the attenuation coefficient and the curing age. When these two figures are joined in unison, the relationship between intrinsic attenuation and compressive strength seems to increase, as there is a decrease in attenuation as the curing age increases, and an increase in compressive strength as the attenuation decreases. These two relationships align as the strength of concrete tends to increase as the curing age increases.

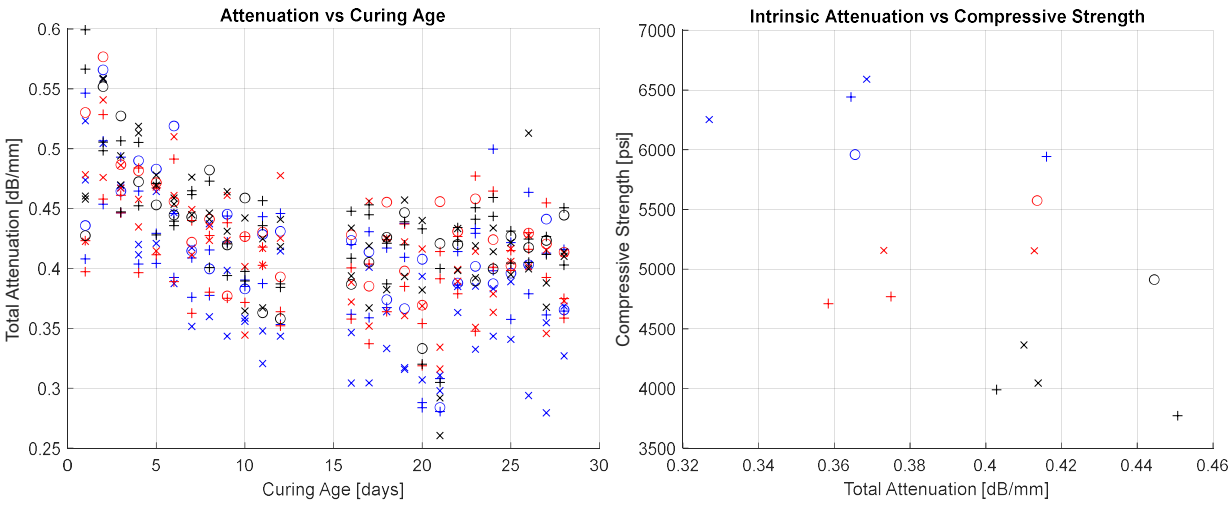

Figure 3.21: Total attenuation vs curing age (left) and vs compressive strength (right)

Next, the relationship between the two intrinsic attenuation coefficients, diffusivity and dissipation were compared with the curing age and compressive strength. For all four of the relationships, there does not appear to be any relationship at all, as data is scattered all around the plot with little correlation, as shown in Figure 3.22. The belief for the lack of correlation between the plots was that the contact conditions while testing were not ideal due to the roughness of the ends of the concrete cylinders.

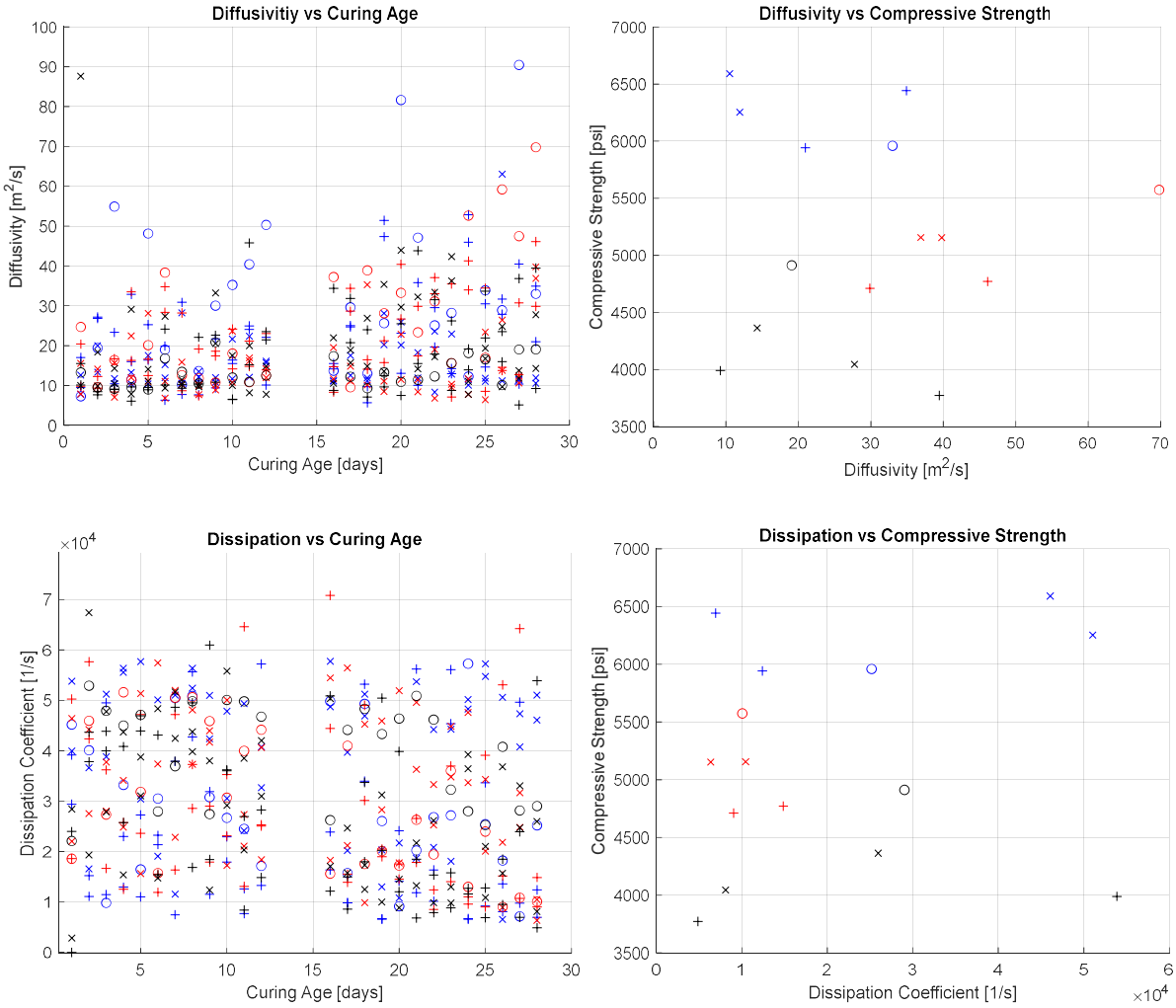

Figure 3.22: Intrinsic attenuation coefficients vs curing and compressive strength

Next, the relationship between the formation factor and ultrasonic pulse velocity was investigated. This is best displayed by curing conditions, with the first being the saturated specimens, as shown in Figure 3.23. Based on this plot, there appears to be an exponential relationship between the ultrasonic pulse velocity and the formation factor. This is significant due to the previously shown relationship between the ultrasonic pulse velocity and strength. The formation factor is a property that is representative of the concrete microstructure, so by correlating the two, there is the potential to obtain information on the compressive strength of the concrete, along with its microstructural properties, through a single property. Additionally, the ultrasonic pulse velocity is a property which can be quick and easy to calculate.

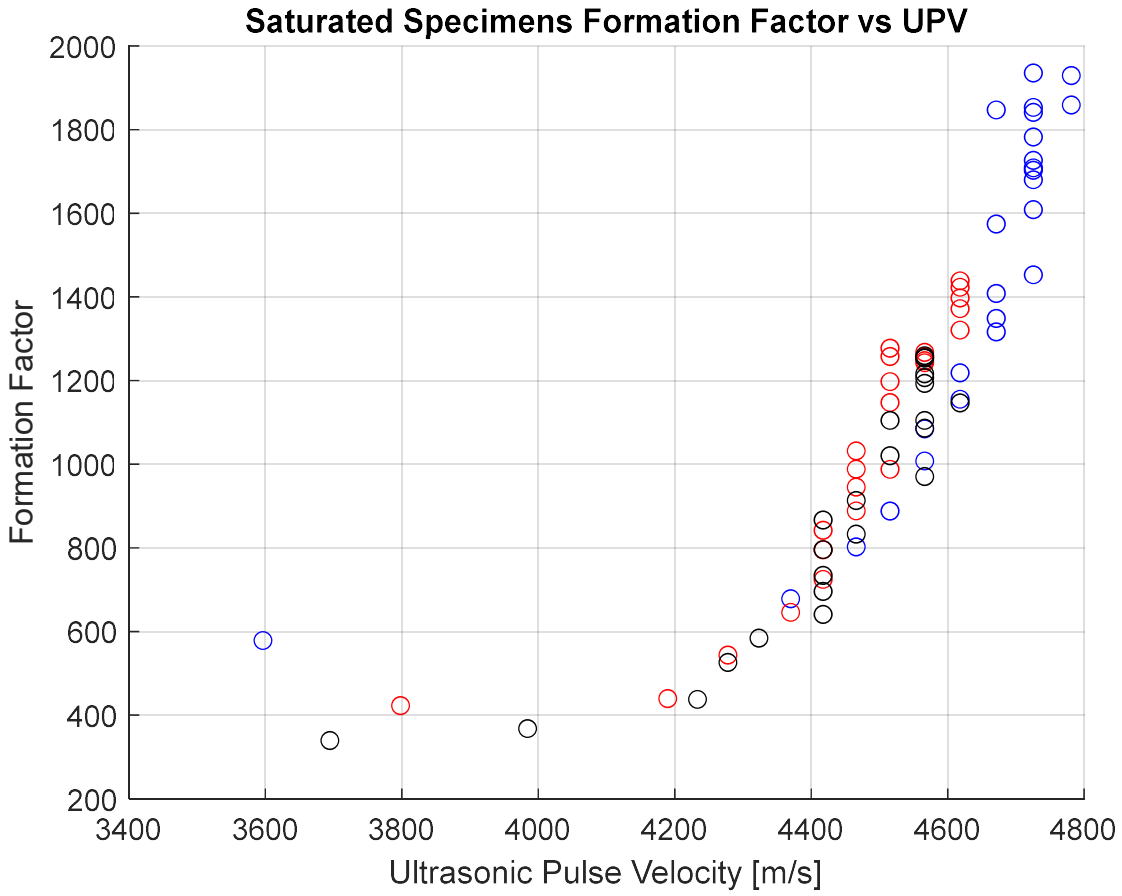

Figure 3.23: Formation factor vs ultrasonic pulse velocity for saturated specimens

Next, the relationship between the formation factor and ultrasonic pulse velocity for the sealed and air dried curing conditions are presented, shown in Figure 3.24. Again, while these formation factors are not adjusted for the saturation, there is still an apparent exponential relationship between the ultrasonic pulse velocity and formation factor.

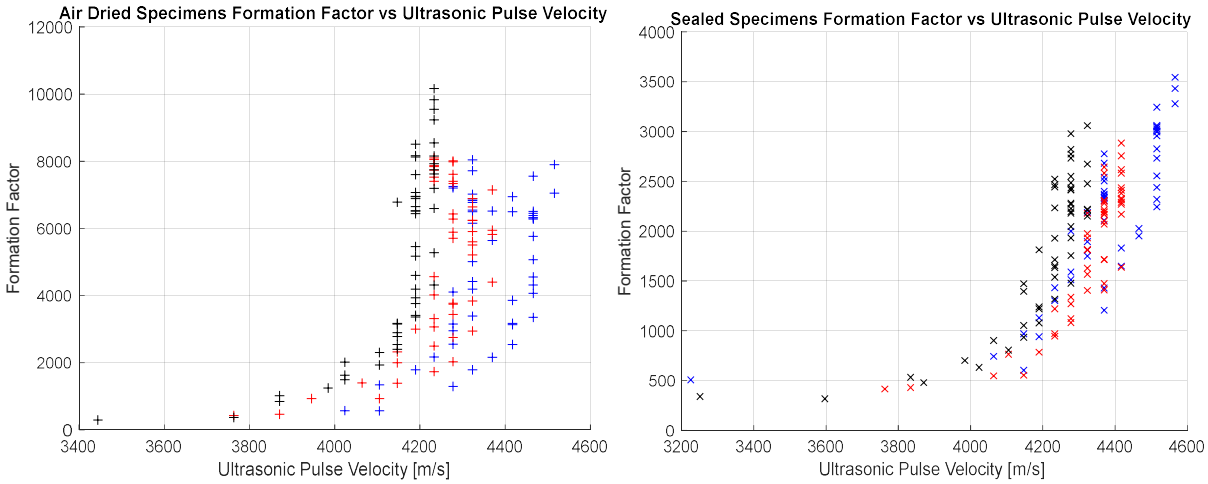

Figure 3.24: Formation factor vs ultrasonic pulse velocity for air dried and sealed specimens

3.2.6 Conclusion

The hypothesis for this experiment was that by combining the two non-destructive evaluation techniques, for a variety of specimens, that a relationship could be found between the two methods such that more information on the material could be found. This hypothesis was achieved based on the relationship found between the formation factor and ultrasonic pulse velocity. The significance of this relationship is derived from the simplicity of the ultrasonic pulse velocity. Since the ultrasonic pulse velocity shows some relationship with compressive strength, as shown in Figure 3.23, and the formation factor characterizes the microstructure for a given material, this relationship creates the potential for determining both compressive strength along with microstructural properties using a single measurement. Additionally, the ultrasonic pulse velocity is a quick and simple calculation, making it feasible for field applications for industrial practices.

3.2.7 Plans for Improvement

To improve upon this procedure, the saturation factor needed to be known for each specimen. In order to have the true value of formation factor without the need for an adjustment factor via a saturation function, all specimens should be saturated. This would help further investigate the relationship between the formation factor and ultrasonic pulse velocity by having more specimens. Another improvement that could be made to this procedure would be to flatten the ends of the specimens in order to remove the possibility that the uneven ends altered ultrasonic measurements. During the measurement process, it was difficult to obtain data on some specimens due to the uneven specimen ends, and flattening these ends would allow for more consistent and accurate measurements.

3.3 Experiment 3: Multi Method Setup

3.3.1 Methodology

The third experiment took place in January and February 2022. This experiment attempted to build off the first multi-method experiment. Based on the conclusion of the second experiment, this experiment was planned in order to maintain each specimen at full saturation, while also investigating the effect of moisture on ultrasonic measurements. In order to do so, the concrete specimens were dried. Following the drying of the concrete, the concrete was rehydrated and measured incrementally to investigate the effect that moisture has on ultrasonic measurements. In terms of drying, several methods can be applied, as investigated by Zhang et al. (2011), Galan et al. (2016) and Zhang et al. (2019). These methods include oven drying, microwave drying, dry ice method, percolate drying, and vacuum drying.

Oven drying is the most common method in concrete. This is typically performed at 60^{o}C or 105^{o}C, although temperatures between can also be used. The advantage of oven drying methods is that it is simple and effective at removing evaporable water (Zhang 2011). The downside of oven drying methods is that the process of drying can remove the evaporable water from ettringite and C-S-H formations, along with damaging the pore structure of the element (Galle 2001). Microwave drying is a method that can provide significant time savings through the use of electromagnetic radiation. The pitfall of the microwave method is that the microstructure of the sample can be significantly altered by the build-up of vapor pressure within the pores due to the rapid temperature changes in the pore liquid (Zhang 2011). Dry ice methods utilize the combination of solid carbon dioxide along with alcohol in concert with a vacuum pump and dry ice. This method is effective at removing unreacted water within the pore system. The downside of this method is the rate of water removal is relatively slow, but this method is otherwise considered the best drying method in concrete and cementitious materials (Zhang 2011). Percolate drying is a specific technique which involves placing the specimen on drying magnesium

perchlorate hydrates. The vacuum drying method is performed at low pressure, and is found to be less effective at removing unreacted water than oven drying methods, while also causing significant damage to the pore structure (Zhang 2011).

In terms of measurement practices for resistivity and ultrasonic wave propagation, the methodology of this experiment mimics that of the first multi-method experiment. The hypothesis for this experiment was that the relationship between formation factor and ultrasonic pulse velocity could be further cemented by including a greater number of specimens, and that a relationship could be found between the degree of saturation and ultrasonic measurements.

3.3.2 Specimen Manufacturing and Curing

Similar to experiment two, concrete mixes were selected to be representative of a wide variety of concrete mixes used in industry practices. In addition to the three mixes that were used in the first multi-method experiment, the high performance concrete mix from the fiber orientation experiment was also used. This was done in order to determine if the relationship between fiber orientation and ultrasonic pulse velocity can be extended to high performance mixes.

Similar to experiment two, the cylinders were made in accordance with ASTM C192. The process outlined in section 3.2.2 was followed for making these specimens as well, with the only difference being the creation of the high performance mix. The high performance mix was made following the process described in section 3.1.2, although these mixes were also poured in lifts and vibrated using the vibration table. The day after mixing, the concrete specimens were removed from the specimen molds. After removal, the specimens were cut with a wet saw in order to achieve flat specimen ends. About an inch was removed from each end of the concrete specimens, resulting in specimens of six inches in length. For the days proceeding, the specimens were cured in a lime bath located in the wet room in the

basement of Boardman hall. The lime bath was created using the ratio of 2 grams of calcium hydroxide per liter of water.

The largest change in the specimen curing occurred on the 30th day. On the 30th day, the specimens were placed in conventional ovens. The specimens were dried at 105^{o}C for several days, up until the change in mass for each specimen was less than 0.1% per day. Following this, the specimens were returned to the lime bath to rehydrate.

3.3.3 Procedure

The procedure for experiment three copies that of experiment two in regards to the resistivity and ultrasonic measurements. The uniaxial method and through transmission method were both used, utilizing water and vacuum grease as couplants, respectively. The only differentiations from experiment two stem from the rehydrating of the specimens after oven drying. The mass of each specimen was recorded before and after drying. The specimens were removed at increasing time increments during saturation, recording mass and taking ultrasonic measurements. The goal of recording data and increasing time increments was to take measurements at spaced degrees of saturation. The mass gain of the specimens decreased over time, requiring larger time increments for similar increases in degree of saturation.

3.3.4 Data Analysis and Results

The data analysis of experiment three was similar to that of experiment two. The only additional data analysis was determining the degree of saturation. For this calculation, the mass recorded before drying was considered the saturated mass, and the mass recorded immediately after drying was consider the oven dried mass. Based on this, the degree of saturation was determined using the relationship below.

$$S = \frac{M_{samp} - M_{dry}}{M_{sat} - M_{dry}}$$

Where *S* is the saturation, M_{samp} is the mass of the specimen for a given measurement, M_{dry} is the oven dry mass, and M_{sat} is the saturated mass. Similar to the results section from experiment two, the results in plots are differentiated by colors. The colors for the concrete mixes are the same, with the addition of the high performance concrete mix which is marked by the color green. The saturation of the concrete specimens is summarized in figure 3.25. It should be noted that the degree of saturation for the high performance concrete samples did not get above 0.7, while the normal concrete mixes all reached about 0.9.

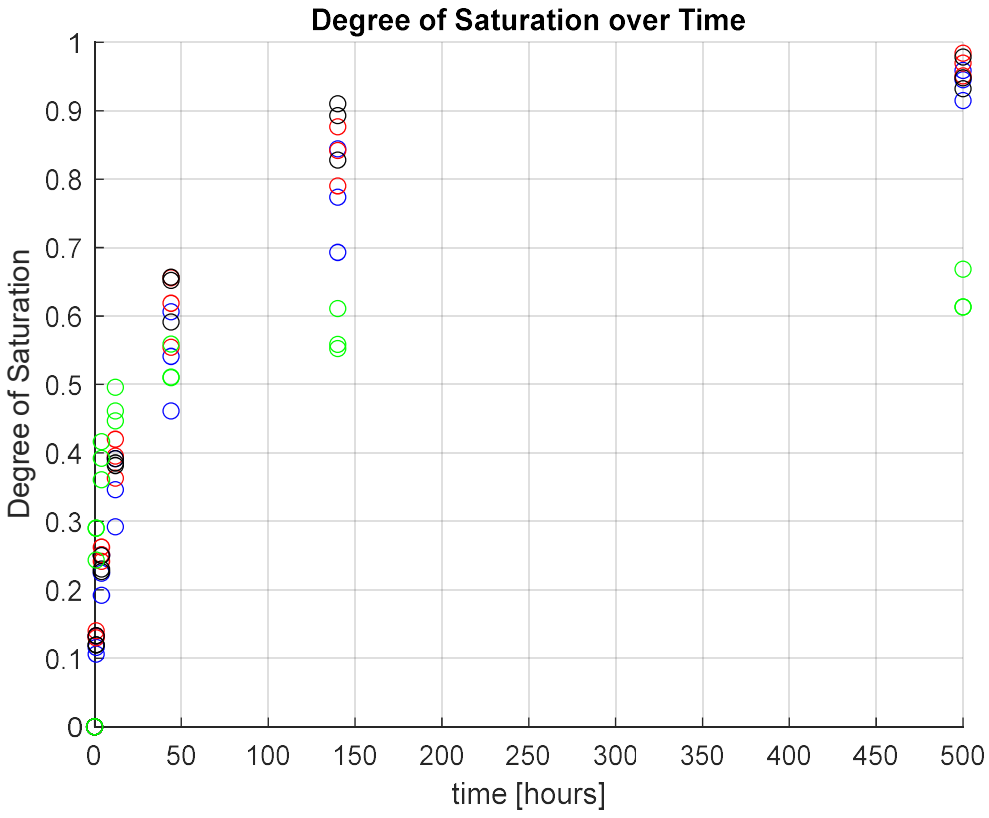

Figure 3.25: Degree of saturation vs time

As done with the second experiment, the relationship between calculated values was compared with time. Since oven drying and saturation were performed, compressive strength testing could not be done in accordance with ASTM standards, no compressive strength data is available for this experiment. First, the formation factor was compared over time, shown in Figure 3.26. The formation factors for the high performance mixes were not included in this plot as they are an order of magnitude higher than the other values, and follow a similar curve. The curve of this plot follow a similar curve as that of the curve from the previous experiment.

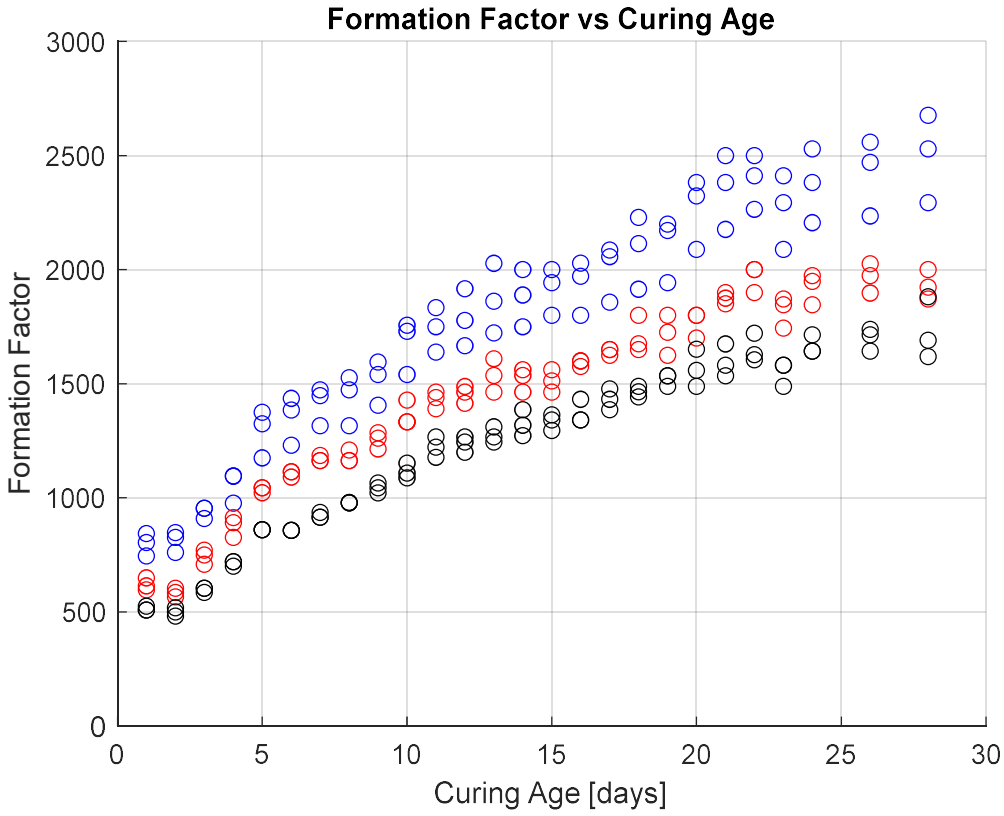

Figure 3.26: Formation factor vs time for normal strength concrete mixes

Next, the ultrasonic pulse velocity was compared with time, as shown in Figure 3.27. This plot is similar to the plot from the previous experiment, but with the addition of the high performance mix. In the previous experiment, it was discussed that the higher strength mixes had higher pulse wave velocity, and this claim seems to be extended for high performance mixes as well, as the high performance mix specimens had the highest pulse wave velocities. Again, no compressive strength data is available to directly compare these two properties, but there appears to be a relationship between the two, as discussed in the results of the previous experiment.

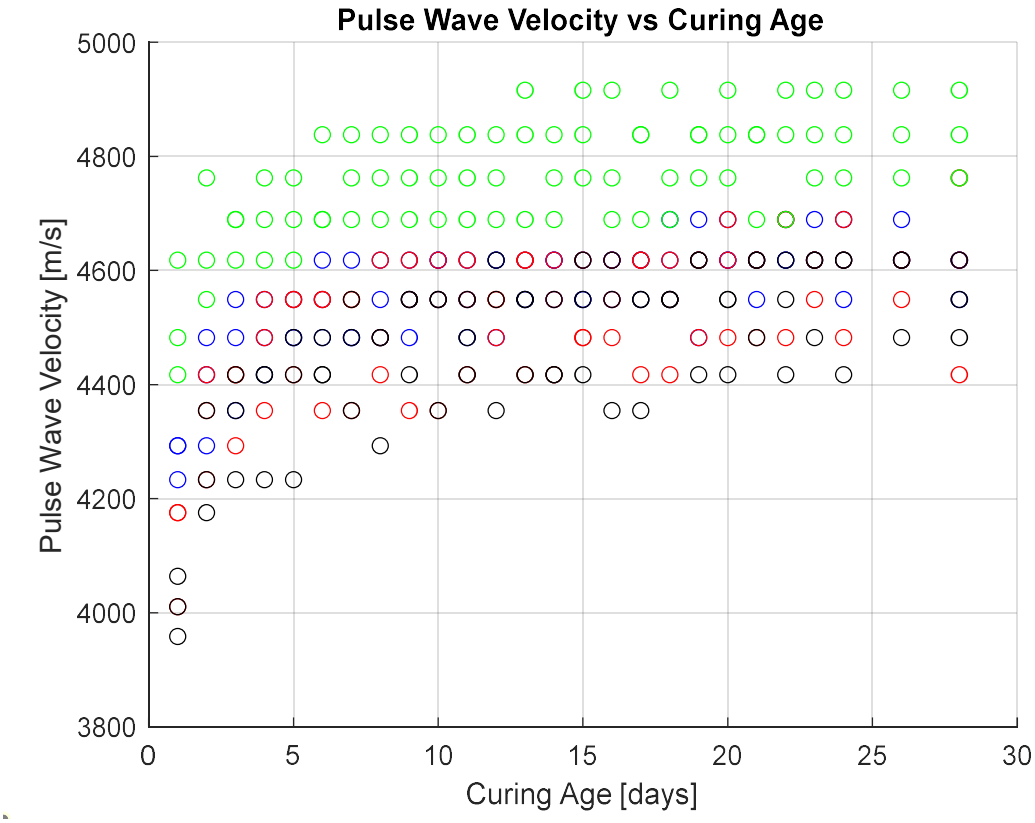

Figure 3.27: Pulse wave velocity vs curing age

Following this, the attenuation coefficient, the diffusivity coefficient, and the dissipation coefficient were all compared with curing age. For the intrinsic attenuation coefficient, there again

appears to be a correlation, as the curing age increases, the attenuation coefficient tends to decrease. This appears to be divided by concrete mix as well. For the other two plots, there appears to be no correlation between the coefficients from the diffusion approximation and the curing age. This is shown in Figure 3.28.

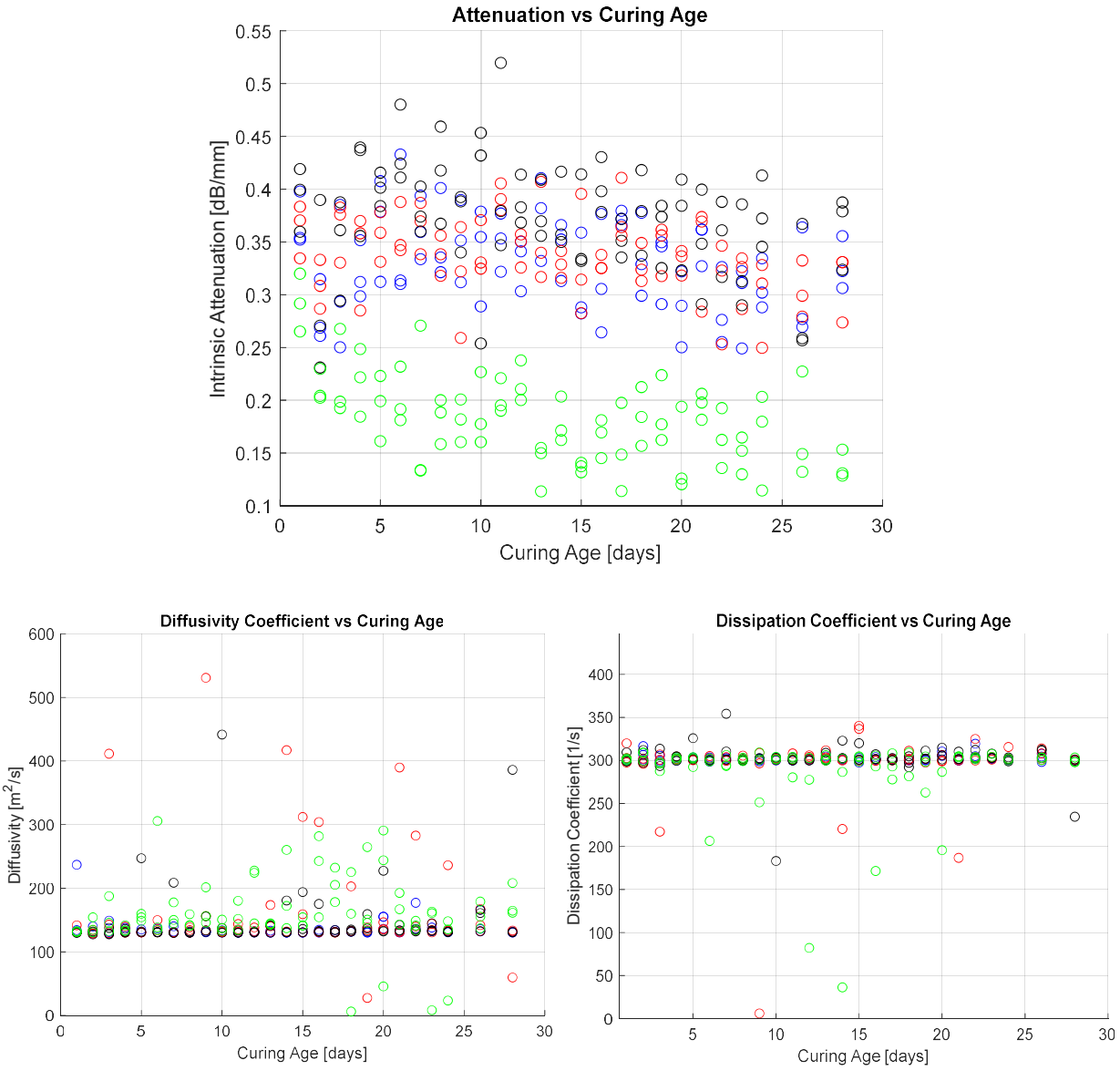

Figure 3.28: Properties of attenuation vs curing age

Next, the formation factor was compared to the ultrasonic pulse velocity. The plots were separated into two plots, the first of which includes the specimens made from normal strength concrete, as shown in Figure 3.29, and the second plot included the specimens made from the high performance concrete mix, shown in Figure 3.30. These two plots both continue to show the exponential relationship between formation factor and ultrasonic pulse velocity. This being said, it should be noted that the increase in ultrasonic pulse velocity is small relative to the increase in formation factor between the two sets of data. The ultrasonic pulse velocities differ by less than 5%, while the formation factor increases by over 10 fold.

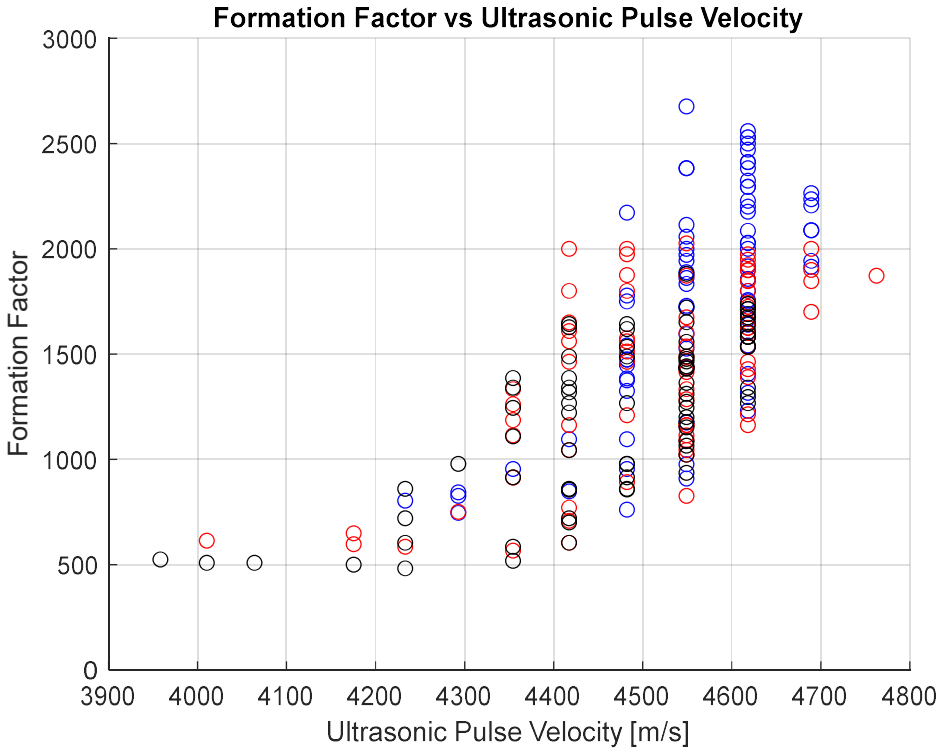

Figure 3.29: Formation factor vs ultrasonic pulse velocity for normal strength concrete

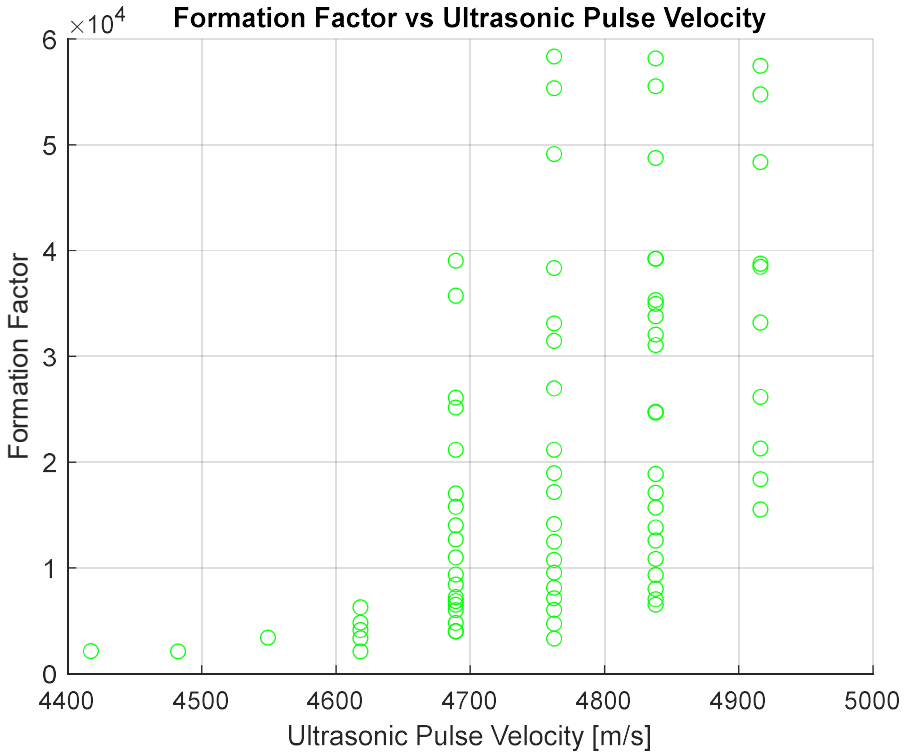

Figure 3.30: Formation factor vs ultrasonic pulse velocity for high performance concrete

The rehydration results were then investigated. Due to the resistance being too high on some samples, only the ultrasonic data could be properly recorded using the bulk resistivity test device utilized in this study. Accordingly, the ultrasonic pulse velocity will be compared with degree of saturation, as shown in Figure 3.31. There doesn't appear to be any trend amongst the high performance concrete, but the ultrasonic pulse velocity of the normal concrete mixes seems to decrease up to about 0.5 degree of saturation, then proceeds to increase afterwards.

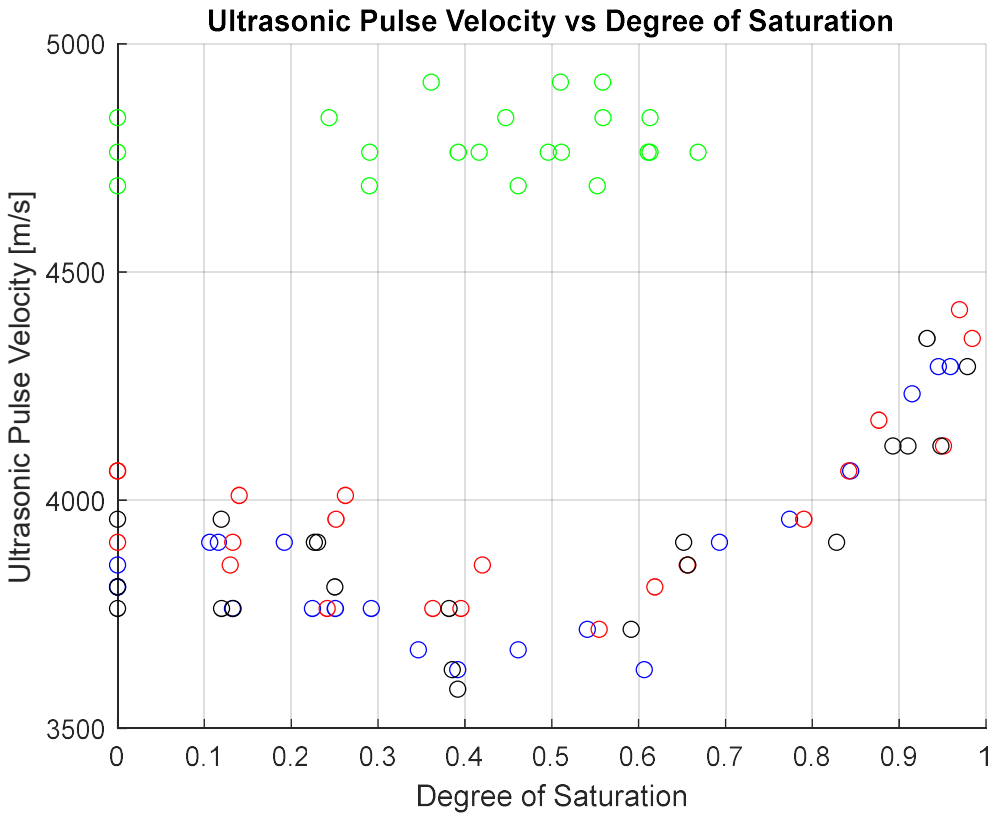

Figure 3.31: Ultrasonic pulse velocity vs degree of saturation

Next, the attenuation coefficient was compared with degree of saturation. As seen in Figure 3.32, the attenuation coefficient tends to increase as the degree of saturation increases. For the individual water-to-cement ratios, there does not seem to be much correlation in these regards, as the different mixes are scattered throughout the upwards trend. For the high performance concrete, there appears to be very little correlation.

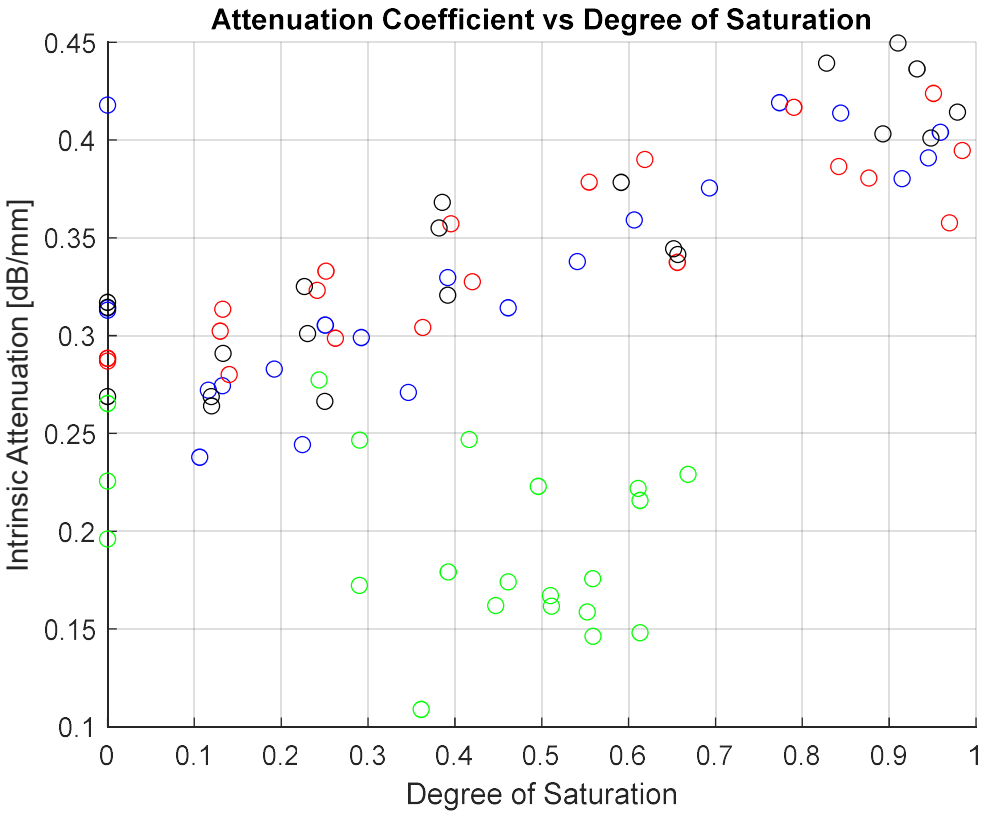

Figure 3.32: Intrinsic attenuation vs degree of saturation

Now, the relationship between the diffusivity and dissipation coefficients will be presented. These two plots are shown in figure 3.33. Yet again, there does not appear to be any trend of correlation amongst the two attenuation coefficients.

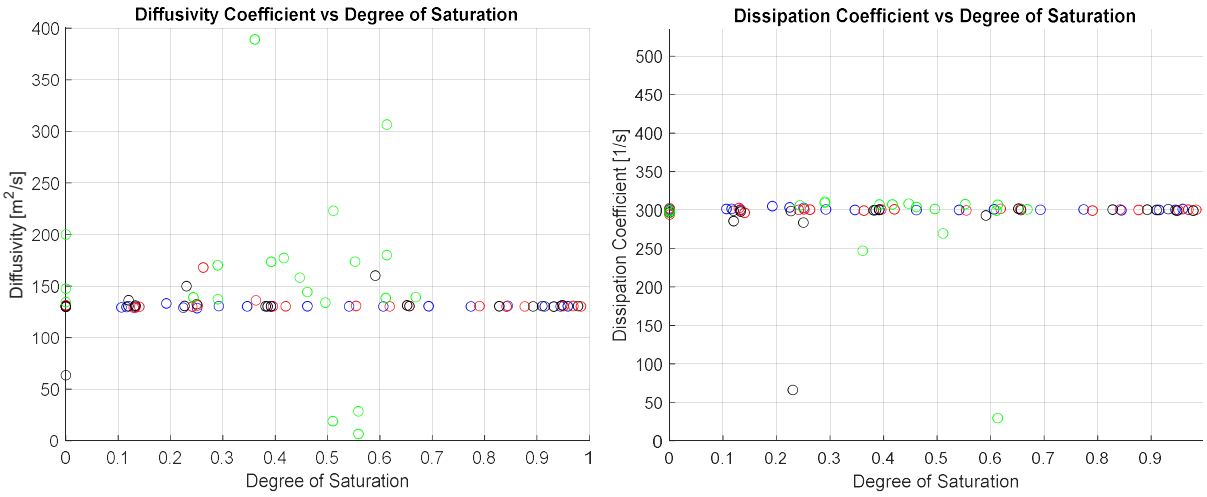

Figure 3.33: Diffusivity and dissipation coefficients vs degree of saturation

3.3.5 Conclusions

The hypothesis of this experiment was that the exponential relationship between the formation factor and ultrasonic wave velocity could be further cemented by running tests with more specimens. This hypothesis was confirmed through this experiment as the exponential relationship between these two properties was displayed for several more sets of specimens. As described in the conclusion of experiment two, the importance of this relationship is that this relationship creates the potential for predicting a significant amount of information about the state of concrete based off a single quick and easy measurement, the ultrasonic pulse velocity.

3.3.6 Suggestions for Future Research

The potential applications of the results of this experiment could be very significant for the non-destructive evaluation of concrete structures in the field. For future research, it would be important to

be able to predict the formation factor and compressive strength based solely on the ultrasonic pulse velocity. A double blind study could be run, where ultrasonic pulse data is recorded, then it is predicted which data sets represent the given specimens. In addition to this, using the ultrasonic pulse data to project the compressive strength and formation factor would be vital in the potential application in the field use as previously proposed.

3.4 Experiment 4: Fiber Orientation

3.4.1 Methodology

The fourth experiment took place in April 2022. This experiment was conducted in an attempt to build off of the first experiment, which attempted to determine the orientation of steel fibers in a high performance concrete panel. Recalling section 3.1, it was concluded that the Wenner probe used may not have been suitable for determining the fiber orientation in the concrete panel. In addition to this, it was concluded that the best course of action may be to adopt the setup used in previous literature (Lataste 2003, Lataste 2008, Barnett 2009, Martinie 2013). This setup required using a four-point probe, but rather than aligning the probes in an array, positioning the probes in a square formation, with two adjacent probes injecting current, and the opposing two probes measuring electrical potential (Lataste 2008). The purpose of this formation of probes was to further reduce the effects of interference and polarization.

As was the objective in the first experiment, the goal of this experiment was to determine the orientation of fibers dispersed within a concrete specimen. The hypothesis of this experiment was that the orientation of fibers could be determined by taking circular measurements about points on a concrete specimen, and using the recorded values of resistivity at each angle, one would be able to determine local resistivity axes and when plotted about their location on the respective specimen, a global resistivity axis could be determined. This hypothesis mimics that of experiment one, just utilizing different equipment.

3.4.2 Specimen Preparation and Procedure

Due to lack of available equipment, new equipment had to be purchased in order to achieve a four-probe square array configuration. In the aforementioned mentioned studies, the Megger DET5/4D earth tester device was used. By the time of this thesis, this product had been replaced by newer models

and was considered obsolete. As a result, the Megger DET4TC2 was purchased to be used for the purpose of recreating the four-probe square device. Similar to the model DET5/4D, the DET4TC2 is a 4-terminal soil resistivity meter. In order to create the square setup, a square wooden block was cut out, then slots for the probes were drilled out using a power drill at a distance of two inches apart, as shown in Figure 3.34. The probes for the square probe configuration were then slotted through the holes in the wooden block. Following this, pieces of sponge were cut out and attached to the end of the probe tips in order to ensure a good electrical contact for measurements. Due to time constraints along with an attempt to build off of the first experiment, the same concrete specimens were utilized in this experiment as were used in the first experiment.

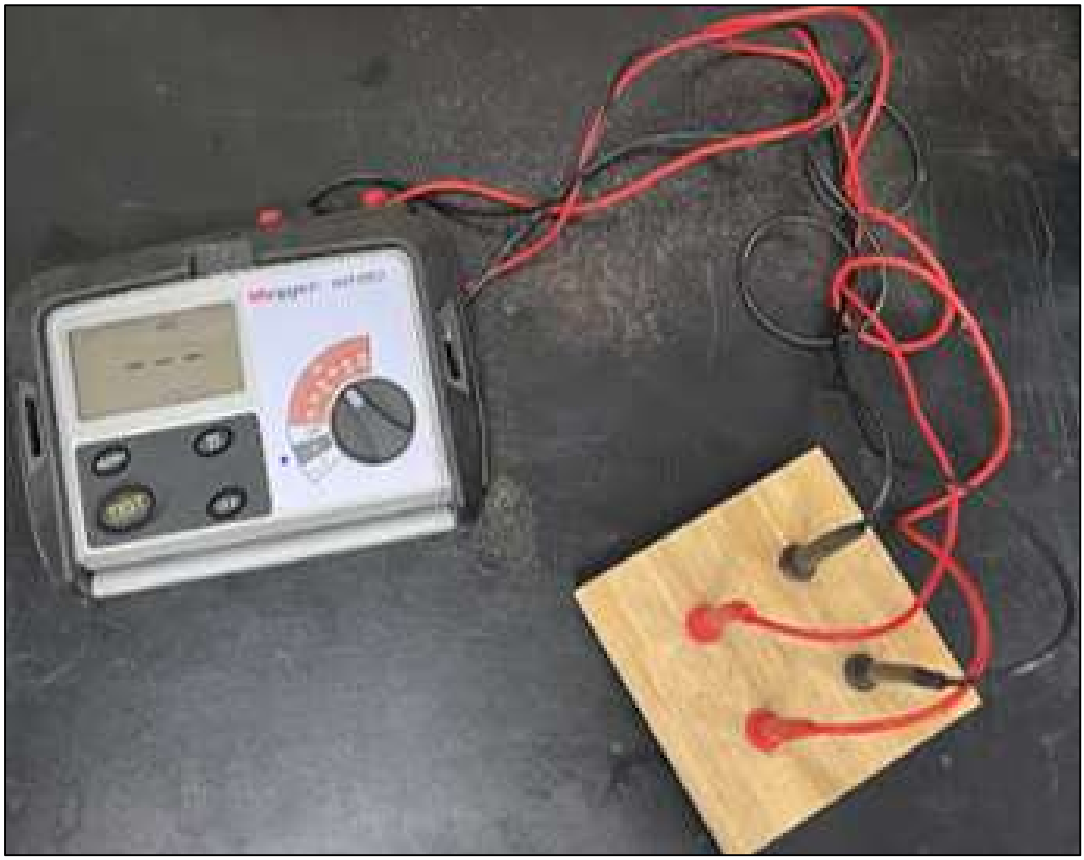

Figure 3.34: Four-probe square device manufactured for experiment four

For the procedure, locations were marked on the specimens for determining fiber orientation. The sponges attached to the end of the probes on the four-probe square array were then wetted with water. The Megger DET4TC2 was then turned on and put into 4-terminal mode. Similar to experiment one, measurements were then taken in 22.5^{o} increments for 16 measurements at each location. It should be noted that the 22.5^{o} increments have no theoretical significance, but are simply a balance between accuracy and time (Lataste 2008, Barnett 2010, Martinie 2013), as this procedure intends to be reasonable for field use. In addition to this, theoretically, the resistivity along an axis should be the same regardless of which side the current is injected and received from, so measurements that are 180^{o} apart should be the same (Lataste 2008). Despite this, all 16 measurements were taken in this experiment at each location for the sake of setting up this method and for creating an easier visualization of local resistivity axes.

3.4.3 Data Analysis and Results

The data analysis for this experiment followed the methodology prescribed by section 3.1.3. The analysis for the data from this experiment was again evaluated through the use of Microsoft Excel. The analysis portion of this experiment follows that of experiment one. In short, the data recorded using the four-probe square array is plotted in polar coordinates for each location that measurements were taken. Using this visualization, the determination of a resistivity axis can be made for each measurement circle. For this experiment, the specimens were significantly older than in experiment one. As a result, the resistivity of the high performance concrete was significantly greater. Consequently, the resistance of the concrete panel without fibers was too high to get a reading using the Megger DET4TC2, so all data came from one high performance concrete panel with fibers.

Figure 3.35: Resistivity vs orientation plots overlaid onto concrete specimen

The results from this experiment show some progress relative to the first fiber orientation experiment. In this experiment, there appear to be defined resistivity axes at each measurement location. Figure 3.35 summarizes these findings by overlaying the resistivity circles over the specimen used. Looking at the plot, the fibers appear to be orientating along the flow of the concrete based on the location that the concrete was poured from. This is depicted more clearly in Figure 3.36. This is contrary to the results of previous studies utilizing this technique. Previous studies utilizing this method show that the fibers orient perpendicular to the direction of flow (Lataste 2008), as shown in Figure 3.37. Thus, there are multiple possibilities regarding why the results from this experiment contrast that of existing literature.

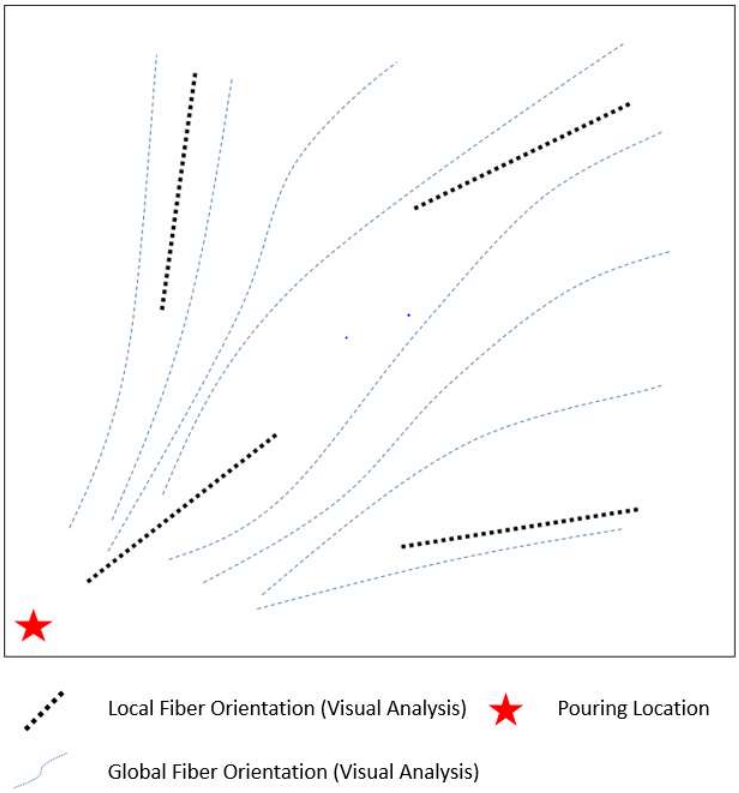

Figure 3.36: Visual analysis of local and global fiber orientation

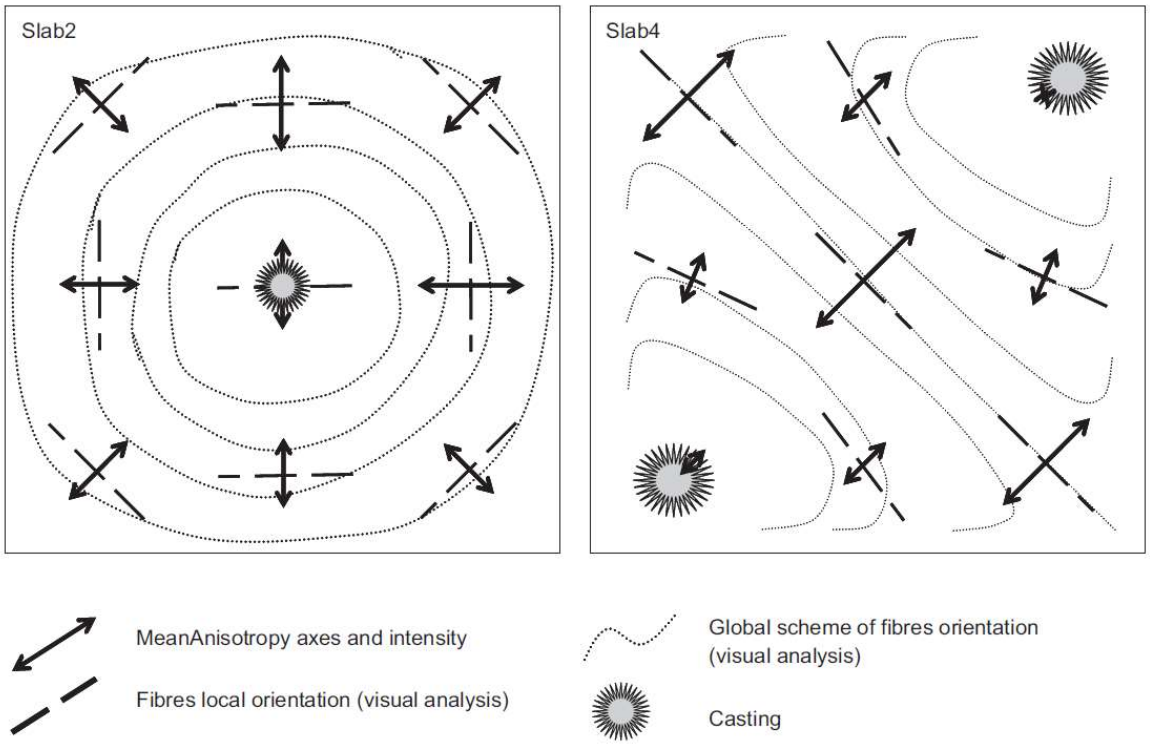

Figure 3.37: Visual analysis of local and global fiber orientation from Lataste et al. (2008)

The first possibility regarding why the results of this experiment differ from those in literature, is that these results may be the product of experimental error. The ratio between the resistivity along an axis that is indicated to have a high fiber alignment and one with low fiber alignment in this experiment is between two and five. Studies found within literature show that this ratio should be orders of magnitude larger, which aligns with the theoretical as the resistivity of concrete and steel are on orders of magnitude difference. As previously stated, if a reading is taken along an axis for which fibers are strongly oriented, the resistivity would be similar to that of steel, and other axes for which fibers are not strongly oriented, the resistivity would be similar to that of concrete without fibers. Since the resistivity axes are oriented perpendicular to what would be expected, it is possible that these resistivity axes are not due to fibers, but rather just experimental error and variability of the concrete. For such an occurrence, the effect of fibers would have to be minimal, so the orientation of the fibers would have to be near isotropic, or the density of fibers would have to be low in the locations where measurements were taken. These both seem unlikely considering the percent of fibers was 3% by mass and reference studies have similar fiber content for ultra-high performance concrete (Martinie 2013). Overall, the solution to this error would be to work on making the existing device better by creating a better electrical connection between the probes and the specimen surface, and create more specimens with higher fiber content to negate the potential that there weren't enough fibers within the specimens to have a large impact on resistivity measurements.

Another possible explanation could be that the fibers are aligned as they are shown in the results, though this would be unlikely given the location of that the concrete was poured from. While the concrete mix was poured in a relatively viscous state, it seems unlikely that there would be enough resistance to prevent the steel fibers from orienting similar to that of previous studies. Similar to the first possible explanation, the solution to this possible error would be to perform more experiments on more specimens to determine what problem exists with the current procedure.

3.4.4 Conclusion

The hypothesis of this experiment was that, using the procedure previously outline, resistivity axes would be found so that the orientation of fibers could be found locally and then globally. This hypothesis was partially fulfilled, as resistivity axes were found, although based on existing studies, it appears that these resistivity axes may not have been accurate. The found resistivity axes were perpendicular to that of what would be expected based on past research. In total, progress was made with the advancement from the Wenner probe device to the four-probe square device. While the desired outcome was not achieved, the upgrade from completely inconclusive data to results showing differentiation in resistivity at incremental orientations may lead to a device and procedure with the capacity to accurately determine the local and global fiber resistivity.

3.4.5 Reflection and Suggestions for Future Research

The ultimate purpose of the fiber orientation experiments was to determine a methodology and procedure that would create the ability to determine the fiber orientation of steel fibers within a concrete specimen. This goal was partially achieved with the manufacturing of the four-probe square device. The design of this device followed that of the equipment used in successful studies (Lataste 2003, Lataste 2008, Barnett 2010, Martinie 2013), but was not as effective in the experiments performed for this thesis. For future research, the existing device should be improved for better electrical contact, which would begin with the sponges attached to the probe tips. Additionally, more specimens should be used, both with normal concrete mixes and high performance mixes, with different fibers (steel, nylon, etc.). This would create a better understanding of the strengths and weaknesses of this method and lead to less variability due to the increase number of specimens. It would also give the opportunity to investigate the potential of identifying other types of fibers. Fibers such as steel are very conductive, making this method viable, but determining whether or not this method would work for less conductive fibers such as nylons, would be of interest. The determination of the impact of other

concrete components such as course aggregates may be important to the implementation of this method in industry practices.

CHAPTER 4
CONCLUSION

The purpose of this thesis was to further investigate the question of can concrete be more effectively assessed in a non-destructive manner by combining the results from multiple non-destructive evaluation techniques. The answer to this question was pursued by performing four experiments, with the first two acting as preliminary studies to the two latter experiments. The first and last studies focused on determining the orientation of steel fibers in concrete plates. These studies led to the development of the four-probe square device, which has the potential to determine the orientation of fibers within a concrete plate. The other two studies focused on the application of a multi method system, combining both electrical resistivity and ultrasonic pulse velocity. These studies further verified the existence of a relationship between ultrasonic pulse velocity and curing age along with compressive strength. In addition to these relationships, this study uncovered a relationship between the ultrasonic pulse velocity and formation factor. In this way, the purpose of this thesis was partially achieved as the combination of these two methods produced a relationship that has the potential for determining more information about the characteristics of the concrete through the calculation of a single property. As shown in this thesis, the ultrasonic pulse velocity has a relationship with compressive strength, and the formation factor characterizes the microstructure of concrete. Consequently, there is the potential for employing a device that has the capability of predicting compressive strength and properties of the concrete microstructure using a quick and easy measurement.

There were several potential improvements that could have been made to the experiments performed during this thesis. First, the results from the fiber orientation studies would be significantly more convincing if there were a larger data set. In experiment four, there were two concrete plates, one of which did not have fibers, and had too high of a resistance, so no measurements could be taken on this plate. Thus the data for experiment four only contained a single specimen, which could also have

been the results of insufficient contact between the probe and the specimen, so improvements could be made there as well. For the multi-method studies, the first study included compressive strength, and the second study included degree of saturation. It would be useful to formulate a procedure in which both compressive strength and degree of saturation can be determined along with the other measurement, especially if the compressive strength is known for more than one point in time. Additionally, if resaturation is going to be done similar the experiment three, then measurements should be taken on resistivity as soon as possible. From these two experiments, it was learned that creating a smooth surface to record measurements on is very advantageous, as it allows for more consistent measurements. Another improvement that could be made to this study would be determining a better means of calculating the diffusivity and dissipation constants for ultrasonic attenuation. The diffusion approximation produced very inconclusive results in this thesis, which may be due to the analysis done to calculate such constants. In the end, the results of this thesis revealed a relationship that could have major implications in the application of non-destructive evaluation techniques for field inspections.

REFERENCES

Abdullah, A., & Sichani, E. F. “Experimental study of attenuation coefficient of ultrasonic waves in concrete and plaster.” *The International Journal of Advanced Manufacturing Technology*, *44*(5), 421-427. 2009.

Aggelis, D. G., & Shiotani, T. Repair evaluation of concrete cracks using surface and through-transmission wave measurements.” *Cement and Concrete Composites*, *29*(9), 700-711. 2007.

Aggelis, D. G., Shiotani, T., Momoki, S., & Hirama, A. “Acoustic emission and ultrasound for damage characterization of concrete elements.” *ACI Materials Journal*, *106*(6), 509.2009.

Alnuaimi, H. N., Sasmal, S., Amjad, U., Nikvar-Hassani, A., Zhang, L., & Kundu, T. “Monitoring concrete curing by linear and nonlinear ultrasonic methods.” *ACI Materials Journal*, *118*(3), 61-69. 2021.

Anugonda, P., Wiehn, J. S., & Turner, J. A. “Diffusion of ultrasound in concrete.” *Ultrasonics*, *39*(6), 429-435. 2001.

Archie, G. E. “The electrical resistivity log as an aid in determining some reservoir characteristics.” *Transactions of the AIME*, *146*(01), 54-62. 1942.

ASTM, “Standard test method for pulse velocity through concrete.” *ASTM International, West Conshohocken, PA*. 2009.

ASTM, “Standard test method for bulk electrical conductivity of hardened concrete,” ASTM C1760-12, ASTM International, 2012.

ASTM, “Standard test method for electrical indication of concrete’s ability to resist chloride ion penetration.” *C1202–18*. 2012.

ASTM, “Standard test method for compressive strength of cylindrical concrete specimens.” ASTM international. 2014.

American Society for Testing and Materials. “Standard practice for making and curing concrete test specimens in the field.” ASTM International. 2016.

ASTM, “Bulk electrical resistivity or bulk conductivity concrete,” ASTM C1876-19, ASTM International, 2019.

Atkins, E. R., & Smith, G. H. “The significance of particle shape in formation resistivity factor-porosity relationships.” *Journal of Petroleum Technology*, *13*(03), 285-291. 1961.

Azarsa, P., & Gupta, R. “Electrical resistivity of concrete for durability evaluation: a review.” *Advances in Materials Science and Engineering*, *2017*.

Barnett, S. J., Lataste, J. F., Parry, T., Millard, S. G., & Soutsos, M. N. “Assessment of fibre orientation in ultra high performance fibre reinforced concrete and its effect on flexural strength.” *Materials and Structures*, *43*(7), 1009-1023. 2010.

Becker, J., Jacobs, L. J., & Qu, J. “Characterization of cement-based materials using diffuse ultrasound.” *Journal of engineering mechanics*, *129*(12), 1478-1484. 2003.

Bratina, W.J., and Mills, D. “Study of fatigue in metals using ultrasonic technique.” Canadian Metallurgical Quarterly, 1:83–97, 1962.

Deroo, F., Kim, J. Y., Qu, J., Sabra, K., & Jacobs, L. J. “Detection of damage in concrete using diffuse ultrasound.” *The Journal of the Acoustical Society of America*, *127*(6), 3315-3318. 2010.

Dugmore, K., Jonson, D., & Walker, M. “A comparison of signal consistency of common ultrasonic couplants used in the inspection of composite structures.” *Composite structures*, *58*(4), 601-603. 2002.

Eik, M., Lohmus, K., Tigasson, M., Listak, M., Puttonen, J., & Herrmann, H. “DC-conductivity testing combined with photometry for measuring fibre orientations in SFRC.” Journal of Materials Science, 48(10), 3745-3759. 2013.

Farooq, M., Park, S. G., Song, Y. S., & Kim, J. H. “Mortar characterization using electrical resistivity method.” *Geophysics and Geophysical Exploration*, *12*(2), 215-220. 2009.

Galan, I., Beltagui, H., García-Maté, M., Glasser, F. P., & Imbabi, M. S. “Impact of drying on pore structures in ettringite-rich cements.” *Cement and Concrete Research*, *84*, 85-94. 2016.

Gebretsadik, B., Jdidirendi, K., Farhangi, V., & Karakouzian, M. “Application of Ultrasonic Measurements for the Evaluation of Steel Fiber Reinforced Concrete.” *Engineering, Technology & Applied Science Research*, *11*(1), 6662. 2021.

Hansson, I. L. H., & Hansson, C. M. “Electrical resistivity measurements of Portland cement based materials.” *Cement and Concrete Research*, *13*(5), 675-683. 1983.

Hassefras, E, “Concrete Microstructure Characterization Using Ultrasound.” (Master’s thesis, Delft University of Technology). 2019.

Henkensiefken, R., Castro, J., Bentz, D., Nantung, T., & Weiss, J. “Water absorption in internally cured mortar made with water-filled lightweight aggregate.” *Cement and Concrete Research*, *39*(10), 883-892. 2009.

Hu, Xiang, et al. "A review on microstructural characterization of cement-based materials by AC impedance spectroscopy." Cement and Concrete Composites 100: 1-14. 2019.

İşleyici, U. “Effect of surface roughness on ultrasonic testing” (Master's thesis, Middle East Technical University). 2005.

Joshi, N. R., & Green Jr, R. E. “Ultrasonic detection of fatigue damage.” *Engineering Fracture Mechanics*, *4*(3), 577-583. 1972.

Ju, T., Achenbach, J. D., Jacobs, L. J., Guimaraes, M., & Qu, J. “Ultrasonic nondestructive evaluation of alkali–silica reaction damage in concrete prism samples.” Materials and structures, 50(1), 1-13. 2017.

Kewalramani, M. A., & Gupta, R. “Concrete compressive strength prediction using ultrasonic pulse velocity through artificial neural networks.” *Automation in Construction*, *15*(3), 374-379. 2006.

Kolsky, H. “Stress waves in solids” (Vol. 1098). Courier Corporation. 1963.

Krautkrämer, J., & Krautkrämer, H. “Ultrasonic testing of materials.” Springer Science & Business Media. 2013.

Landis, E. N., & Shah, S. P. “Frequency-dependent stress wave attenuation in cement-based materials.” *Journal of Engineering Mechanics*, *121*(6), 737-743. 1995.

Landis, E. “Materials: Lecture Notes in Civil Engineering,” 2017.

Landis, E. N., Hassefras, E., Oesch, T. S., & Niederleithinger, E. “Relating ultrasonic signals to concrete microstructure using X-ray computed tomography.” *Construction and Building Materials*, *268*, 121124. 2021.

Larsen, C. K. Sellevold, E. J. Ostvik, J. M. Vennesland, O. “Electrical resistivity of concrete-Part II: influence of moisture content and temperature,” in Proceedings of the 2nd International RILEM Symposium on Advances in Concrete through Science and Engineering, 2006.

Laskar, A. A., Ghosh, P., & Arifin, M. K. “Effect of flaws and its depth on ultrasonic pulse velocity of concrete results under different method of ultrasonic wave transmission through concrete medium.” 2020.

Lataste, J. F., Sirieix, C., Breysse, D., & Frappa, M. ”Improvement of electrical resistivity measurement for non destructive evaluation of concrete.” In *PRO 29: 2nd International RILEM Workshop on Life Prediction and Aging Management of Concrete Structures* (p. 93). RILEM Publications. 2003.

Lataste, J. F., Behloul, M., & Breysse, D. “Characterisation of fibres distribution in a steel fibre reinforced concrete with electrical resistivity measurements.” *Ndt & E International*, *41*(8), 638-647. 2008.

Layssi, H., Ghods, P., Alizadeh, A. R., & Salehi, M. “Electrical resistivity of concrete.” *Concrete International*, *37*(5), 41-46. 2015.

Li, Z., Xiao, L., & Wei, X. “Determination of concrete setting time using electrical resistivity measurement.” *Journal of materials in civil engineering*, *19*(5), 423-427. 2007.

Lootens, D., Schumacher, M., Liard, M., Jones, S. Z., Bentz, D. P., Ricci, S., & Meacci, V. “Continuous strength measurements of cement pastes and concretes by the ultrasonic wave reflection method.” *Construction and Building Materials*, *242*, 117902. 2020.

Macdonald, J. R., and Johnson, W. B., “Fundamentals of Impedance Spectroscopy,” in: “Impedance Spectroscopy; Emphasizing Solid Materials and Systems,” ed. J. R. Macdonald, John Wiley and Sons, New York. 1987.

Martinie, L., & Roussel, N. “Simple tools for fiber orientation prediction in industrial practice.” Cement and Concrete research, 41(10), 993-1000. 2011.

Martinie, L., Lataste, J. F., & Roussel, N. “Fiber orientation during casting of UHPFRC: electrical resistivity measurements, image analysis and numerical simulations.” *Materials and Structures*, *48*(4), 947-957. 2015.

Mazloom, M., Allahabadi, A., & Karamloo, M. “Effect of silica fume and polyepoxide-based polymer on electrical resistivity, mechanical properties, and ultrasonic response of SCLC.” *Advances in concrete construction*, *5*(6), 587. 2017.

Maxwell, J. C. “Electricity and magnetism*”* (Vol. 2). New York: Dover. 1954.

Mehta P.K, Monteiro P. J, “Concrete: microstructure, properties, and materials,” McGraw-Hill, New York, NY, USA, 2nd Edition, 2001.

Mindess S, Young, J. F, & Darwin D, “Concrete,” Pearson, Upper Saddle River, NJ, USA, 2nd Edition, 2003.

Morris, W., Moreno, E. I., & Sagüés, A. A. “Practical evaluation of resistivity of concrete in test cylinders using a Wenner array probe.” *Cement and concrete research*, *26*(12), 1779-1787. 1996.

Netshidavhini, N., & Mabuza, R. B. “Effects of various couplants on carbon steel and aluminium materials using ultrasonic testing.” In *18th World Conference on Nondestructive Testing* (pp. 16-20). 2012.

Ongpeng, J. M. C., Oreta, A. W. C., & Hirose, S. “Contact and noncontact ultrasonic nondestructive test in reinforced concrete beam." *Advances in Civil Engineering*, *2018*.

Papadakis, E. P. “Ultrasonic attenuation caused by scattering in polycrystalline media.” Physical acoustics, 4(Part B), 269-328. 1968.

Philippidis, T. P., & Aggelis, D. G. “Experimental study of wave dispersion and attenuation in concrete.” Ultrasonics, 43(7), 584-595. 2004.

Polder, R. B. “Test methods for on site measurement of resistivity of concrete—a RILEM TC-154 technical recommendation.” *Construction and building materials*, *15*(2-3), 125-131. 2001.

Popovics, J. S., Song, W., Achenbach, J. D., Lee, J. H., & Andre, R. F. “One-sided stress wave velocity measurement in concrete.” *Journal of Engineering Mechanics*, *124*(12), 1346-1353. 1998.

Punurai, W. “Cement-based materials' characterization using ultrasonic attenuation.” Georgia Institute of Technology. 2006.

Punurai, W., Jarzynski, J., Qu, J., Kurtis, K. E., & Jacobs, L. J. “Characterization of dissipation losses in cement paste with diffuse ultrasound.” *Mechanics Research Communications*, *34*(3), 289-294. 2007.

Rajabipour, Farshad, Jason Weiss, and Dulcy M. Abraham. "Insitu electrical conductivity measurements to assess moisture and ionic transport in concrete (A discussion of critical features that influence the measurements)." Proceedings of the International RILEM Symposium on Concrete Science and Engineering: A Tribute to Arnon Bentur. Rilem, Paris, France, 2004.

Rajabipour, F. “In situ electrical sensing and material health monitoring of concrete structures,” Ph.D. Dissertation, Purdue University, West Lafayette, Indiana, 2006.

Rajabipour, F., & Weiss, J. “Electrical conductivity of drying cement paste.” *Materials and Structures*, *40*(10), 1143-1160. 2007.

Ravikumar, Deepak, and Narayanan Neithalath. "An electrical impedance investigation into the chloride ion transport resistance of alkali silicate powder activated slag concretes." Cement and Concrete Composites 44: 58-68. 2013.

Rivard, P., & Saint-Pierre, F. “Assessing alkali-silica reaction damage to concrete with non-destructive methods: From the lab to the field.” *Construction and Building Materials*, *23*(2), 902-909. 2009.

Roth, M., & Korn, M. “Single scattering theory versus numerical modelling in 2-D random media.” Geophysical Journal International, 112(1), 124-140. 1993.

Sallehi, H., Ghods, P., & Isgor, O. B. “Formation factor of fresh cementitious pastes.” *Cement and Concrete Composites*, *91*, 174-188. 2018.

Sanish, K. B., Neithalath, N., & Santhanam, M. “Monitoring the evolution of material structure in cement pastes and concretes using electrical property measurements.” *Construction and Building Materials*, *49*, 288-297. 2013.

Sant, G., Bentz, D., & Weiss, J. “Capillary porosity depercolation in cement-based materials: Measurement techniques and factors which influence their interpretation.” Cement and Concrete Research, 41(8), 854-864. 2011.

Seidel, K., & Lange, G. “Direct current resistivity methods.” In *Environmental geology* (pp. 205-237). Springer, Berlin, Heidelberg. 2007.

Shah, S. P., Popovics, J. S., Subramaniam, K. V., & Aldea, C. M. “New directions in concrete health monitoring technology.” *Journal of engineering mechanics*, *126*(7), 754-760. 2000.

Sharisha K, “To Study the Effect of Cellulose Nano Fibrils on Cement Paste Micro Structure using Electrical Resistivity Measurement” University of Maine, Orono, Maine 2017.

Sharisha, K. “Electrical Resistivity Measurements Concepts on Hardened Cement Pastes.” University of Maine, Orono, Maine. 2019.

Shimizu, Y. “An Electrical Method for Measuring the Setting Time of Portland Cement.” Mill Section of Concrete, Vol. 32, No. 5, pp. 111–113. 1928.

Slawinski, A. “Conductivity of an Electrolyte Containing Dielectric Bodies.” *Jour. Chem. Phys*, *23*, 710. 1926.

Solgaard, A. O. S., Geiker, M., Edvardsen, C., & Küter, A. “Observations on the electrical resistivity of steel fibre reinforced concrete.” *Materials and structures*, *47*(1), 335-350. 2014.

Spragg, R., Bu, Y., Snyder, K., Bentz, D., & Weiss, J. “Electrical testing of cement-based materials: Role of testing techniques, sample conditioning, and accelerated curing.” 2013.

Spragg, R. The Rapid Assessment of Transport Properties of Cementitious Materials Using Electrical Methods. M.S.C.E. Purdue University, West Lafayette, Indiana, 2013.

Spragg, R., Villani, C., Snyder, K., Bentz, D., Bullard, J. W., & Weiss, J. “Factors that influence electrical resistivity measurements in cementitious systems.” *Transportation research record*, *2342*(1), 90-98. 2013.

Suaris, W., and Fernando, V. “Ultrasonic pulse attenuation as a measure of damage growth during cyclic loading of concrete.” ACI Materials Journal, 84:185– 193, 1987.

Tang, S. W., Cai, X. H., He, Z., Zhou, W., Shao, H. Y., Li, Z. J., ... & Chen, E. “The review of pore structure evaluation in cementitious materials by electrical methods.” *Construction and Building Materials*, *117*, 273-284. 2016.

Torquato, Salvatore, and H. W. Haslach Jr. “Random heterogeneous materials: microstructure and macroscopic properties.” Appl. Mech. Rev. 55.4, 2002.

Verma, S. K., Bhadauria, S. S., & Akhtar, S. “Review of nondestructive testing methods for condition monitoring of concrete structures.” *Journal of construction engineering*, *2013*(2008), 1-11. 2003.

Veselý, V., Lehner, P., Pieszka, D., & Žídek, L. “Electrical resistivity and ultrasonic measurements during sequential fracture test of cementitious composite.” *Frattura ed Integrità Strutturale*, *8*(30), 263-272. 2014.

Veselý, V., Konečný, P., & Lehner, P. “Influence of crack propagation on electrical resistivity and ultrasonic characteristics of normal concrete assessed by sequential TPB fracture test.” *Theoretical and Applied Fracture Mechanics*, *80*, 2-13. 2015.

Villagran Zaccardi, Y. A., & Di Maio, Á. A. “Electrical resistivity measurement of unsaturated concrete samples.” *Magazine of Concrete Research*, *66*(10), 484-491. 2014.

Weaver, R. “Ultrasonics in an aluminum foam.” *Ultrasonics*, *36*(1-5), 435-442. 1998.

Weiss, J. Snyder, K. Bullard, J. Bentz, D. “Using a saturation function to interpret the electrical properties of partially saturated concrete.” J Mater Civ Eng 25:1097–1106. 2013.

Weiss, W.J., Barrett, T.J., Qiao, C., Todak, H. “Toward a specification for transport properties of concrete based on the formation factor of a sealed specimen.” Adv. Civ. Eng. Mater. 5(1), 179–194 2016.

Weiss, W.J., Ley, T., Isgor, O.B., Van Dam, T. “Toward performance specifications for concrete durability: using the formation factor for corrosion and critical saturation for freeze-thaw.” Transportation Research Board, Washington, DC. 2017.

Woo, L. Wansom, S. Ozyurt, N. Mu, B. Shah, S. Mason, T. “Characterizing fiber dispersion in cement composites using AC-impedance spectroscopy,” Cem. Concr. Compos. 27 (6) 627–636. 2004.

Yaman, I. O., Inci, G., Yesiller, N., & Aktan, H. M. “Ultrasonic pulse velocity in concrete using direct and indirect transmission.” *ACI Materials Journal*, *98*(6), 450. 2001.

Yang, R. B., & Mal, A. K. “Multiple scattering of elastic waves in a fiber-reinforced composite.” Journal of the Mechanics and Physics of Solids, 42(12), 1945-1968.

Zamen, S., & Dehghan-Niri, E. “Fractal analysis of nonlinear ultrasonic waves in phase-space domain as a quantitative method for damage assessment of concrete structures.” *NDT & E International*, *111*, 102235. 2020.

Zhang, J., Qin, L., & Li, Z. “Hydration monitoring of cement-based materials with resistivity and ultrasonic methods.” *Materials and Structures*, *42*(1), 15-24. 2009.

Zhang, J., & Scherer, G. W. “Comparison of methods for arresting hydration of cement.” *Cement and Concrete Research*, *41*(10), 1024-1036. 2011.

Zhang, Z., Zhu, Y., Zhu, H., Zhang, Y., Provis, J. L., & Wang, H. “Effect of drying procedures on pore structure and phase evolution of alkali-activated cements.” *Cement and Concrete Composites*, *96*, 194-203. 2019.

Zhou, R., Li, Q., Wang, J., Zhou, K., He, R., & Fu, C. “Assessment of Electrical Resistivity and Oxygen Diffusion Coefficient of Cementitious Materials from Microstructure Features.” *Materials*, *14*(12), 3141. 2021.

Zhu, Yu, et al. "Electrochemical impedance spectroscopy (EIS) of hydration process and drying shrinkage for cement paste with W/C of 0.25 affected by high range water reducer." Construction and Building Materials 131: 536-541. 2017.

APPENDIX: MATLAB CODES

Data Averaging:

```
function [Data] = DataAveraging(x)
readmatrix(x);

x = ans;
RL = length(x(1,:)); %Row Length
CL = length(x(:,1)); %Column Length
x = x(5:CL,:); %Data without headers
time = x(:,1); %Time

Data = zeros(size(CL-4,1)); %Initialization
for i = 1:RL/2
   Data = Data + x(:,2*i); %Adds columns with data together
end
Data = Data/(RL/2); %Divide by # of tests
Data = [time Data];
%Plotting
clf
plot(Data(:,1),Data(:,2),'m')
hold on
xlabel('Time [sec]')
ylabel('Voltage [V]')
title('Averaged Signal')
hold off
```

Ultrasonic Pulse Velocity:

```
function [pwv,counter] = USStart(a,x)

x = x*0.0254; %convert to meters
counter = 1050;
diff = 0;
   while abs(diff) < 0.0005
   diff = a(2,counter+1)-a(2,counter);
   counter = counter + 1;
   end

pwv = x/(a(1,counter)-0.0005);
```

Attenuation Coefficient:

```
function [alpha] = Attenuation(data)
load('Base150.mat');
```

```
time = Base150(1,:);
base = Base150(2,:);

%Frequency Domain
ts = time(2)-time(1); %Sampling interval
N = length(time); %Number of Data Points
fn = 1/(2*ts); %Nyquist Frequency (1/sec)
df = 1/(ts*N); %Change in frequency (1/sec-sample)
f = (0:N-1)*df; %Frequency Vector (1/sec)
Basefft = fft(base); %Fast Fourier Transform of base
BaseMag = abs(Basefft); %Magnitude of Base FFT
Datafft = fft(data); %Fast Fourier Transfrom of data
DataMag = abs(Datafft);

%Calculations
Ao = max(BaseMag);
Ar = max(DataMag);
alpha = -20/(8*25.4)*log(Ar/Ao); %dB/mm
```

Spectral Energy Density:

```
function [t,E] = psd2(time,data)
t =[];
E = [];
n = 5;

for i = (1+n):length(time)-n
   t(i-n) = time(i);
   subD = data(i-n:i+n).*hamming(2*n+1)';
   four = abs(fft(subD));
   psd = four.^2;
   f = linspace(160000,340000,length(four));
   E(i-n) = trapz(f,psd);
end
clf
plot(t,log(E))
```

Curve Fitting for Diffusion Approximation:

```
function [phi] = UltrasonicRegression(t,d)
%Solve using lsqnonlin
for i = 1:7
   phi(i,:) = lsqnonlin(@(p) nllsr(t',d(i,:)',p),[10;15;1]);
end
```

```
function err = nllsr(t,data,a)

r = 6*0.0254;
rModel = a(3).*exp(-r^2./(4*a(1)*t)).*exp(-a(2)*t)./sqrt(4*a(1)*pi*t);
err = data - rModel;
```

BIOGRAPHY OF THE AUTHOR

Justin Harris was born in Maine on November 27th, 1998. He was raised in South China, Maine and graduated from Erskine Academy in 2017 as the class Valedictorian. He then attended the University of Maine, and graduated in 2020 with a Bachelor's degree in Civil Engineering. He further continued his education by pursuing a Master's degree in Civil Engineering at the University of Maine. After receiving his degree, Justin will be joining VHB in their Augusta and Portland offices, a structural design firm located throughout the east coast of the United States. Justin is a candidate for the Master of Science degree in Civil Engineering from the University of Maine in August 2022.